

6193

NATIONAL LIBRARY  
OTTAWA



BIBLIOTHÈQUE NATIONALE  
OTTAWA

NAME OF AUTHOR... *N. Naveena Chandra*...

TITLE OF THESIS... *MICROSEISMS IN*...  
*CANADA*.....

.....

UNIVERSITY... *University of Alberta*.....

DEGREE FOR WHICH THESIS WAS PRESENTED... *Ph. D.*.....

YEAR THIS DEGREE GRANTED... *1970, Spring*.....

Permission is hereby granted to THE NATIONAL LIBRARY  
 OF CANADA to microfilm this thesis and to lend or sell copies  
 of the film.

The author reserves other publication rights, and  
 neither the thesis nor extensive extracts from it may be  
 printed or otherwise reproduced without the author's  
 written permission.

(Signed) *N. Naveena Chandra*

PERMANENT ADDRESS:

*3-5-37, Narayana*  
*Hyderabad, A.P.*  
*INDIA*.....

DATED... *April 27*... 19 *70*

THE UNIVERSITY OF ALBERTA

MICROSEISMS IN CANADA

by



N. NAVEENA CHANDRA

A THESIS

SUBMITTED TO THE FACULTY OF GRADUATE STUDIES

IN PARTIAL FULFILMENT OF THE REQUIREMENTS FOR THE DEGREE  
OF DOCTOR OF PHILOSOPHY

DEPARTMENT OF PHYSICS

EDMONTON, ALBERTA

SPRING, 1970

UNIVERSITY OF ALBERTA  
FACULTY OF GRADUATE STUDIES

The undersigned certify that they have read,  
and recommend to the Faculty of Graduate Studies for  
acceptance, a thesis entitled Microseisms in Canada  
submitted by N. Naveena Chandra in partial fulfilment  
of the requirements for the degree of Doctor of  
Philosophy.

*G. L. Cumming*  
.....  
Supervisor

*D. J. Goulet*  
.....

*A. Roy House*  
.....

*[Signature]*  
.....

E. R. Kanarewicz

*Robert M. Ellis*  
.....  
External Examiner

Date... *April 6, 1970* .....

*University of British Columbia*  
.....

## ABSTRACT

Microseisms at five observatories viz. Victoria, Penticton, Edmonton, Resolute and Ottawa are studied with special reference to their content of physical wave types, mechanism of their propagation in the crust and the direction of approach.

Correction for the instrument response is made using a transfer function of fourth order in frequency. Plot of this function is matched with the calibration curves supplied by the observatories. The matching shows that in the case of Ottawa only the critical response conditions are met; but at Victoria, Penticton and Resolute the seismometer is overdamped and the galvanometer underdamped, while at Edmonton the seismometer is underdamped and the galvanometer overdamped.

Peaks in the autopower and the crosspower spectra occur at around 6.5 seconds, 4.5 seconds and 2.5 seconds. The main peak is at 6.5 seconds at all stations although the sedimentary layers at Edmonton seem to have a pronounced effect in accentuating the shorter period peak at 2.5 seconds. Coherency between the vertical and horizontal components is in general very low (often much less than 0.7) while that between the horizontal components is usually around 0.8 or greater. The phase values between the vertical and horizontal components strongly suggest that body waves (perhaps LP

modes of Phinney) make up a considerable portion of microseisms. This is reinforced by the sequential peaks in the velocity sensitivity spectra and by the studies on synthetic microseisms. White noise with a peak to peak amplitude twenty times that of the signal is required to change the phase and coherency for a simple Rayleigh type of motion by the amount observed in the data. The same amount of white noise would also distort the shape of the microseisms as recorded on the instruments. But since the microseisms appear as sinusoids on the records, it is felt that "noise" associated with Rayleigh or Love type of motion is not background white noise but some seismic wave with the properties of body waves and pseudo-surface waves. Interference of Rayleigh waves and the long period body waves would then be explained as a reason for low coherency between the vertical and horizontal components.

Studies on directional spectra indicate that the uncertainty of direction of approach increases as the distance from the coast increases. This is attributed to the coastal effect rather than due to the source of microseisms. It is suggested that the elastic vibrations set up in the ocean bottom by the second order fluctuations are channeled in the oceanic crust and travel in different directions until they reach the coast from whence the waves travel in the continent along different paths so that the sites near the coast have a smaller angle of vision of the source of elastic energy and the farther sites have a larger angle of vision resulting in greater uncertainty.

## ACKNOWLEDGEMENTS

With sincere and deep appreciation I wish to thank Dr. G. L. Cumming whose guidance, work and encouragement have been invaluable throughout the entire programme.

A special vote of thanks has to be extended to Dr. E. R. Kanasewich for very stimulating discussions which were extremely useful in several phases of this work.

The seismic records were obtained from the Dominion Observatory, Ottawa, and they also made the seismogram digitizer available to the author. I am deeply indebted to the personnel of the Dominion Observatory for their very kind help, especially to Dr. F. Kollar who extended unreserved guidance in using the digitizer.

During the course of his research, the author was supported by a Graduate Service Assistantship from the Faculty of Graduate Studies and by a Graduate Teaching Assistantship from the Department of Physics, University of Alberta.

TABLE OF CONTENTS

	Page
ABSTRACT . . . . .	i
LIST OF ILLUSTRATIONS. . . . .	iii
CHAPTER I. INTRODUCTION . . . . .	1
CHAPTER II. METHOD OF ANALYSIS . . . . .	13
CHAPTER III. POWER SPECTRA OF MICROSEISMS . . . . .	32
CHAPTER IV. WAVE TYPES IN MICROSEISMS. . . . .	46
CHAPTER V. JENSEN'S DIAGRAMS AND PARTICLE MOTION TRAJECTORIES. . . . .	72
CHAPTER VI. DIRECTIONAL SPECTRA. . . . .	81
CHAPTER VII. GENERAL DISCUSSION . . . . .	97
BIBLIOGRAPHY. . . . .	100

## LIST OF ILLUSTRATIONS

- Fig. II.1 Standard Seismic Stations in Canada
- Fig. II.2 Comparison of the traces from the record with the digitized traces.
- Fig. II.3 Asymptotic form of the Transfer Function of Seismometer and Galvanometer
- Fig. II.4 Calibration Curve of the Instrument at Ottawa
- Fig. II.5 Response of the Seismometer-Galvanometer System at Ottawa
- Fig. II.6 Comparison of the digitized trace with the phase corrected trace.
- Fig. II.7a Surface Weather Maps of the Pacific Ocean  
to on January 1-5, 1965.  
7e
- Fig. III.1.a Auto-power Spectrum of Microseisms at Edmonton
- Fig. III.1.b Auto-power Spectrum of Microseisms at Victoria
- Fig. III.2 Auto-power peaks at Victoria
- Fig. III.3 Auto-power peaks at Penticton
- Fig. III.4 Auto-power peaks at Edmonton Vertical Component
- Fig. III.5 Auto-power peaks at Edmonton North-South Component
- Fig. III.6 Auto-power peaks at Edmonton East-West Component
- Fig. III.7 Auto-power peaks at Ottawa
- Fig. III.8 Auto-power peaks at Resolute
- Fig. III.9 Variation of Auto-power with Distance
- Fig. III.10 Velocity Sensitivity Spectra at Victoria
- Fig. III.11 Velocity Sensitivity Spectra at Penticton
- Fig. III.12 Velocity Sensitivity Spectra at Edmonton
- Fig. III.13 Cross-power peaks at Victoria



- Fig. III.14 Cross-power peaks at Penticton
- Fig. III.15 Cross-power peaks between Vertical North-South Components at Edmonton
- Fig. III.16 Cross-power peaks between North-South and East-West Components at Edmonton
- Fig. III.17 Cross-power peaks between East-West and Vertical Components at Edmonton
- Fig. III.18 Cross-power peaks at Resolute
- Fig. III.19 Cross-power peaks at Ottawa
- Fig. III.20 Phase and Coherency between Vertical and East-West Components
- Fig. V.1 Power Spectrum of the Unfiltered Data
- Fig. V.2 Power Spectrum of the Filtered Data Band Pass 0.05-0.10 hz
- Fig. V.3 Power Spectrum of the Filtered Data Band Pass 0.10-0.20 hz
- Fig. V.4 Jensen's Diagram at Victoria
- Fig. V.5 Jensen's Diagram at Penticton
- Fig. V.6 Jensen's Diagram at Edmonton
- Fig. V.7 Particle Trajectories at Victoria
- Fig. V.8 Particle Trajectories at Penticton
- Fig. VI.1.a Cross-power between Vertical and Horizontal Components at Victoria
- Fig. VI.1.b Coherency between Vertical and Horizontal Components at Victoria
- Fig. VI.1.c Cross-power between the Horizontal Components at Victoria
- Fig. VI.1.d Coherency between the Horizontal Components at Victoria
- Fig. VI.2.a Cross-power between Vertical and Horizontal Components at Penticton

- Fig. VI.2.b Coherency between Vertical and Horizontal Components at Penticton
- Fig. VI.2.c Cross-power between the Horizontal Components at Penticton
- Fig. VI.2.d Coherency between the Horizontal Components at Penticton
- Fig. VI.3.a Cross-power between Vertical and Horizontal Components at Edmonton
- Fig. VI.3.b Coherency between Vertical and Horizontal Components at Edmonton
- Fig. VI.3.c Cross-power between the Horizontal Components at Edmonton
- Fig. VI.3.d Coherency between the Horizontal Components at Edmonton
- Fig. VI.4.a Cross-power between Vertical and Horizontal Components at Resolute
- Fig. VI.4.b Coherency between Vertical and Horizontal Components at Resolute
- Fig. VI.4.c Cross-power between the Horizontal Components at Resolute
- Fig. VI.4.d Coherency between the Horizontal Components at Resolute
- Fig. VI.5.a Cross-power between Vertical and Horizontal Components at Ottawa
- Fig. VI.5.b Coherency between Vertical and Horizontal Components
- Fig. VI.5.c Cross-power between the Horizontal Components at Ottawa
- Fig. VI.5.d Coherency between the Horizontal Components at Ottawa

## CHAPTER I

### INTRODUCTION

I.1 Bertelli (Macelwane, 1952) seems to be the first to have systematically studied microseismic phenomenon. He did this by means of several thousands of observations on free pendulums and on reflections from the surface of mercury. Darwin & Darwin (Macelwane, 1952) had to abandon their study of lunar tides in the solid earth because of this phenomenon, which interfered with their experiments. Milne (Macelwane, 1952), on the basis of work extended over several years (1880-1887) and done in different parts of the earth (Japan, Italy, France and England), concluded that the whole globe is affected by these phenomena and he called them "microseismical disturbances." He was also the first to recognize a "microseismic storm" and to coin the phrase, in addition to observing that these disturbances can travel for long distances. Meanwhile E. Von Rebeur-Pachwitz (Macelwane, 1952) on the basis of work done in Germany during the period 1892-1894, submitted a report on Earth tides in 1895 wherein a section was devoted to observations on microseisms. Omori (1901) recognized the periods of these pulsations to be about 4 sec. and 8 sec. By this time interest in microseisms was widespread and at meetings of the International Seismological Association (Macelwane, 1952) a standing committee was appointed for the study of microseisms.

I.2 Many theories have been proposed to explain the origin of microseisms but the surf theory seems to be the one with some historical importance. Weichert (Macelwane, 1952) proposed this theory during the second international conference in Strasbourg. Surf approaching a continental boundary imparts energy to it which is then transmitted as microseisms in the continent. Gutenberg (Macelwane, 1952), in a doctoral dissertation, vigorously supported the surf theory on the basis of a strong correlation between the occurrence of microseisms and waves approaching the Norwegian Coast. However, Banerji (1930) and Gherzi (Macelwane, 1952) found that the strongest microseisms occurred some hours before the storm reached the Coast. To meet this objection the surf theory was modified to state that the wave energy produced by the storm radiates in the ocean to form a swell until it reaches the continental boundary where, by a mechanism not specified in the theory, it is imparted to the continents.

I.3 Imbo (Macelwane, 1952), by comparing waves in the Mediterranean with microseisms in Sicily, found that the period of the microseisms was half that of the ocean waves. A similar result was reported by Deacon (1947) and Darbyshire (1950). This clearly can not be explained by the surf theory.

The theory of oceanic storms as proposed by Banerji (1929, 1930, 1935) and Gherzi (Macelwane, 1952) suffered from the objection that the internal pressures

due to water waves in deep water die off too rapidly with depth to be effective in imparting energy to the ocean floor.

As early as 1831 Faraday (Longuet-Higgins, 1952) knew that fluid resting on a vibrating elastic plate will form itself into standing waves. He also showed that the period of the standing waves in the fluid was twice that of the elastic vibrations in the plate. Rayleigh (Longuet-Higgins, 1952) repeated Faraday's experiment in 1883 and verified by a slightly different method the doubling of the period. Neither Faraday nor Rayleigh evaluated the second order terms involved in the analysis of standing waves. Miche (Longuet-Higgins, 1952) using a Lagrangian System of coordinates noticed the unattenuated terms and evaluated them. Longuet-Higgins (1950) expanded the standing wave theory where the second order terms do not vanish with depth and if the water area concerned is large they could cause microseisms on the continents. Theoretically then the period of ocean waves would be twice that of the microseisms.

I.4 Longuet-Higgins (ibid) suggests that interference of waves travelling in opposite directions may be necessary to cause the second order fluctuations. The opposite travelling groups of waves may occur in cyclones or by reflection of sea waves from a coast. The interference of these waves should set up a standing wave, where as shown by Miche, the second order fluctuations do not attenuate with depth

and are independent of the depth of the liquid body concerned. If the period of the seismic wave is  $T$  and its wavelength  $L$ , then the pressure applied on an area sufficiently small compared with  $L$  may be considered to have been applied at a point. The time difference involved in applying any pressure at another point of the area would be small compared with  $T$ . The seismic wavelength is very large compared with the length of a gravity wave (sea wave) of comparable period. Hence it is appropriate to consider the properties of the mean pressure over a large number of wavelengths in any gravity wave.

It can be easily shown that the pressure fluctuations in a progressive wave over a multiple of wavelengths is too insignificant to cause seismic waves in the sea bed. In a progressive wave the contributions to the disturbance from different parts of the sea bed tend to cancel one another out. A second reason why pressure fluctuations in a progressive wave are ineffectual in causing seismic oscillations on the sea bed is that not only the mean pressure but also the pressure difference decreases rapidly (exponentially) below a wavelength.

Now consider two progressive waves of equal wavelength and amplitude travelling in opposite directions. The mean pressure on the bottom between two nodal points vanishes to a first approximation. But the addition is not exact and the superposability is not exact as the equations

of motion are nonlinear. Consider the mass of water contained between the standing wave on the free surface, the sea bottom, the two anti-nodal planes and a unit length in a direction orthogonal to the direction of wave propagation. Since there is no flow of mass across the nodal planes, this mass consists always of the same particles; therefore the motion of center of gravity of this mass is that due to external forces alone which act upon it. Comparing the motion of water with that of a pendulum, it can be seen that when the pendulum passes through the center of oscillation the equivalent surface of the water is relatively flat and when the pendulum reaches the point of its maximum displacement, there will be a corresponding crest on the water surface. The center of gravity of the mass is higher when crests are formed than when it is relatively flat. The center of gravity is thus raised and lowered in one complete cycle. The external forces acting on this mass of water are 1) that due to gravity which is constant, 2) the atmospheric pressure  $P$  on the surface is constant or it gives a constant downward force of  $\lambda P_0$ , where  $\lambda$  is the wavelength, 3) the forces across the vertical planes which must have zero vertical components, the motion being symmetrical about these planes, 4) the force on the bottom which equals  $\lambda \bar{P}$ . Since all the forces other than  $\lambda \bar{P}$  are constant,  $\lambda \bar{P}$  must fluctuate with time. In other words  $\bar{P}$  must fluctuate with time. The mean pressure fluctuation is proportional to the square of the wave amplitude on the free surface.

If  $F$  is the force acting vertically,  $z$  is the vertical coordinate dependent on time,  $m$  is the mass of the water,

$$F = \frac{\Sigma m \frac{\partial^2 z}{\partial t^2}}{\partial t^2} = \frac{\partial^2}{\partial t^2} \Sigma mz$$

In an incompressible fluid

$$\Sigma mz = \rho \int_0^\lambda \frac{1}{2} \zeta^2 dx + \text{constant}$$

where  $\zeta$  is the vertical displacement of the free surface,  $x$  is the horizontal coordinate,  $\rho$  density and  $\lambda$  the wavelength. But the force  $F = \lambda (\bar{P} - P_0 - \rho gh)$ ,  $\bar{P}$  is the density,  $\bar{P}$  the mean pressure at the bottom,  $h$  is the mean depth of water,  $P_0$  pressure at the free surface.

The standing wave can be represented by

$$\zeta = a \cos kx \cos \sigma t$$

where  $a$  is the amplitude of the wave,  $k = 2\pi/\lambda$ ,  $\sigma = 2\pi/\tau$ , ( $\tau$ , being the period of the wave), higher order terms being omitted.

After simplification we find

$$(\bar{P} - P_0)/\rho - gh = -1/2 a^2 \sigma^2 \cos 2\sigma t$$

This shows that, to the second order, the mean pressure  $\bar{P}$  fluctuates sinusoidally with twice the frequency of the original wave, and with an amplitude proportional to the square of the wave amplitude. The pressure fluctuation is independent of depth, for a given frequency of the wave, though the frequency itself is dependent on the depth,



given by

$$\sigma^2 = gk \tanh(kh)$$

For two progressive waves we have

$$\frac{\bar{p}-P_0}{\rho} - gh = -2a_1 a_2 \sigma \cos 2\sigma t$$

For an incompressible liquid

$$\frac{\bar{p}-P_0}{\rho} - gh = -1/2 a^2 \sigma^2 \frac{\cos(2\sigma(z-h)/c')}{\cos(2\sigma h/c')} \cos 2\sigma t$$

very nearly, where  $c'$  is the velocity of sound in water.

For sea waves,

$$\zeta(x,y,t) = \operatorname{Re} \int_{-\infty}^{\infty} \int_{-\infty}^{\infty} A(u,v) e^{i(ukx+vky+\sigma t)} du dv$$

where  $x, y$  are the horizontal coordinates,  $k$  is a constant, and  $\sigma$  is  $\sigma(u,v)$ .

$$\sigma^2 = gk/(u^2 + v^2) \tanh kh/(u^2 + v^2)$$

$A(u,v)$  is in general complex and  $\operatorname{Re}$  denotes the real part.

Longuet-Higgins goes on to prove that mean pressure variation for a three dimensional case is

$$\frac{\bar{p}-P_0}{\rho} - 1/2 g \lambda_g = \frac{\partial^2}{\partial t^2} \frac{1}{4R^2} \int_{-\infty}^{\infty} \int_{-\infty}^{\infty} 1/2 \zeta'^2 dx dy$$

where

$$\zeta' = \operatorname{Re} \int_{-\infty}^{\infty} \int_{-\infty}^{\infty} A'(u,v) e^{i(ukx+vky+\sigma t)} du dv$$

where

$$A'(u,v) = \int_{-\infty}^{\infty} \int_{-\infty}^{\infty} A(u_1, v_1) \frac{\sin(u-u_1)\pi}{(u-u_1)\pi} \frac{\sin(v-v_1)\pi}{(v-v_1)\pi} e^{-i(\sigma-\sigma_1)t} du_1 dv_1$$

where  $\sigma_1 = \sigma(u,v)$ . In other words  $A'$  is the weighted average of values of  $A$  over neighbouring wavelengths and

directions. This is true of a square region S with side 2R, where  $k = \pi/R$ . R should be very large compared with the wavelengths associated with most energy in the spectrum.  $\zeta'$  also vanishes outside S. Further simplification results in

$$\frac{\bar{p} - p_0}{\rho} - 1/2g\lambda_g = -\text{Re} \int_{-\infty}^{\infty} \int_{-\infty}^{\infty} \sigma^2 A' A'_- e^{i2\sigma t} du dv$$

$A'_-$  stands for  $A'$  ( $-u, -v$ ), and is the amplitude of the wave component opposite to  $A$  ( $u, v$ ). This shows that 1) fluctuations in the mean pressure  $p$  arise only from opposite pairs of wave components in the spectrum; 2) that the contribution to  $\bar{p}$  from any opposite pair of wave components is twice their frequency and proportional to the product of their amplitudes; 3) and that the total pressure fluctuation is the integrated sum of the contributions from all opposite pairs of wave components, taken separately.

For a more rigorous treatment of the subject, the reader is referred to the original work of Longuet-Higgins.

I.5 It should be noted here that the earlier work on microseisms was mainly connected with the oscillations whose frequency was .25 to .125 hz or lower. It was not until later that the study of high frequency microseisms was feasible when proper instrumentation was made available. Earlier workers were also contented with temporal comparison of microseisms. An attempt was made first in Ottawa (Macelwane, 1952) during the conferences of the Eastern Section of the Seismological Society of America to correlate and map

microseisms in Canada and the U.S., but nothing seems to have come out of this study, at least no literature can be cited. It was in 1952 that a programme was initiated by the Association of Seismology of the International Geodetic and Geophysical Union to record simultaneously microseisms of the whole globe. Like its predecessor it did not seem to attract the attention of many workers or at least no work came to the notice of the present writer.

I.6 In addition to the temporal and spatial correlations of microseisms, attempts were made to determine the direction of approach of microseismic waves by assuming that microseisms are Rayleigh waves. Tromsdorff (Macelwane, 1952) and Ramirez (1940) independently, using the tripartite method, found that the bearings determined from arrival time differences across the array, pointed towards a low pressure area over the sea. Later attempts by the U. S. Naval Aerological Service under Gilmore (1946) in tracking cyclones by the Ramirez method did not prove too encouraging. Jensen (1958), on the assumption of a Rayleigh wave nature of microseisms, devised a vector method for determination of direction of approach. He mentions that at the moments at which the Z component is maximum, the slopes of the two horizontal records are read. The plot between these two slopes gives the velocity of the earth particle. The mean of several velocity vectors gives the direction of approach. Jensen (1958, 1959, 1961, 1965) using this method determined the direction of

approach at Copenhagen and at several places in Greenland. He found a strong correlation between the direction of approach and the bearings of an atmospheric low pressure area over the North Sea. Darbyshire (1954) using Lee's method of direction of approach arrived at results which agreed with meteorological charts. In Lee's method (1935) first the seismograms are corrected for instrument phase response and then the phases are read off the record for each component. Phase differences between each pair of the three components are then calculated. These phase differences are used to determine the nature of microseismic waves. Lee (ibid) concluded that all microseisms recorded at Kew Observatory were Rayleigh waves. On the other hand Darbyshire (op. cit.) showed that there were appreciable love waves present in the microseisms he studied. This was in accord with observations made by Leet (Lee, 1935). In Lee's case the measurements were very few. The phase response for each instrument was calculated at a few discrete periods and the correction was made in the time domain. This method is inferior to one in which the overall response of the instrument is computed and then matched to the measured calibration curve of the instrument. In none of the papers cited there is ever a mention of matching of the observed calibration curves against calculated values as is discussed later in this work. A more serious source of error lies in the measurement of the phases which are read directly from the traces. Darbyshire (op.cit.)

magnified the traces. Even with magnification inaccuracies are bound to result in these measurements.

The workers on the North American continent, however, did not find the determination of the direction of approach so simple. Tripartite stations were set up to determine the direction of approach. Considering that an equilateral triangle will come closest to giving the most accurate results, Dinger (1952) points out that the estimate of direction even in this case is  $\pm 11^\circ$ ; a spread of  $22^\circ$ . The waves often come from different directions resulting in a very low coherency. The wave trains differ not only in their direction of arrival but in period and wave type. Thus, as will be confirmed in this work, a simple straightforward method does not seem to yield any satisfactory results, though claims contrary to this do exist in literature.

I.7 The most intricate problem connected with microseisms seems to be the physical nature of these waves. That they are not purely Rayleigh waves is now established. In addition to the fundamental Rayleigh mode, the existence in microseisms of higher Rayleigh modes and also of different Love modes, has been reported by workers such as Gutenberg (1958), Ewing et al (1957, p 185 - 189). Phinney (1961), in a theoretical consideration, suggested possible existence of leaking P modes which could be propagated over long distances. Douze (1964) obtained results, using seismometers at different depths, which point out that noise in general consists

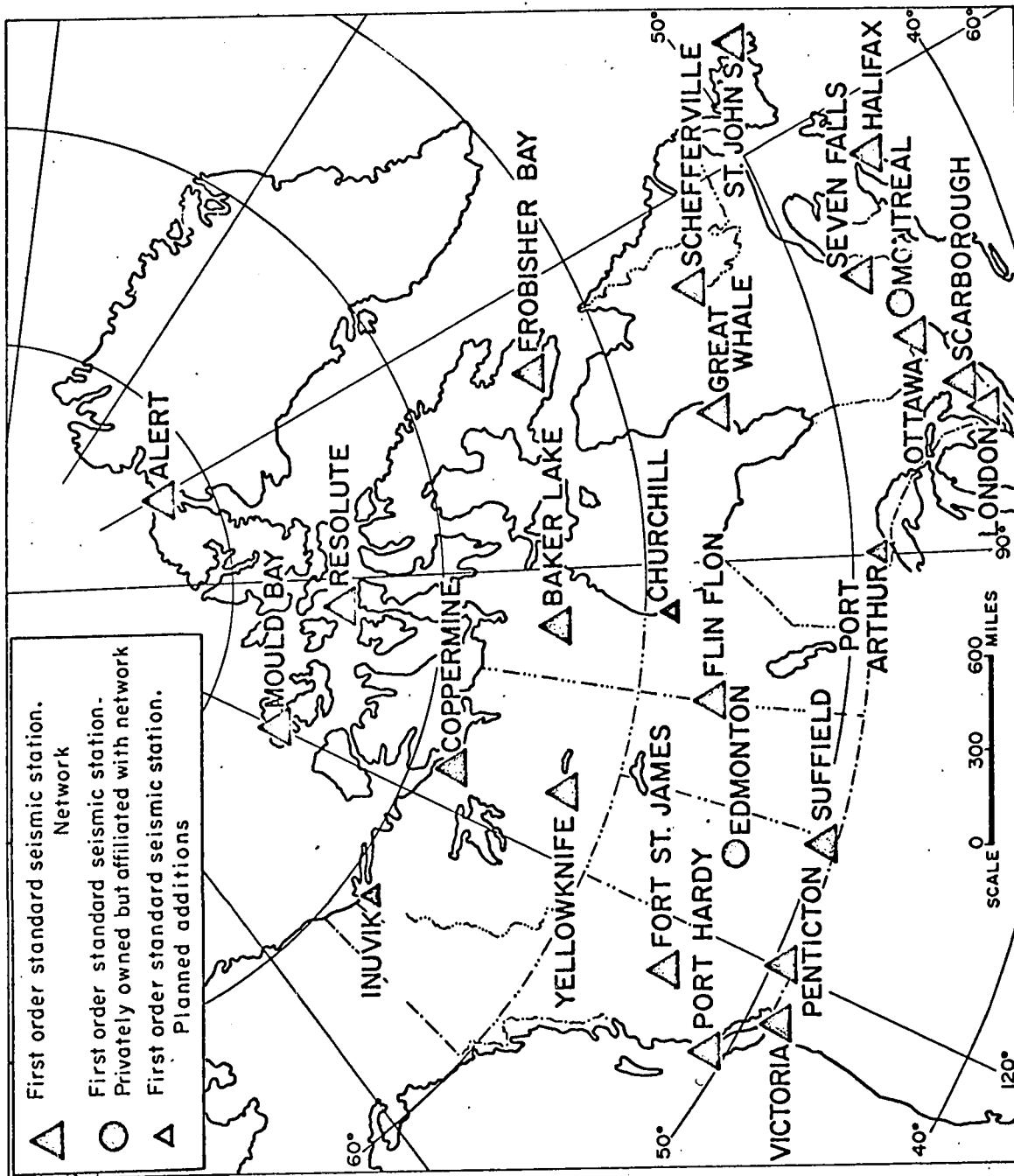
of an arbitrary combination of several Rayleigh modes. Several authors have discussed the possible existence of body waves in the short period microseisms, (Roden (1965), Seriff et al (1965), and Gupta (1965)). Douze (1967) states "Previous studies of short period seismic noise have often assumed that only surface waves are present in short period noise. However, the experimental results obtained to date cannot, in general, be explained in this fashion. The presence of random body wave noise must also be taken into consideration." Having examined the noise in the range 6.0 - 0.3 sec, Douze concludes that surface waves generally predominate at the longer periods (of the period range discussed), mostly 4 - 6 sec., while the body waves appear at shorter periods, mostly 0.3 - 2 sec., at quiet sites. He also states that not all the data could be interpreted to define the wave type present.

## CHAPTER II

### METHOD OF ANALYSIS

II.1 The aim of the present work is to compare the microseismic waves at different stations in Canada and try to identify the wave types present in the data. In other words more emphasis is placed on the mechanism of propagation of microseisms from station to station which are separated by large distances. There is an excellent network of seismograph stations in Canada (see Fig. II.1) and most of these have the facility for recording on three short period and on three long period instruments. A casual observation of these records shows existence of unmistakable microseisms on the records. Long period instruments especially show the sinusoidal type of motion with beat phenomenon superimposed on it. Winter months seem to be the time when microseismic activity is maximum with a peak activity in January (Basham and Whitham, 1966).

January 1965 records showed very good trains of these complex waves and records for January 1-5 were picked out at the Leduc observatory some 20 miles south of Edmonton. Preliminary work showed a good possibility for identification of Rayleigh and Love waves. It was then thought worthwhile to examine the records at some of the other operating stations for the same dates and times and to attempt a temporal and spatial correlation of these waves. The records for the same time were obtained from Victoria, Penticton, Resolute



STANDARD SEISMIC STATIONS IN CANADA

Fig. II. 1



and Ottawa stations. All of them showed good microseismic activity for the period mentioned. The next step then was to statistically analyse these records for which it was necessary to digitize the seismograms. The seismogram digitizer as developed by Wickens and Kollar (1967) at the Dominion Observatory, Ottawa was used for this work.

II.2 The general principle of the digitizer is that the seismogram is mounted on a drum, the same in physical dimensions as the recording drums used in the network stations, and the drum is driven by a motor; the trace is followed optically while the drum is rotating, and the transverse movement of the drum required to follow the fluctuations of the trace can be changed into equivalent voltages by a precise linear potentiometer; potentiometer measurements are then fed to a digital voltmeter; once a sample is held in the voltmeter it only remains to punch this in suitable format onto cards. For more details the reader is referred to the paper cited.

For the purpose of this work the voltage sensitivity was kept at .0325 volts/mm. The calibration was done before each day's work and an average figure was taken.

For the Edmonton records the total length of the record digitized was five minutes. Edmonton records are run twice as fast as those at other stations. The total length of record digitized at the other stations was twenty minutes.

There are twelve hundred samples in each case so that the digitizing interval for Edmonton records was one fourth that of other stations, the actual figures being 0.25 sec and 1.0 sec. Thus the nyquist frequency for Edmonton records is 2.0 hz and that for the records at other stations 0.5 hz. The shortest period estimate in these two cases are thus 0.5 sec and 2 sec, respectively.

II.3 Digitization, or sampling of data at discrete intervals places a restriction on the data. Statistical estimates of the data for frequencies above  $1/2 \Delta t$ , where  $\Delta t$  is the sampling rate, do not exist in a mathematical form. As a result, if such a frequency does exist in the data, and if we call it  $(1/2 \Delta t + \Delta)$ , then it will be folded down to  $(1/2 \Delta t - \Delta)$ , since  $\text{Cos}(\pi + \delta) = \text{Cos}(\pi - \delta)$ . This process is called aliasing. The frequency  $(1/2 \Delta t)$  is called the "folding" or nyquist frequency,  $f_N$ . The frequencies  $f$ ,  $2f_N - f$ ,  $2f_N + f$ ,  $4f_N - f$ ,  $4f_N + f$ , and so on are called the "aliases" of one another, and  $f$  is called the principal "alias". The "aliased spectrum"  $P_a(f)$  is the result of "aliasing"  $P(f)$ . The principal part of the aliased spectrum  $P_A(f)$  is the part of  $P_a(f)$  which corresponds to principal aliases, positive and negative. Thus the contributions to the power spectrum from frequencies greater than  $f_N$  cause problems of aliasing.

Aliasing is an unavoidable consequence of digitization. It seems desirable to evolve a workable scheme of

digitizing the data in some definite, but not at equally distributed intervals, and estimate the power spectrum without aliasing. No such scheme seems to have been developed so far.

Aliasing causes more serious problems with data like microseisms, where signal to noise ratio is low. Contributions to the power spectrum from high frequency noise present in microseisms because of aliasing poses an important and potential threat to the statistical analysis of the data. Identification of wave types may become difficult because of the presence of high frequency noise folded into the data band.

II.4 If one is looking for an event whose frequency is much lower than the folding frequency, one can safely assume that aliasing problems are not statistically important provided the sampling rate is sufficiently high so that negligible power is present in the original data above the folding frequency. Due to the frequency response of the instruments it is believed that this is not a serious problem for the present data. As mentioned in II.2 the lowest period estimate for Edmonton records is 0.5 sec and the same for other records is 2.0 sec. For the microseisms with a peak amplitudes at 6 sec and 4 sec, the statistical estimate for Edmonton records is more reliable than that for other stations because the folded power will be less serious a problem in this case. An example of the original trace from the seismogram as compared with that of the digitized

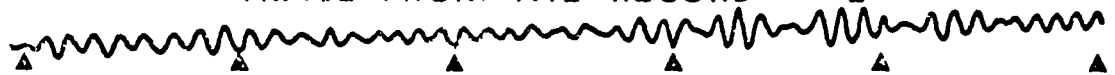
TRACE FROM THE RECORD - Z



TRACE FROM THE RECORD - N



TRACE FROM THE RECORD - E



(Minute marks as shown)

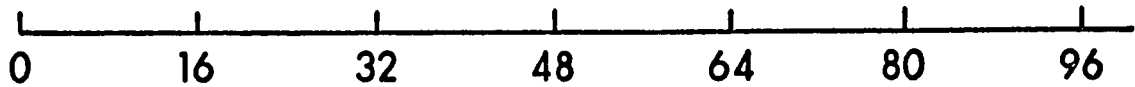
DIGITIZED TRACE Z



DIGITIZED TRACE N



DIGITIZED TRACE E



TIME IN SEC ( $\times 10^1$ )

Fig. II.2

trace is shown in figure II.2.

II.5 In order to identify the wave types it is useful to determine the cross correlation function for two given traces and also find the phase difference between the two. Before making this calculation it is necessary to determine the phases of the two instruments involved and make the necessary correction. After this phase correction is made, any calculation of phase difference between the two instruments becomes meaningful.

There are two ways of doing this phase correction. In the first method, one calculates the phases from the transfer function of the instrument for given periods and takes the phase value for a given instrument at the period one is interested in. In the case of microseisms it is around 6 sec. Then one reads the phases off the trace and makes the necessary correction depending on whether the instrument is leading or lagging. The disadvantages in this method are:

1. The trace that appears on the seismogram is not exactly a "6 sec" event. It is composed of various other frequencies. Assuming that this trace is purely of one given frequency is erroneous.
2. The method of determining the phase from the trace is crude and inaccurate.

In the second method one calculates the transfer function in the frequency domain. Let us call this  $H(\omega)$ .

Then one takes the Fourier transform of the digitized trace also in the frequency domain. Let us call this  $F(\omega)$ . The division of  $F(\omega)$  by  $H(\omega)$  in the frequency domain then gives the corrected frequency content of the signal. In this method phases at all frequencies are taken care of. The inverse Fourier transform of  $F(\omega)/H(\omega)$  thus puts the trace back into time domain with phase corrected. In the series  $F(\omega)$ , the first term is the d.c. level of the trace, a meaningless quantity in the present context. The next two terms correspond to periods 1024 sec and 512 sec for Victoria, Penticton, Resolute and Ottawa, and 256 sec and 128 sec for Edmonton. The effect of these long periods is removed by equating the Fourier coefficients for these frequencies to zero, since most of the power at these very long periods is due to instrumental drift.

II.6 It is now necessary to examine the transfer function for the galvanometer-seismometer system of the long period instruments used in recording the microseisms. The galvanometer is a low pass and the seismometer is a high pass device in terms of frequency. The velocity sensitivity for the seismometer can be easily shown to be

$$\frac{E(s)}{V(s)} = G (s/\omega_S)^2 \frac{1}{1 + 2\zeta_S (s/\omega_S) + (s/\omega_S)^2} \quad (1)$$

ASYMPTOTIC FORM OF THE TRANSFER FUNCTION  
OF SEISMOMETER AND GALVANOMETER

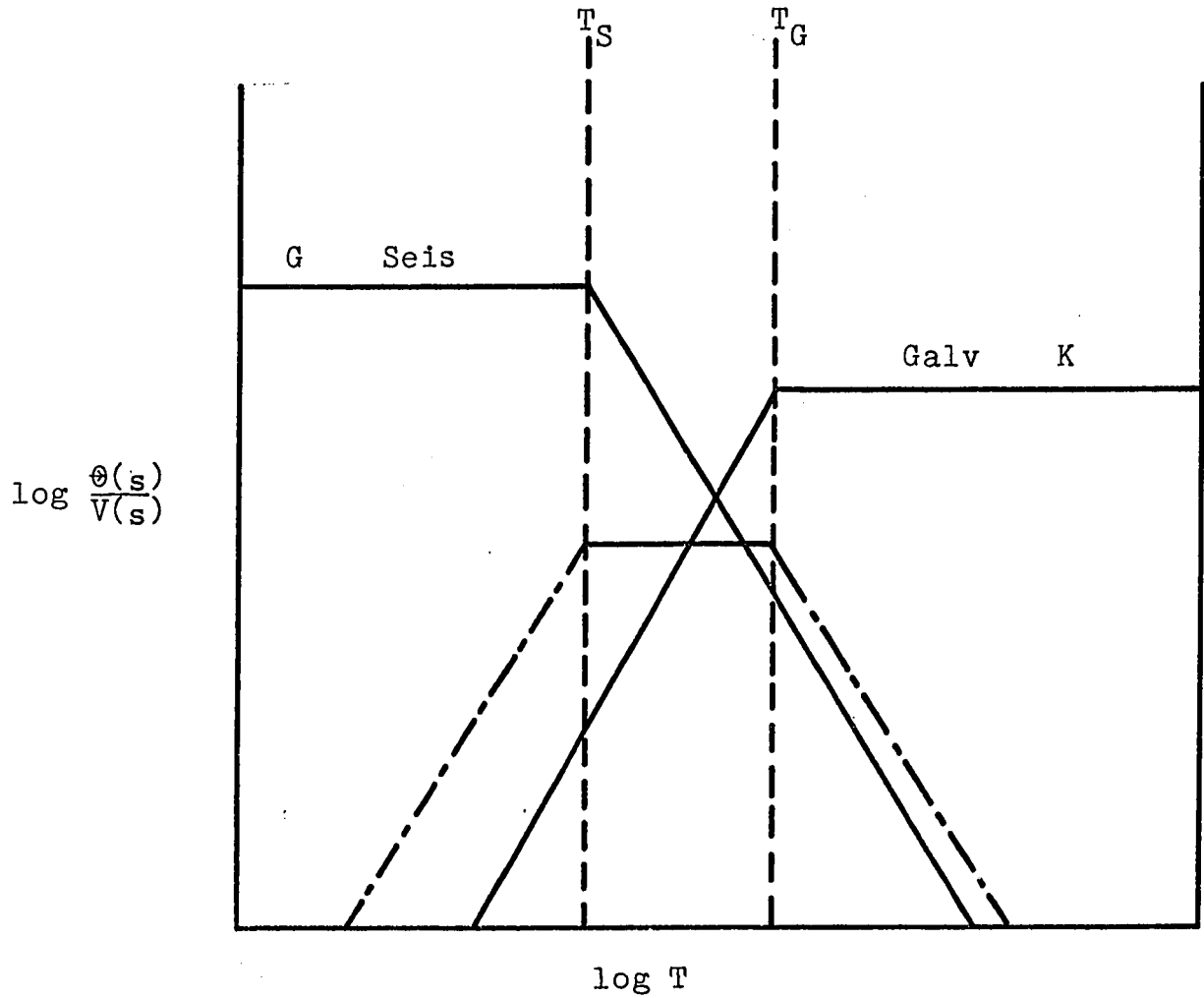


FIG II.3

$$\frac{\theta(s)}{V(s)} = G \left( \frac{s}{\omega_S} \right)^2 \frac{1}{1 + 2\zeta_S s/\omega_S + (s/\omega_S)^2} K \frac{1}{1 + 2\zeta_G s/\omega_G + (s/\omega_G)^2}$$

$$s = i\omega, \omega = 2\pi/T$$

and the velocity sensitivity for the galvanometer is

$$\frac{\Theta(s)}{E(s)} = K \frac{1}{1 + 2\zeta_G(s/\omega_G) + (s/\omega_G)^2} \quad (2)$$

where  $E(s)$  is the voltage developed in the coil,  $s=i\omega$ ,  $\omega$  being the frequency,  $\omega_S$  and  $\omega_G$  the natural frequencies of the seismometer and galvanometer,  $\zeta_S$  and  $\zeta_G$  are the damping coefficients for seismometer and galvanometer,  $\Theta(s)$  and  $V(s)$  are the velocity sensitivities for galvanometer and seismometer respectively. Multiplication of (1) by (2) gives  $\frac{\Theta(s)}{V(s)} = T_S(s) \times T_G(s)$ , where  $T_S(s)$  and  $T_G(s)$  are the transfer functions of seismometer and galvanometer respectively as given by (1) and (2), assuming negligible coupling between the two systems.

For the seismometer, since  $\omega = 2\pi/T$ , from (1)

- i) as  $T \rightarrow 0$ ,  $E(s)/V(s) \rightarrow G$ , a constant and the phase difference is  $0^\circ$ . Or
- ii) as  $T \rightarrow \infty$ ,  $\omega \rightarrow 0$  hence  $E(s)/V(s) \rightarrow -G(\omega/\omega_S)^2$  a line of slope 2 on a log-log plot ie. 12db/octave, and the phase difference is  $180^\circ$ .

Similar results hold for the galvanometer and these asymptotic values are shown in Figure II.3.



At the natural frequency of the seismometer  $\omega = \omega_s$

hence

$$\frac{E(s)}{V(s)} = \frac{iG}{2\zeta_s} \quad \text{so the phase is } 90^\circ$$

- i) If  $\zeta_s = 1$ ,  $\left| \frac{E(s)}{V(s)} \right| = \frac{G}{2}$  down 6db from maximum or  
 ii) using  $\zeta_s = \frac{1}{\sqrt{2}}$  the common condition for maximum linear frequency response, then  $\left| \frac{E(s)}{V(s)} \right| = \frac{G}{\sqrt{2}}$  down 3db from maximum.

II.7 The exact determination of the transfer function is not possible but can be achieved very closely by comparing the transfer function with the calibration curves measured routinely at the various observatories. Calibrated curves which give velocity sensitivity vs. period on log-log plot are available for each instrument at each station. A cursory look at the curves indicate that there is no appreciable phase difference between any two given instruments at a given station. A typical calibration is shown in Figure II.4. The curve in this figure was drawn approximately, by fitting a smooth curve through the measured points.

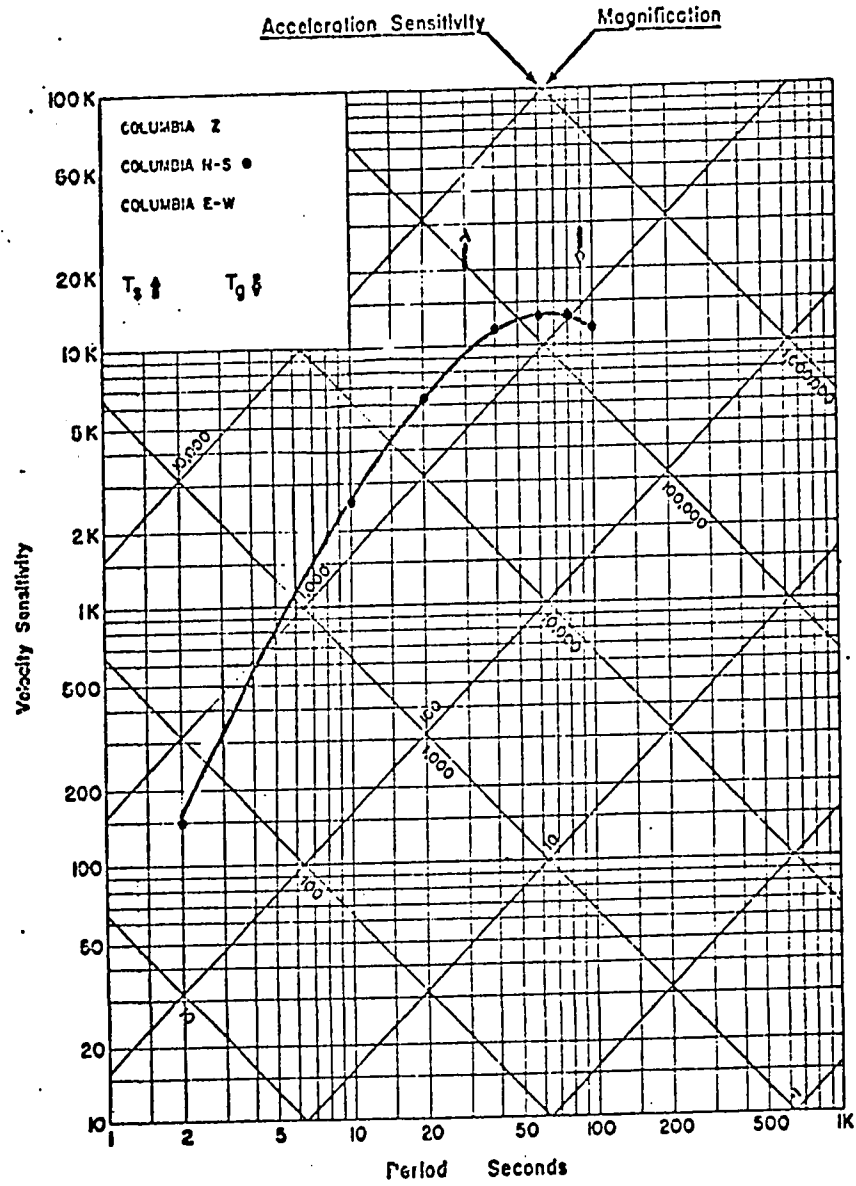
The transfer function as given in II.6 can be written as

$$\frac{\Theta(s)}{E(s)} = A \frac{s^2}{\omega_s^2} \frac{1}{1 + 2\zeta_s \frac{s}{\omega_s} + \frac{s^2}{\omega_s^2}} \frac{1}{1 + 2\zeta_G \frac{s}{\omega_G} + \frac{s^2}{\omega_G^2}}$$

STATION: OTTAWA

$\phi = 45^{\circ}23'38''N$      $\lambda = 75^{\circ}42'57''W$     Altitude 83M

Foundation: Boulder clay on limestone



Dates of Calibration:

COLUMBIA Z

COLUMBIA N-S • Feb. 7 - 1964

COLUMBIA E-W

Fig. II.4

The quantities  $\omega_S$ ,  $\omega_G$  natural frequencies of seismometer and galvanometer are known.  $s=i\omega$ , ( $\omega=2\pi/T$ ) can be changed at regular intervals to give  $\frac{\theta(s)}{E(s)}$  as a function of  $s$ .  $\zeta_S$  and  $\zeta_G$  the damping coefficients of seismometer and galvanometer can be varied to give a family of curves of  $\theta(s)/E(s)$  as a function of  $s$ . For each  $\zeta_S$  and  $\zeta_G$  there will be one such curve. We have the measured velocity sensitivity at a series of frequencies from the observatories. These are then matched with the family of curves obtained as above. The closest matched curve as illustrated in Figure II.5 is considered as the velocity sensitivity response to period and the damping coefficients may be noted for this curve. In table II.1 are enumerated these damping coefficients for all stations as determined from matching of the observed curve with the calculated curve. Matching does not necessarily mean matching at all frequencies. The discussion of the transfer function for seismometer and galvanometer indicates that matching has to be done only in the region between  $T_S$  and  $T_G$  where  $T_S$  and  $T_G$  are the natural periods of the seismometer and galvanometer respectively. Once the portion of the curve between the two points is closely matched, the gain factor  $A$  is computed from the calibration curve. Table II.2 gives these gain factors. Figure II.6 shows a comparison between the digitized traces and the phase corrected traces. Note that there is a change in amplitude between the sets of traces due to normalization

RESPONSE OF THE SEISMOMETER-GALVANOMETER SYSTEM  
AT OTTAWA

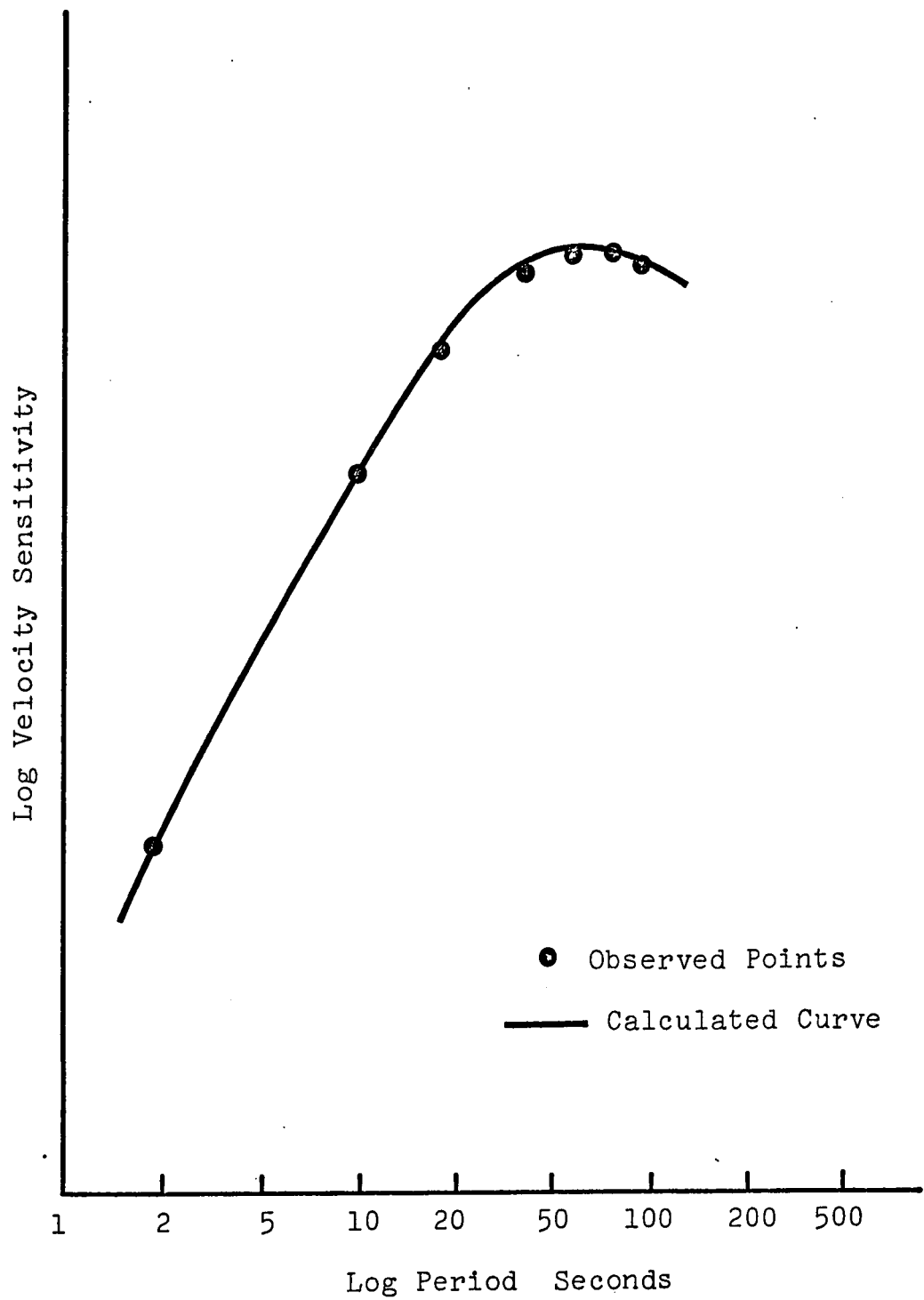


FIG II.5

## DAMPING COEFFICIENTS

TABLE II.1

	VERTICAL		NORTH-SOUTH		EAST-WEST	
	Seis	Galv	Seis	Galv	Seis	Galv
Victoria	1.4	0.35	1.4	0.35	1.4	0.35
Penticton	1.4	0.35	1.4	0.35	1.4	0.35
Edmonton	0.5	0.7	0.5	0.7	0.5	0.7
Resolute	0.9	.35	0.7	0.7	0.9	0.35
Ottawa	0.7	0.7	0.7	0.7	0.7	0.7

## MAGNIFICATION FACTORS

TABLE II.2

	VERTICAL	NORTH-SOUTH	EAST-WEST
Victoria	344	480	324
Penticton	275	205	180
Edmonton	390	384	372
Ottawa	1000	1200	1400
Resolute	3000	1000	3037

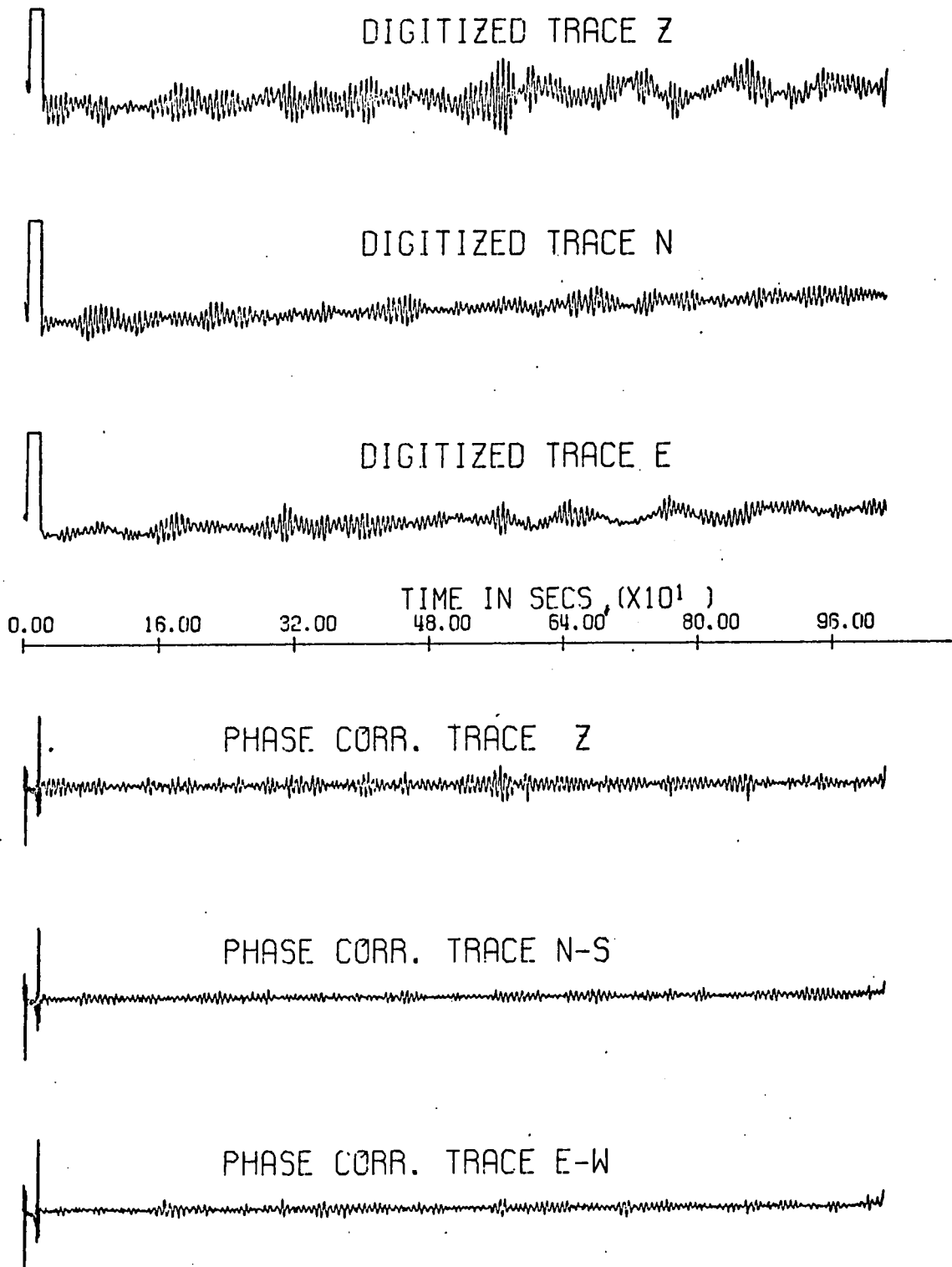


Fig. II.6

TIMES FOR THE DATA AT VICTORIA

TABLE II.3

(All times in GMT)

Record	Date	Digitized Time (hrs)	Digitizing Interval	Length of the record	Record # on Too413	Record # Too472	Remarks
1	Jan. 1	2141-2201	1 second	20 minutes	1	1	Not analysed
2	Jan. 2	0341-0401			2	2	"
3		0941-1001			3	3	
4		1538-1558			4	4	
5		2049-2109			5	5	
6	Jan. 3	0245-0305			6	6	
7		0845-0905			7	7	
8		1445-1505			8	8	
9		2139-2159			9	9	
10	Jan. 4	0337-0357			10	10	
11		0939-0959			11	11	
12		1539-1559			12	12	
13		1939-1959			13	13	
14	Jan. 5	0139-0159			14	14	
15		0739-0759			15	15	
16		1339-1359			16	16	

Total number of digital points at Victoria  
14 x 3 x 1024  
= 43,008

TIMES FOR THE DATA AT PENTICTON

TABLE II.4

Record	Date	Digitized Time (hrs)	Digitizing Interval	Length of the record	Record# on Too413	Record# on Too472	Remarks
1	Jan. 1	1945-2005	1 second	20 minutes	17	17	not analysed
2	Jan. 2	0145-0205			18	18	
3		0745-0805			19	19	Total number of
4		1345-1405			20	20	digital points
5		1945-2005			21	21	at Penticton
6	Jan. 3	0145-0205			22	22	7 x 3 x 1024
7		0745-0805			23	23	= 21,504
8		1345-1405			24	24	



TABLE II.5

## TIMES FOR THE DATA AT EDMONTON

(All times in GMT)

Record	Date	Digitized time (hrs)	Digitizing Interval	Length of the record	Record# on T00802	Record# on T00472	Remarks
1	Jan. 1	1927-1932	0.25 seconds	5 minutes	1	25	
2		2156-2159			2	26	
3	Jan. 2	0001-0005			3	27	
4		0201-0206			4	28	
5		0551-0556			5	29	
6		0644-0649			6	30	
7		1038-1043			7	31	
8		1232-1237			8	32	
9		1454-1459			9	33	
10		1656-1659			10	34	
11		1754-1759			11	35	Total number of
12		1935-1940			13	37	digital points at
13		2217-2222			14	38	Edmonton
14		2332-2337			15	39	119,808
15	Jan. 3	0348-0353			16	40	
16		0434-0439			17	41	
17		0648-0653			18	42	
18		0832-0837			19	43	
19		1047-1052			20	44	
20		1312-1317			21	45	
21		1508-1513			22	46	
22		1643-1648			23	47	
23		1806-1811					Not on tape
24	Jan. 4	1239-1244			24	48	
25		1339-1344			12	36	
26		1439-1444			37	61	
27		1539-1544			38	62	

TABLE II.5 (Cont'd)

TIMES FOR THE DATA AT EDMONTON

(All times in GMT)

Record	Date	Digitized time (hrs)	Digitizing Interval	Length of the record	Record # on T00802	Record # on T00472	Remarks
28		1639-1644			39	63	
29		1754-1759			25	49	
30		1954-1959			26	50	
31		2154-2159			27	51	
32		2354-2359			28	52	
33	Jan. 5	0154-0159			29	53	
34		0357-0402			30	54	
35		0554-0559			31	55	
36		0754-0759			32	56	
37		0957-1002			33	57	
38		1154-1159			34	58	
39		1354-1359			35	59	
40		1554-1559			36	60	
41		1754-1759					not on tape

TIMES FOR THE DATA AT RESOLUTE (All times in GMT)

TABLE II.6

Record	Date	Digitized Time (hrs)	Digitizing Interval	Length of the record	Record# on Too802	Record# Too472	Remarks
1	Jan. 1	2139-2159	1 second	20 minutes	48	72	Total number of digital points at Resolute 39,936
2	Jan. 2	0338-0358			49	73	
3		0938-0958			50	74	
4		1538-1558			51	75	
5		2138-2158			52	76	
6	Jan. 3	0338-0358			53	77	
7		0938-0958			54	78	
8		1538-1558			55	79	
9		2138-2158			56	80	
10	Jan. 4	0338-0358			57	81	
11		0938-0958			58	82	
12		1538-1558			59	83	
13		2138-2158			60	84	

TIMES FOR THE DATA AT OTTAWA (All times in GMT)

TABLE II.7

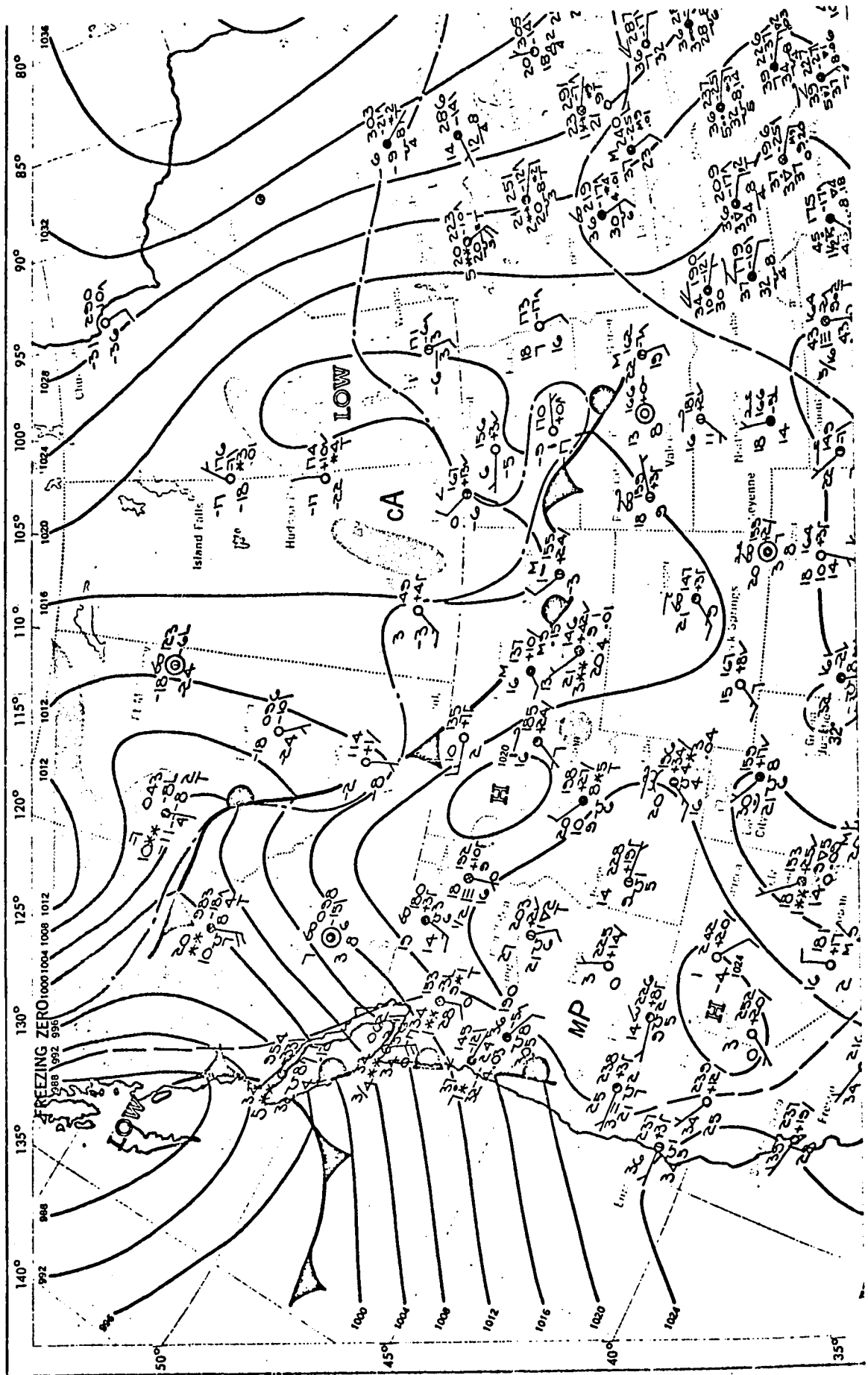
Record	Date	Digitized Time(hrs)	Digitizing Interval	Length of the record	Record# on Too802	Record# on Too472	Remarks
1	Jan. 1	2239-2259	1 second	20 minutes	40	64	
2	Jan. 2	0439-0459			41	65	Total number of
3		0939-0959			42	66	digital points
4		1739-1759			43	67	at Ottawa
5		2239-2259			44	68	24,576
6	Jan. 3	0539-0559			45	69	
7		2257-2311			46	70	
8	Jan. 4	0439-0459			47	71	

and that the very long period components have been removed as mentioned previously.

II.9 The information available for the present study lies in the digitized results for the three components Vertical, North-South and East-West at the recording sites of Victoria, Penticton, Edmonton, Resolute and Ottawa. The dates on which the data were taken are January 1, through 5 of 1965 when there was an atmospheric low pressure area on the Pacific Ocean, as shown in figure II.7.

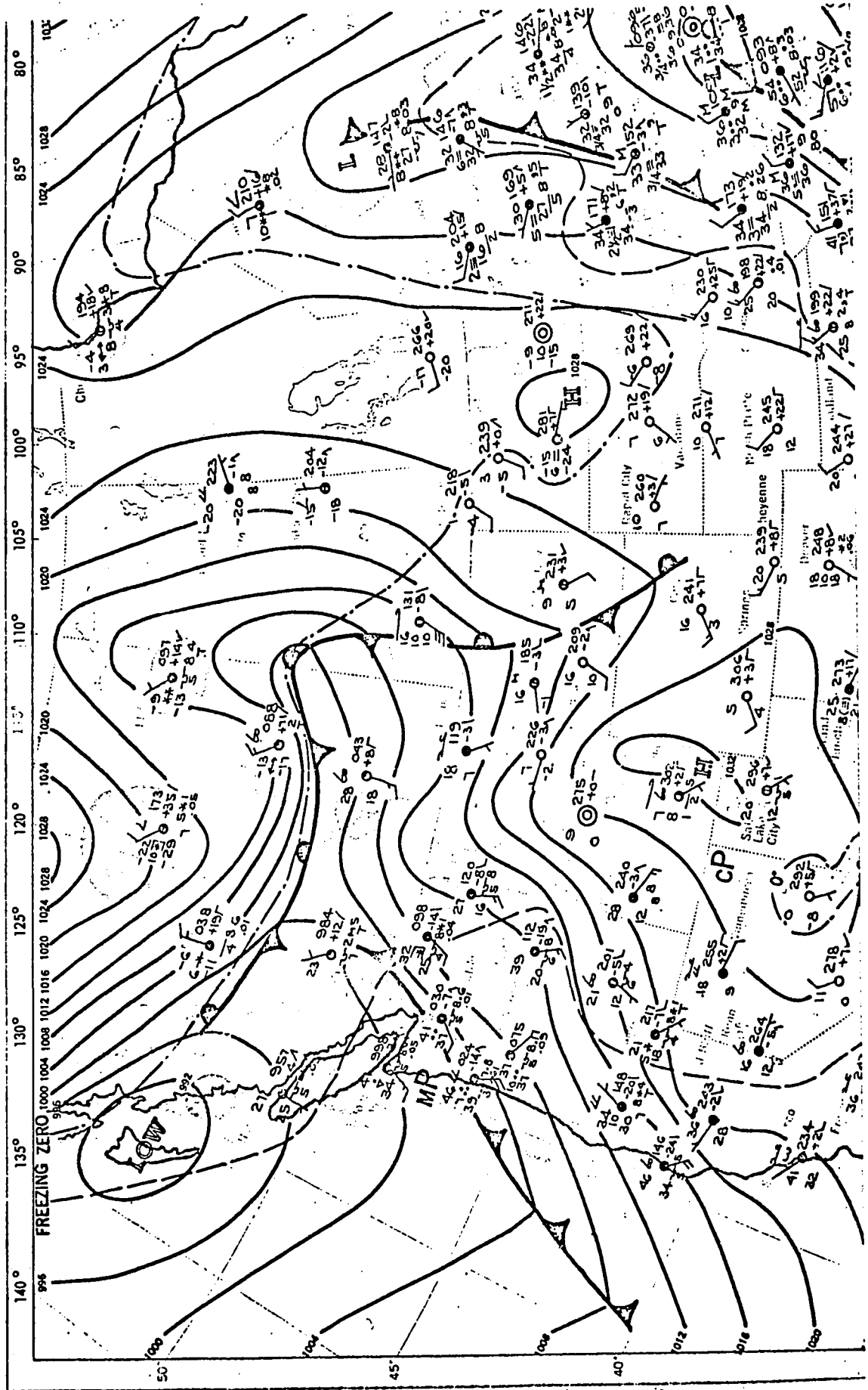
Tables II.3-7 give the starting time of digitization, the number of "records" digitized, the length of each "record" and the interval time between the records. From these tables it can be seen that there are 16 records for Victoria, 8 for Penticton, 39 for Edmonton, 13 for Resolute and 8 for Ottawa. Two records for Victoria and one for Penticton could not be analyzed as alpha-characters were punched on the cards instead of numbers in the process of digitization. All the data was stored on tape and the tape was subsequently used for the whole analysis.

The center of the storm did not remain stationary during the time January 1-5. The atmospheric low pressure area on the Pacific Ocean changed its position from day to day. From the known coordinates of the storm centre and the recording sites, distances between each site and each location of atmospheric low pressure area and the bearings from one to the other were calculated. These distances and bear-



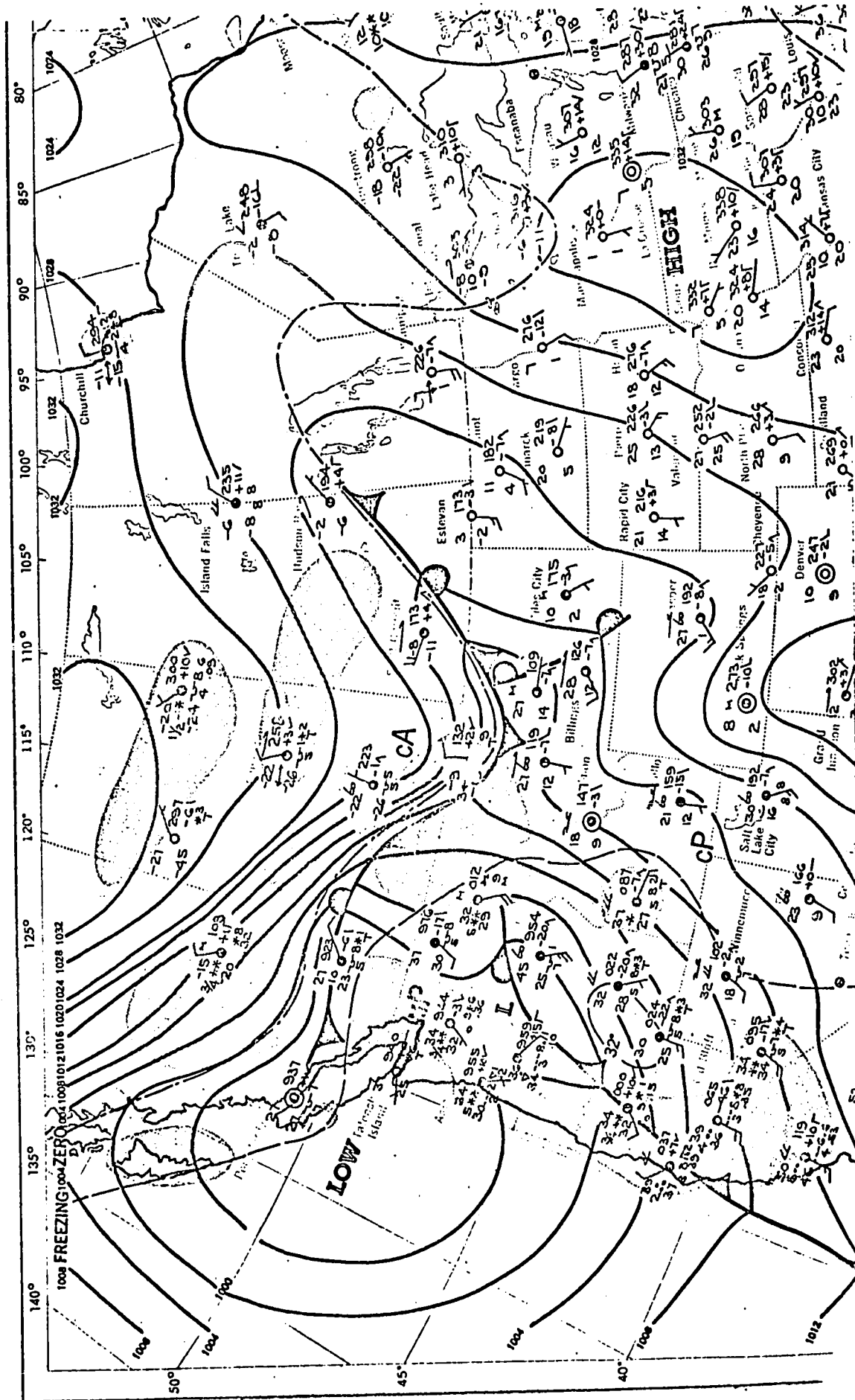
SURFACE WEATHER MAP AT 1:00 A.M., E.S.T., JANUARY 1, 1965

Fig. II.7.a



SURFACE WEATHER MAP AT 1:00 A.M., E.S.T., JANUARY 2, 1965

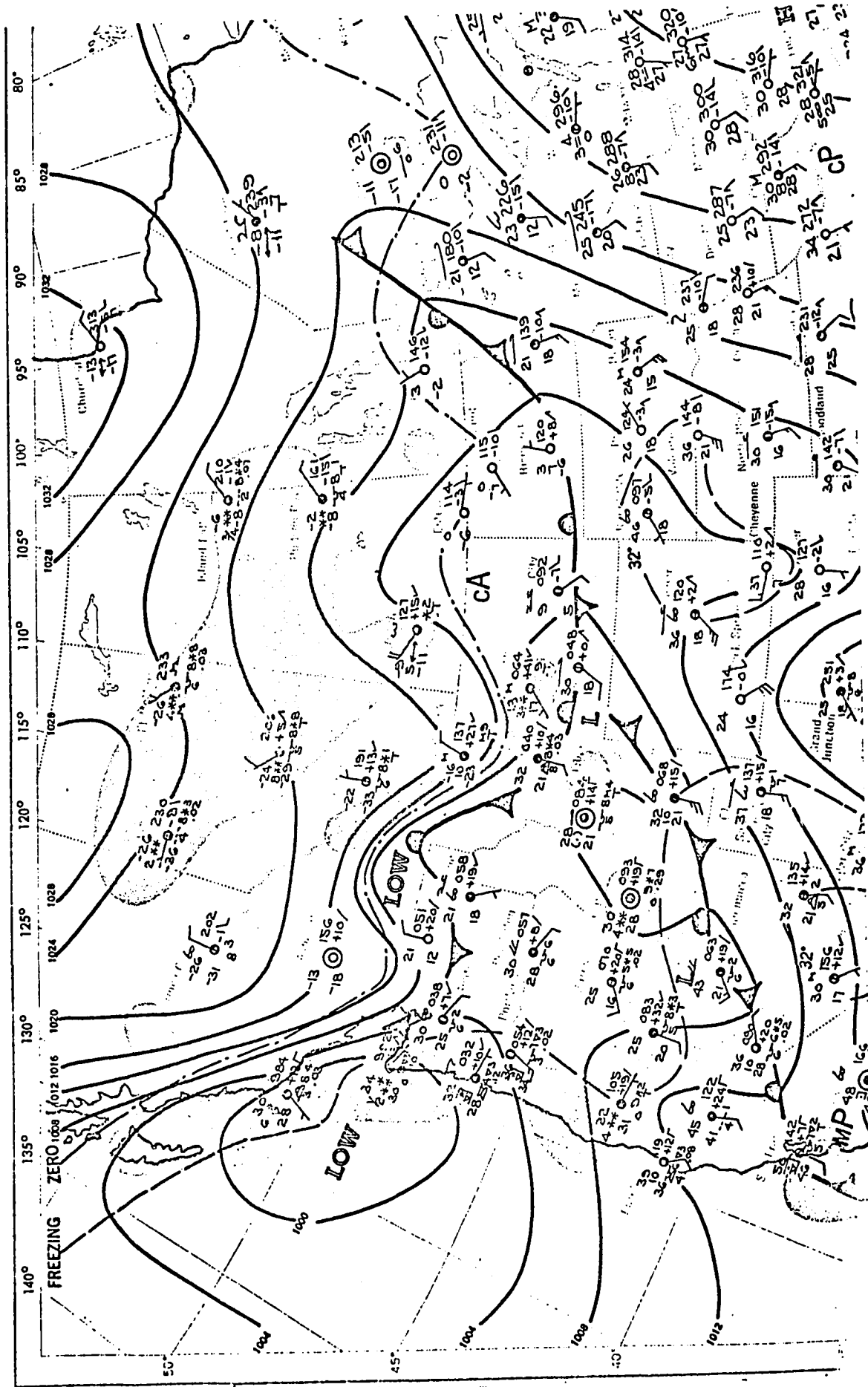
Fig. II.7.b

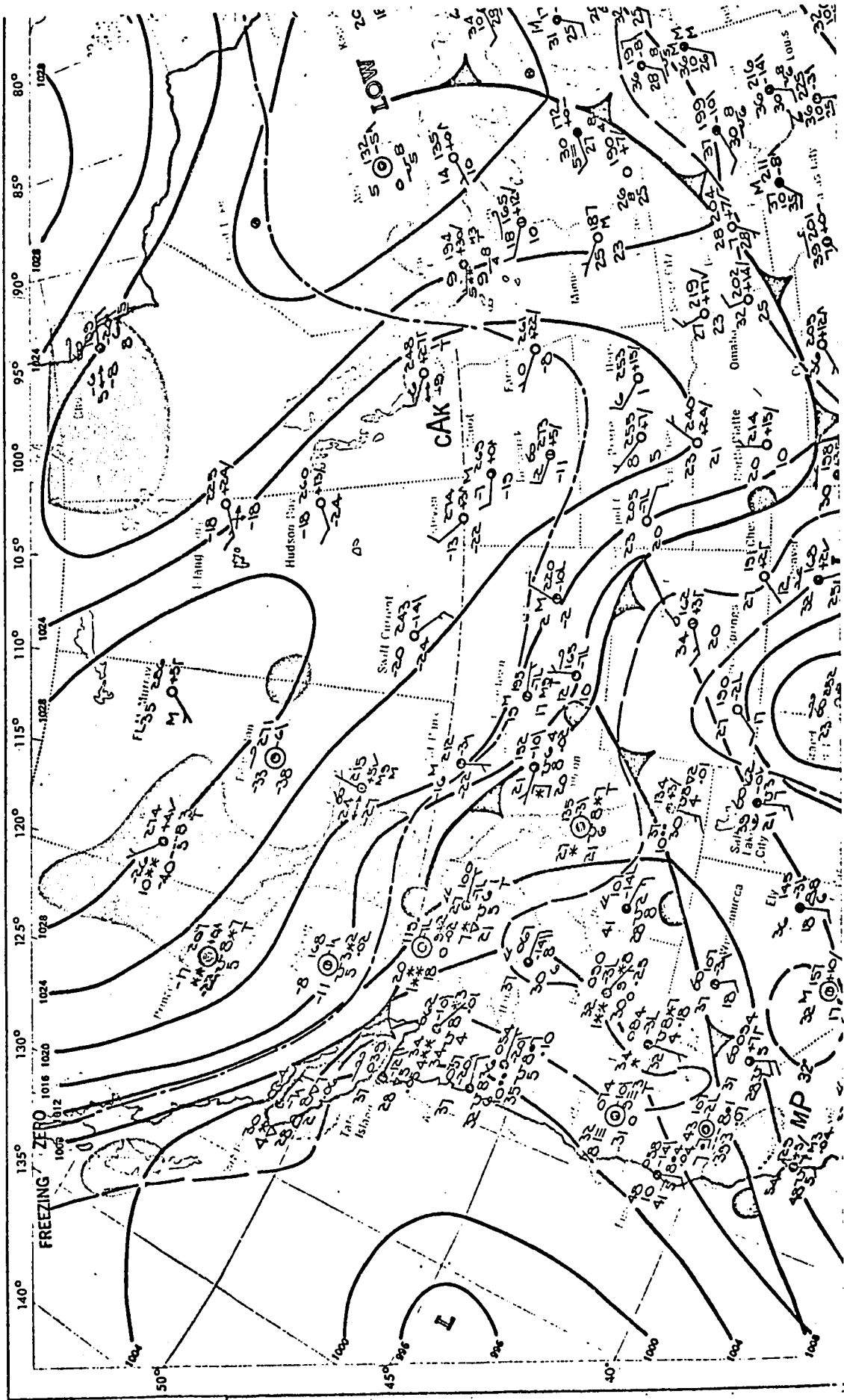


SURFACE WEATHER MAP AT 1:00 A.M., E.S.T., JANUARY 3, 1965

Fig. II.7.c







SURFACE WEATHER MAP AT 1:00 A.M., E.S.T., JANUARY 5, 1965

Fig. II.7.e

ings are shown in Tables II.8a-83.

II.8 Calculation of the autopower spectrum of a stationary time series has been dealt with by Weiner (1964), Blackman and Tukey (1958), and Lee (1964) among others. The methods have been standardized and used by geophysics researchers as routine procedures. A discussion of these methods is avoided in this work because of the availability of more exhaustive treatments elsewhere. Suffice it to say that Fourier analysis technique is exploited to obtain the power of the series. The Fourier transform of the series is first calculated, a filtering or smoothing if necessary is done in the frequency domain, correlation techniques are performed in the lag domain and finally inverse Fourier transform of the series gives the power as calculated at discrete values of period or frequency. The basic assumption is that stationary time series is composed of a large number of sinusoidal waves varying in frequency. The Fourier analysis of the data calculates the power at all those frequencies present in the data which are below the nyquist frequency. The peaks in the power spectrum correspond to the "signal" otherwise obscured by noise in the time series. The same techniques can be used for two series to obtain the power between them. In one case the power is called "autopower" of the series and in the second case it is called "crosspower" between the two series. Crosspower calculation also has an option whereby phases and coherencies between two given series are cal-

TABLE II.8a

DISTANCES BETWEEN THE STORM CENTRES AND THE STATIONS				
	53.00000	13.30000	113.00000	21.00000 EDMONTON
	54.00000	50.00000	134.00000	30.00000PACIFIC CENTRE
<hr/>				
FORWARD AZIMUTH	4.990RADIAN		1392.189KILOMETERS	
BACKWARD AZIMUTH	1.548RADIAN		1392.189KILOMETERS	
	53.00000	13.30000	113.00000	21.00000 EDMONTON
	53.00000	0.0	132.00000	30.00000PACIFIC CENTRE
<hr/>				
FORWARD AZIMUTH	4.827RADIAN		1278.831KILOMETERS	
BACKWARD AZIMUTH	1.418RADIAN		1278.831KILOMETERS	
	53.00000	13.30000	113.00000	21.00000 EDMONTON
	47.00000	30.00000	127.00000	30.00000PACIFIC CENTRE
<hr/>				
FORWARD AZIMUTH	4.247RADIAN		1188.008KILOMETERS	
BACKWARD AZIMUTH	0.914RADIAN		1188.008KILOMETERS	
	53.00000	13.30000	113.00000	21.00000 EDMONTON
	47.00000	30.00000	127.00000	30.00000PACIFIC CENTRE
<hr/>				
FORWARD AZIMUTH	4.247RADIAN		1188.008KILOMETERS	
BACKWARD AZIMUTH	0.914RADIAN		1188.008KILOMETERS	
	53.00000	13.30000	113.00000	21.00000 EDMONTON
	44.00000	0.0	132.00000	30.00000PACIFIC CENTRE
<hr/>				
FORWARD AZIMUTH	4.216RADIAN		1736.191KILOMETERS	
BACKWARD AZIMUTH	0.821RADIAN		1736.191KILOMETERS	

TABLE II.8b

DISTANCES BETWEEN THE STORM CENTRES AND THE STATIONS  
 74.00000 41.20000 94.00000 54.00000 RESOLUTE  
 54.00000 50.00000 134.00000 30.00000PACIFIC CENTRE

FORWARD AZIMUTH 4.189RADIANS 2798.212KILOMETERS  
 BACKWARD AZIMUTH 0.409RADIANS 2798.212KILOMETERS  
 74.00000 41.20000 94.00000 54.00000 RESOLUTE  
 53.00000 0.0 132.00000 30.00000PACIFIC CENTRE

FORWARD AZIMUTH 4.117RADIANS 2936.937KILOMETERS  
 BACKWARD AZIMUTH 0.372RADIANS 2936.937KILOMETERS  
 74.00000 41.20000 94.00000 54.00000 RESOLUTE  
 47.00000 30.00000 127.00000 30.00000PACIFIC CENTRE

FORWARD AZIMUTH 3.941RADIANS 3402.179KILOMETERS  
 BACKWARD AZIMUTH 0.285RADIANS 3402.181KILOMETERS  
 74.00000 41.20000 94.00000 54.00000 RESOLUTE  
 47.00000 30.00000 127.00000 30.00000PACIFIC CENTRE

FORWARD AZIMUTH 3.941RADIANS 3402.179KILOMETERS  
 BACKWARD AZIMUTH 0.285RADIANS 3402.181KILOMETERS  
 74.00000 41.20000 94.00000 54.00000 RESOLUTE  
 44.00000 0.0 132.00000 30.00000PACIFIC CENTRE

FORWARD AZIMUTH 4.018RADIANS 3884.979KILOMETERS  
 BACKWARD AZIMUTH 0.286RADIANS 3884.984KILOMETERS

TABLE II.8c

DISTANCES BETWEEN THE STORM CENTRES AND THE STATIONS			
49.00000	19.00000	119.00000	37.00000 PENTICTON
54.00000	50.00000	134.00000	30.00000PACIFIC CENTRE
<hr/>			
FORWARD AZIMUTH	5.354RADIAN	1187.329	KILOMETERS
BACKWARD AZIMUTH	2.007RADIAN	1187.329	KILOMETERS
49.00000	19.00000	119.00000	37.00000 PENTICTON
53.00000	0.0	132.00000	30.00000PACIFIC CENTRE
<hr/>			
FORWARD AZIMUTH	5.225RADIAN	988.259	KILOMETERS
BACKWARD AZIMUTH	1.909RADIAN	988.259	KILOMETERS
49.00000	19.00000	119.00000	37.00000 PENTICTON
47.00000	30.00000	127.00000	30.00000PACIFIC CENTRE
<hr/>			
FORWARD AZIMUTH	4.431RADIAN	617.273	KILOMETERS
BACKWARD AZIMUTH	1.187RADIAN	617.273	KILOMETERS
49.00000	19.00000	119.00000	37.00000 PENTICTON
47.00000	30.00000	127.00000	30.00000PACIFIC CENTRE
<hr/>			
FORWARD AZIMUTH	4.431RADIAN	617.272	KILOMETERS
BACKWARD AZIMUTH	1.187RADIAN	617.273	KILOMETERS
49.00000	19.00000	119.00000	37.00000 PENTICTON
44.00000	0.0	132.00000	30.00000PACIFIC CENTRE
<hr/>			
FORWARD AZIMUTH	4.256RADIAN	1147.389	KILOMETERS
BACKWARD AZIMUTH	0.951RADIAN	1147.389	KILOMETERS

TABLE II.8d

DISTANCES BETWEEN THE STORM CENTRES AND THE STATIONS				
45.00000	23.66000	75.00000	57.95000	OTTAWA
54.00000	50.00000	134.00000	30.00000	PACIFIC CENTRE
<hr/>				
FORWARD AZIMUTH	5.344RADIANS	4184.328	KILOMETERS	
BACKWARD AZIMUTH	1.388RADIANS	4184.325	KILOMETERS	
45.00000	23.66000	75.00000	57.95000	OTTAWA
53.00000	0.0	132.00000	30.00000	PACIFIC CENTRE
<hr/>				
FORWARD AZIMUTH	5.286RADIANS	4094.273	KILOMETERS	
BACKWARD AZIMUTH	1.369RADIANS	4094.271	KILOMETERS	
45.00000	23.66000	75.00000	57.95000	OTTAWA
47.00000	30.00000	127.00000	30.00000	PACIFIC CENTRE
<hr/>				
FORWARD AZIMUTH	5.104RADIANS	3893.404	KILOMETERS	
BACKWARD AZIMUTH	1.289RADIANS	3893.403	KILOMETERS	
45.00000	23.66000	75.00000	57.95000	OTTAWA
47.00000	30.00000	127.00000	30.00000	PACIFIC CENTRE
<hr/>				
FORWARD AZIMUTH	5.104RADIANS	3893.404	KILOMETERS	
BACKWARD AZIMUTH	1.289RADIANS	3893.403	KILOMETERS	
45.00000	23.66000	75.00000	57.95000	OTTAWA
44.00000	0.0	132.00000	30.00000	PACIFIC CENTRE
<hr/>				
FORWARD AZIMUTH	5.042RADIANS	4389.326	KILOMETERS	
BACKWARD AZIMUTH	1.177RADIANS	4389.326	KILOMETERS	

TABLE II.8e

DISTANCES BETWEEN THE STORM CENTRES AND THE STATIONS			
48.00000	31.18000	123.00000	24.91000 VICTORIA
54.00000	50.00000	134.00000	30.00000PACIFIC CENTRE
<hr/>			
FORWARD AZIMUTH	5.5289RADIANS	1037.706	KILOMETERS
BACKWARD AZIMUTH	2.235RADIANS	1037.706	KILOMETERS
48.00000	31.18000	123.00000	24.91000 VICTORIA
53.00000	0.0	132.00000	30.00000PACIFIC CENTRE
<hr/>			
FORWARD AZIMUTH	5.434RADIANS	810.973	KILOMETERS
BACKWARD AZIMUTH	2.169RADIANS	810.973	KILOMETERS
48.00000	31.18000	123.00000	24.91000 VICTORIA
47.00000	30.00000	127.00000	30.00000PACIFIC CENTRE
<hr/>			
FORWARD AZIMUTH	4.383RADIANS	325.137	KILOMETERS
BACKWARD AZIMUTH	1.188RADIANS	325.137	KILOMETERS
48.00000	31.18000	123.00000	24.91000 VICTORIA
47.00000	30.00000	127.00000	30.00000PACIFIC CENTRE
<hr/>			
FORWARD AZIMUTH	4.383RADIANS	325.137	KILOMETERS
BACKWARD AZIMUTH	1.188RADIANS	325.137	KILOMETERS
48.00000	31.18000	123.00000	24.91000 VICTORIA
44.00000	0.0	132.00000	30.00000PACIFIC CENTRE
<hr/>			
FORWARD AZIMUTH	4.149RADIANS	861.053	KILOMETERS
BACKWARD AZIMUTH	0.892RADIANS	861.053	KILOMETERS



culated. Crosspower is more effectively used in detecting a signal common to both series. Thus it is helpful in detecting any kind of phenomenon which is recorded on two instruments simultaneously.

II.10 Microseisms can be assumed to be stationary in time if the record is long compared with the period of the event concerned. Inherent in the assumption is the point that it is possible to predict the statistical behaviour of the time series at a time  $T$ , if its behaviour is known at some earlier time. The general procedure adopted by the workers in the field has been directed

- 1) to identify the wave type.
- 2) to determine the direction of approach of microseisms.
- 3) to find the effect of the geological features on their propagation.
- 4) to investigate the possibility of tracking down the storms on the ocean.

The present work deals mainly with the mechanism of propagation of microseisms over a continent and an attempt at the identification of different wave types present in microseisms. An attempt is also made to determine the direction of approach. Since the data is available on three components at each station at different times, the crosspower analysis between vertical and horizontal components would yield information on the presence or otherwise of Rayleigh wave, and that between two horizontals would give the same information about Love waves.

## CHAPTER III

### POWER SPECTRA OF MICROSEISMS

III.I Autopower spectrum was calculated for a total number of seventy-nine records, thirteen of which were taken from Victoria, seven from Penticton, thirty-nine from Edmonton, eight from Ottawa and twelve from Resolute. In each record there are three traces, viz. one vertical and two horizontal components. Three sets of crosspower were also calculated along with the coherencies and phases, one between vertical and east-west components, a second between vertical and north-south components and a third between the two horizontal components, east-west and north-south. Figure III.1 is a sample of autopower spectrum as a function of period. In Fig. III.1a the autopower spectrum for Edmonton is shown and in Fig. III.1b the same is shown for Victoria.

At Edmonton three peaks on the vertical component at 2.3 sec, 3.3 sec and 8.0 sec and two on the east-west and north-south components at 2.5 sec and 6.4 sec can be observed. The long period event does not peak either at 8.0 sec or at 6.4 sec on all records; the period varies from record to record, the range of variation being 5.5-8.0 sec. Similarly the 3.3 sec event varies in time, variation being 3.3-4.9 sec. On some records these two peaks vanish but a new peak at 5.2 sec is clearly shown, The short period event is always present,

AUTO-POWER SPECTRUM OF MICROSEISMS AT EDMONTON

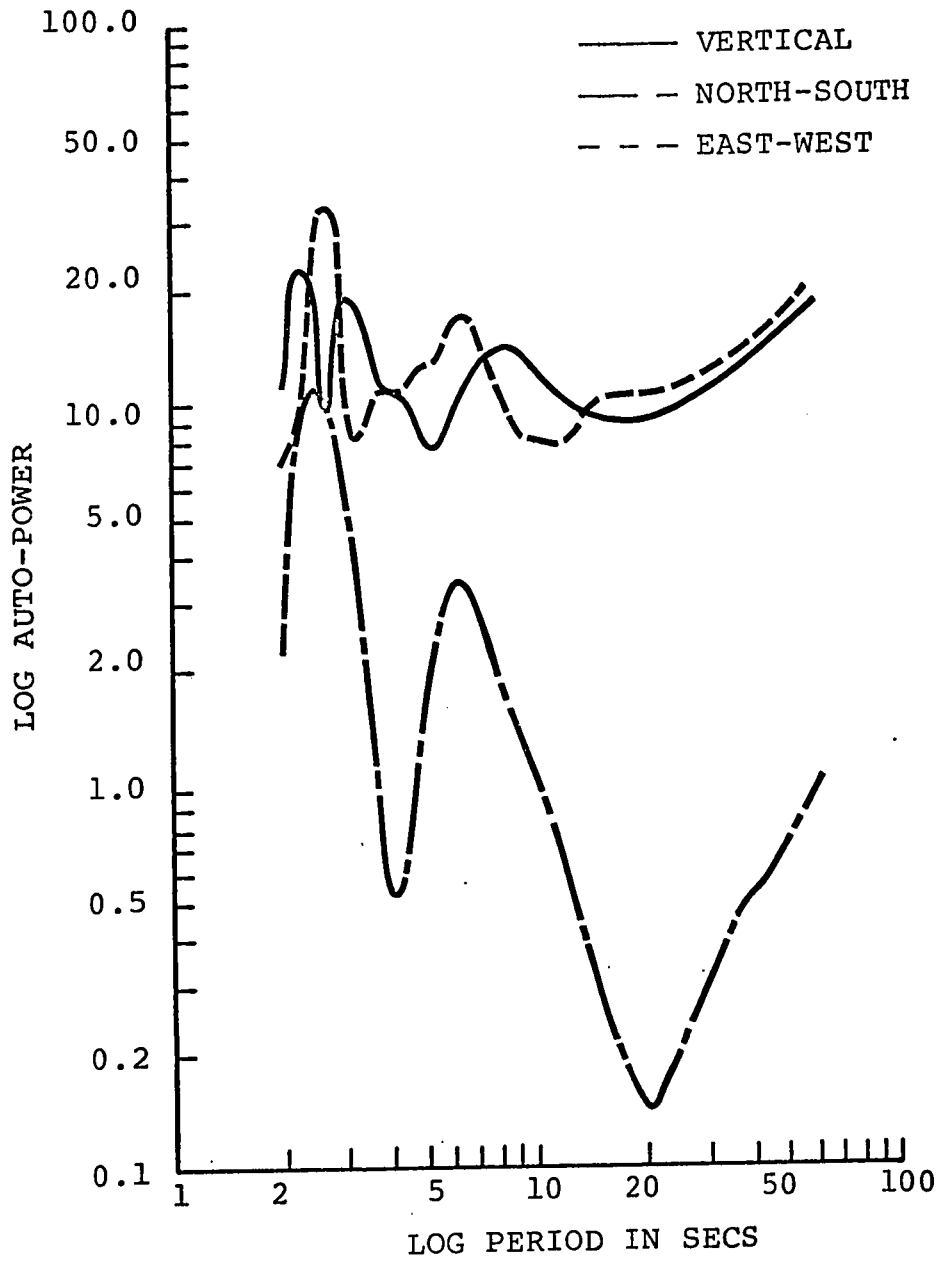


FIG III.1.a

AUTO-POWER SPECTRUM OF MICROSEISMS AT VICTORIA

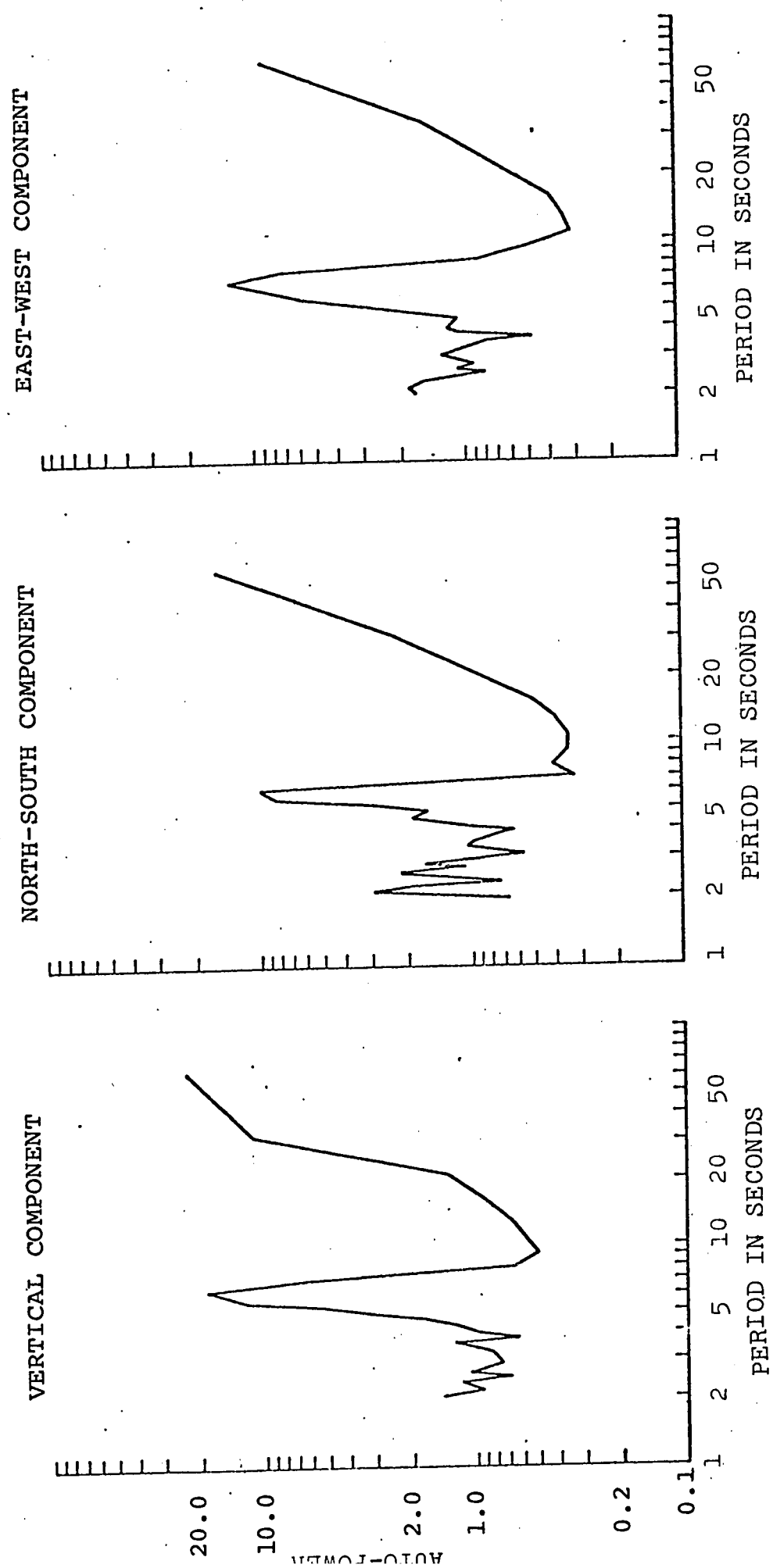


FIG III.1.1.b

its range of variation in time being 2.3-2.6 seconds. The power in the short-period event is equal to or greater than the power in the longer period events.

At Victoria the 6.4 sec peak is present on all three components. A peak around 2.2 sec can be seen on the two horizontal components along with another at 4.0 sec for the example shown which also appears on the vertical component. The period varies in time, the range of variation being 5.4-6.6 sec, 4.0-4.6 sec and 2.0-2.2 sec for the three events mentioned. Unlike at Edmonton, more power is concentrated in the 6.0 sec event than in the other two. The power in the shortest period event is almost negligible compared to the power in the two long period events on most records. The spectral behavior of microseisms at Penticton, Resolute and Ottawa is very similar to that at Victoria.

This marked contrast between Edmonton and the other stations in the behavior of spectra especially with respect to the 2.3 sec event presumably is related to the contrast in crustal layering at these recording sites. The thick sedimentary section at Edmonton probably accentuates the short-periods.

III.2 In figures III.2-8 is shown the temporal variation of autopower spectra for the three components at each recording station. The upper curve in these diagrams shows the variation of magnitude of power in time, the lower curve shows

AUTO-POWER PEAKS AT VICTORIA

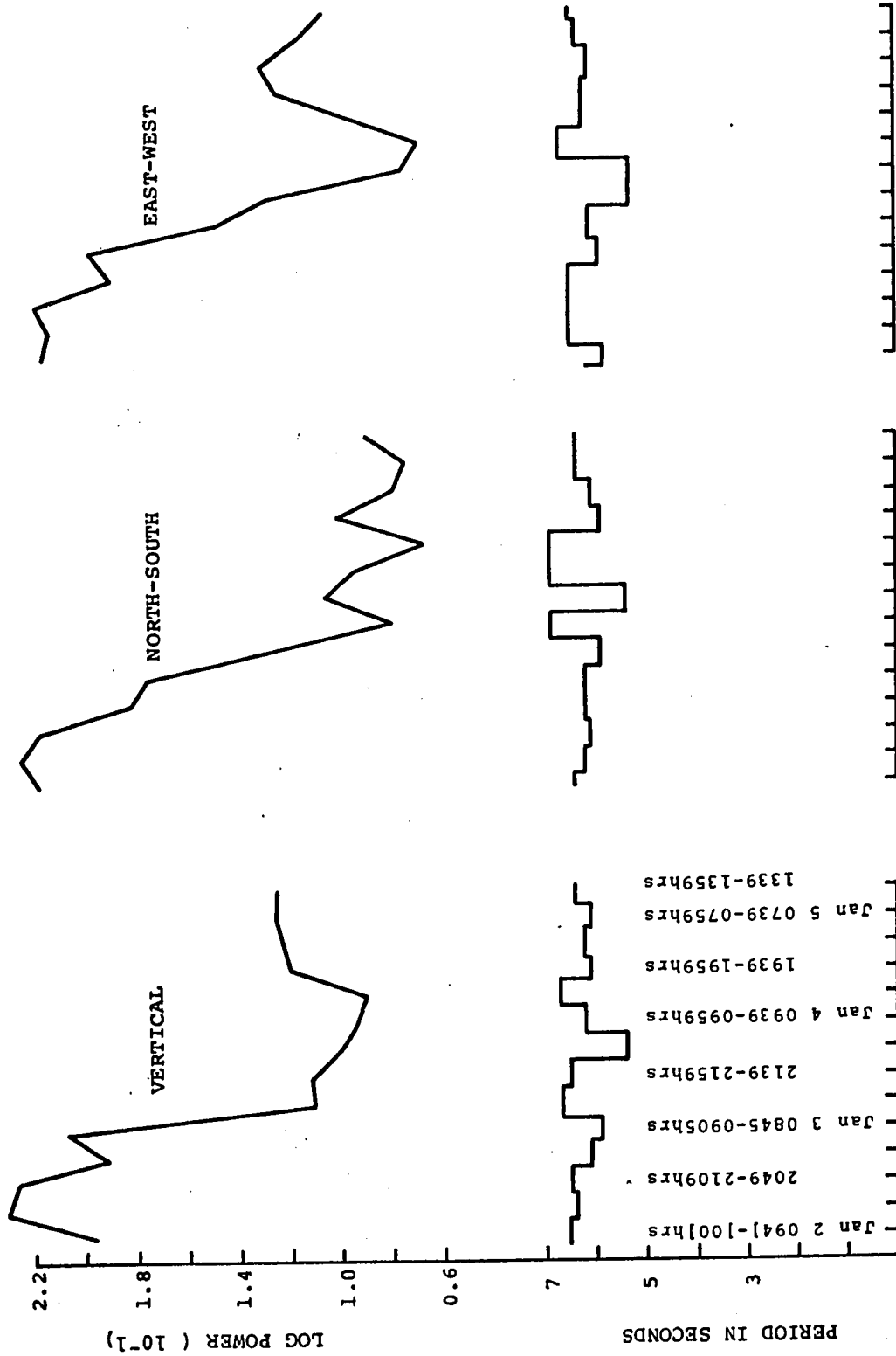


FIG III.2

AUTO-POWER PEAKS AT PENTICTON

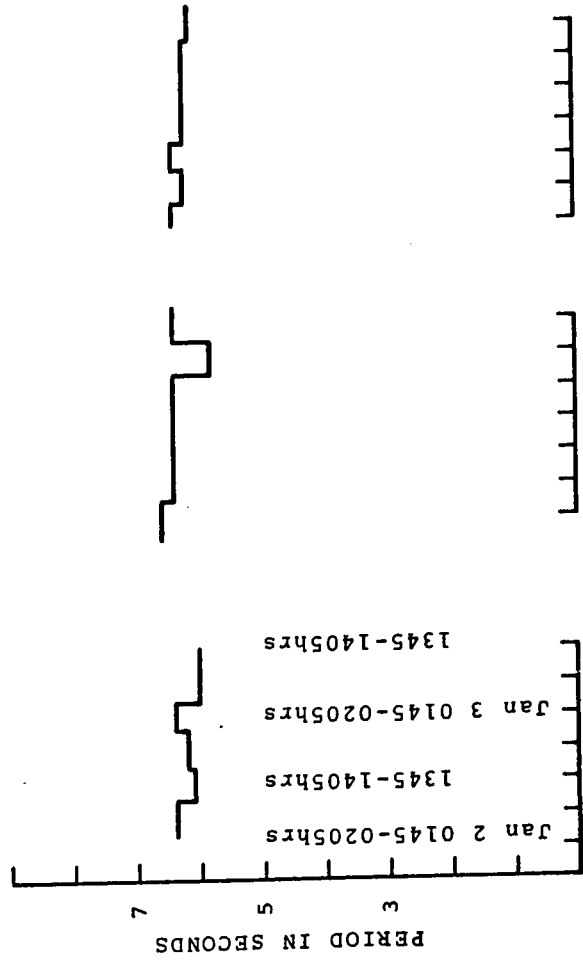
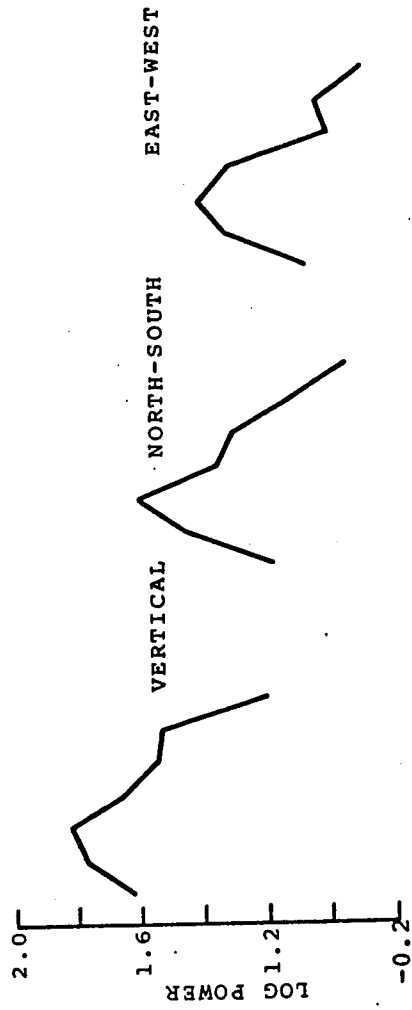


FIG III.3

AUTO-POWER PEAKS AT EDMONTON VERTICAL COMPONENT

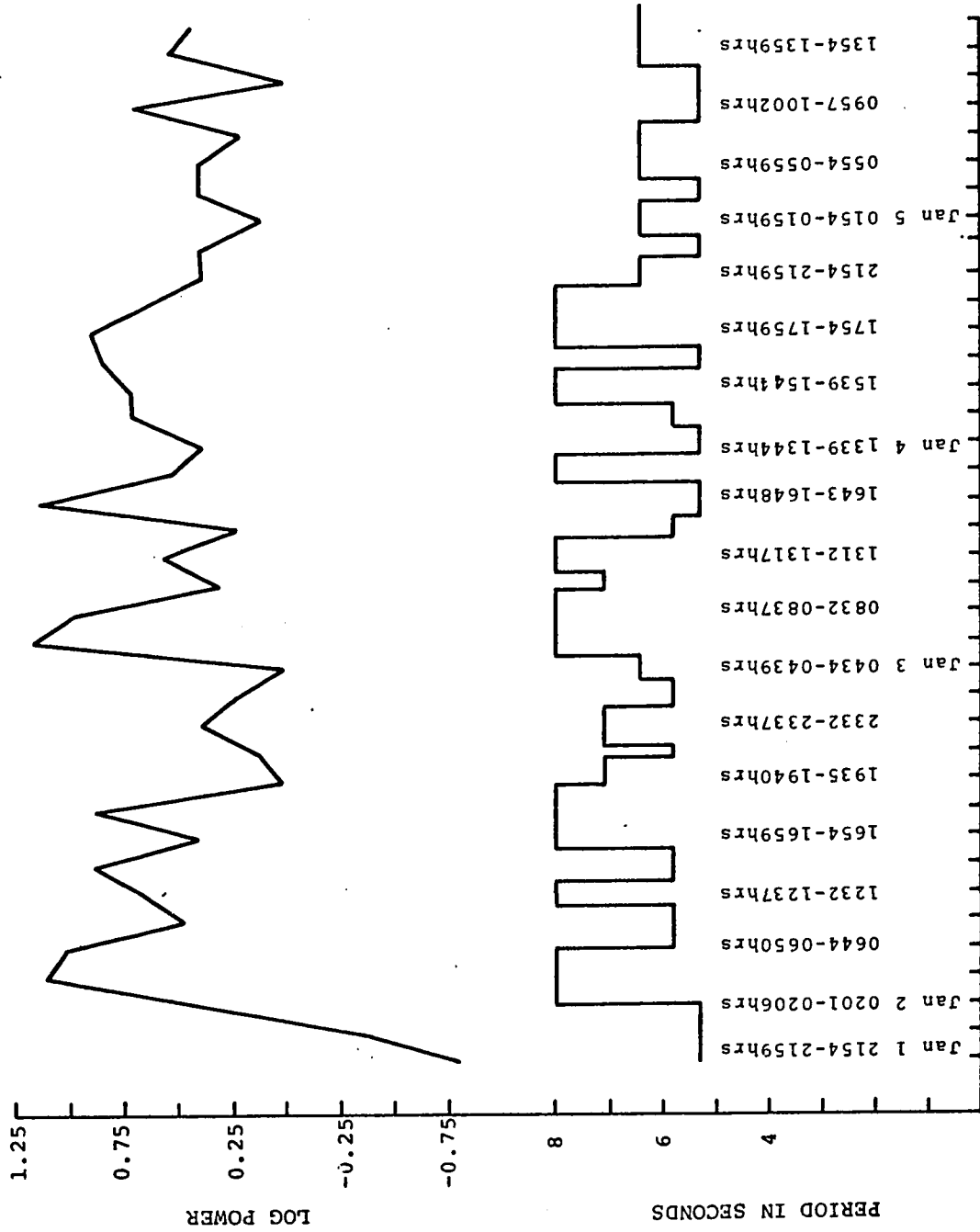


FIG III.4



AUTO-POWER PEAKS AT EDMONTON NORTH-SOUTH COMPONENT

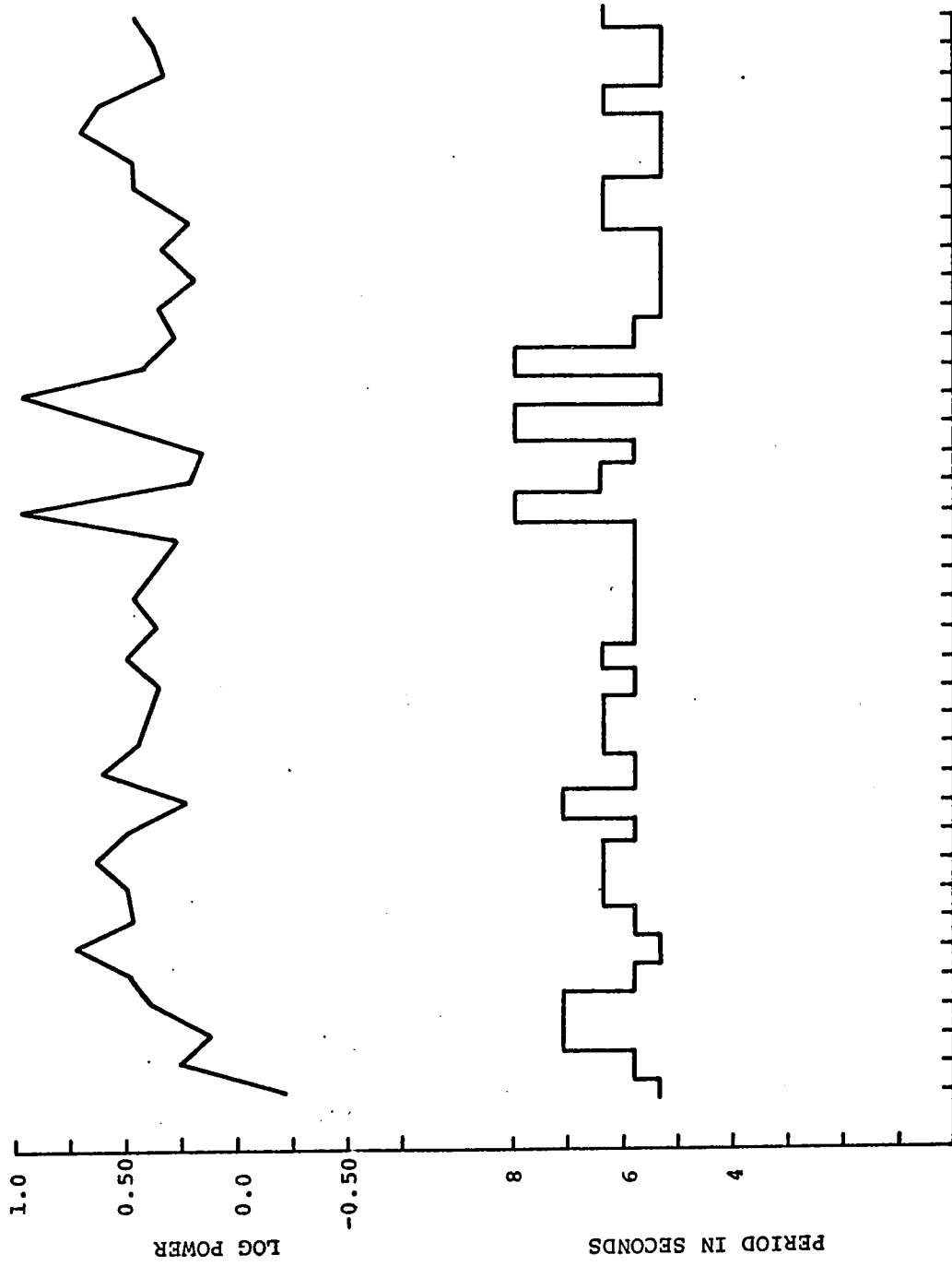


FIG III.5

AUTO-POWER PEAKS AT EDMONTON EAST-WEST COMPONENT

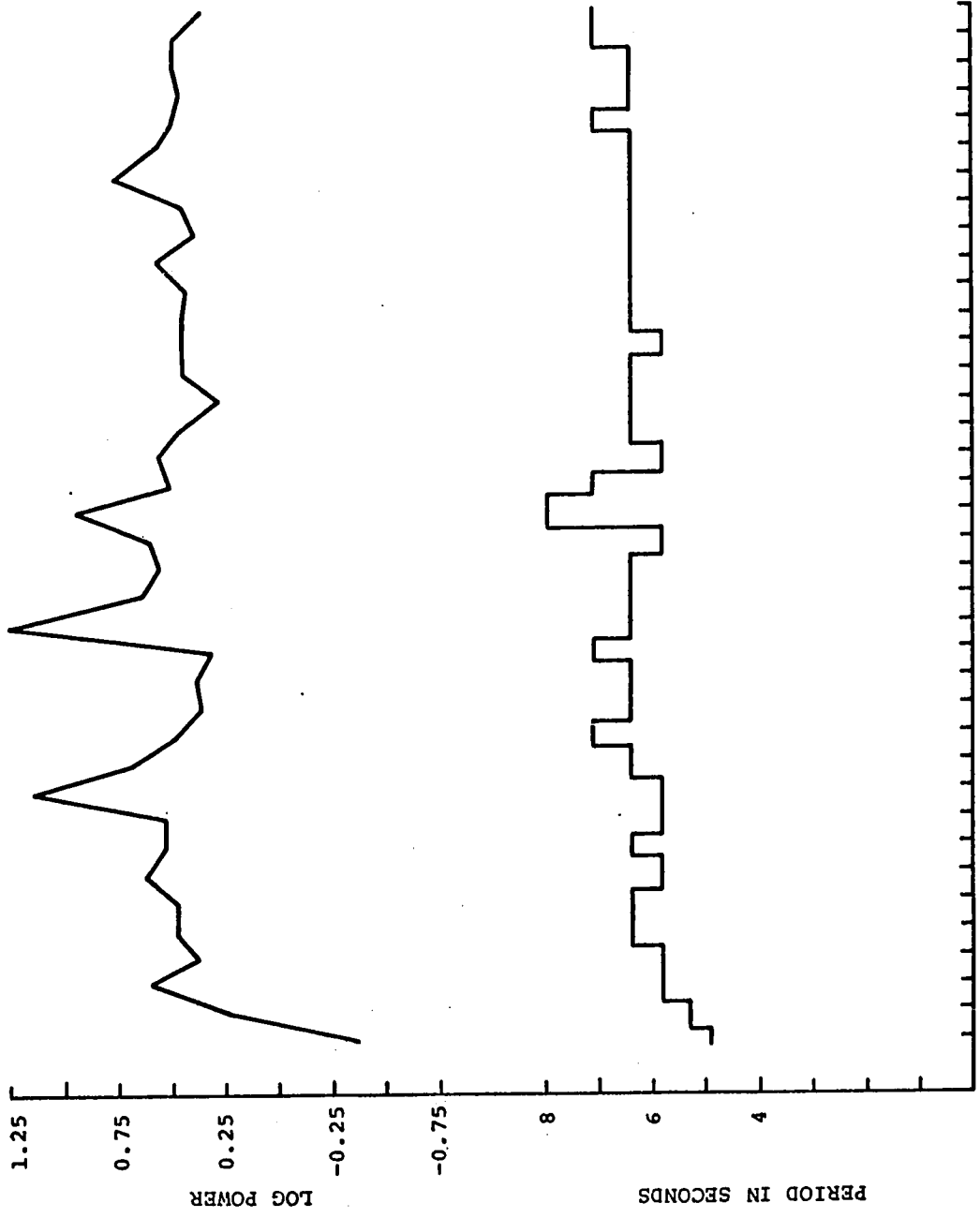


FIG III.6

AUTO-POWER PEAKS AT OTTAWA

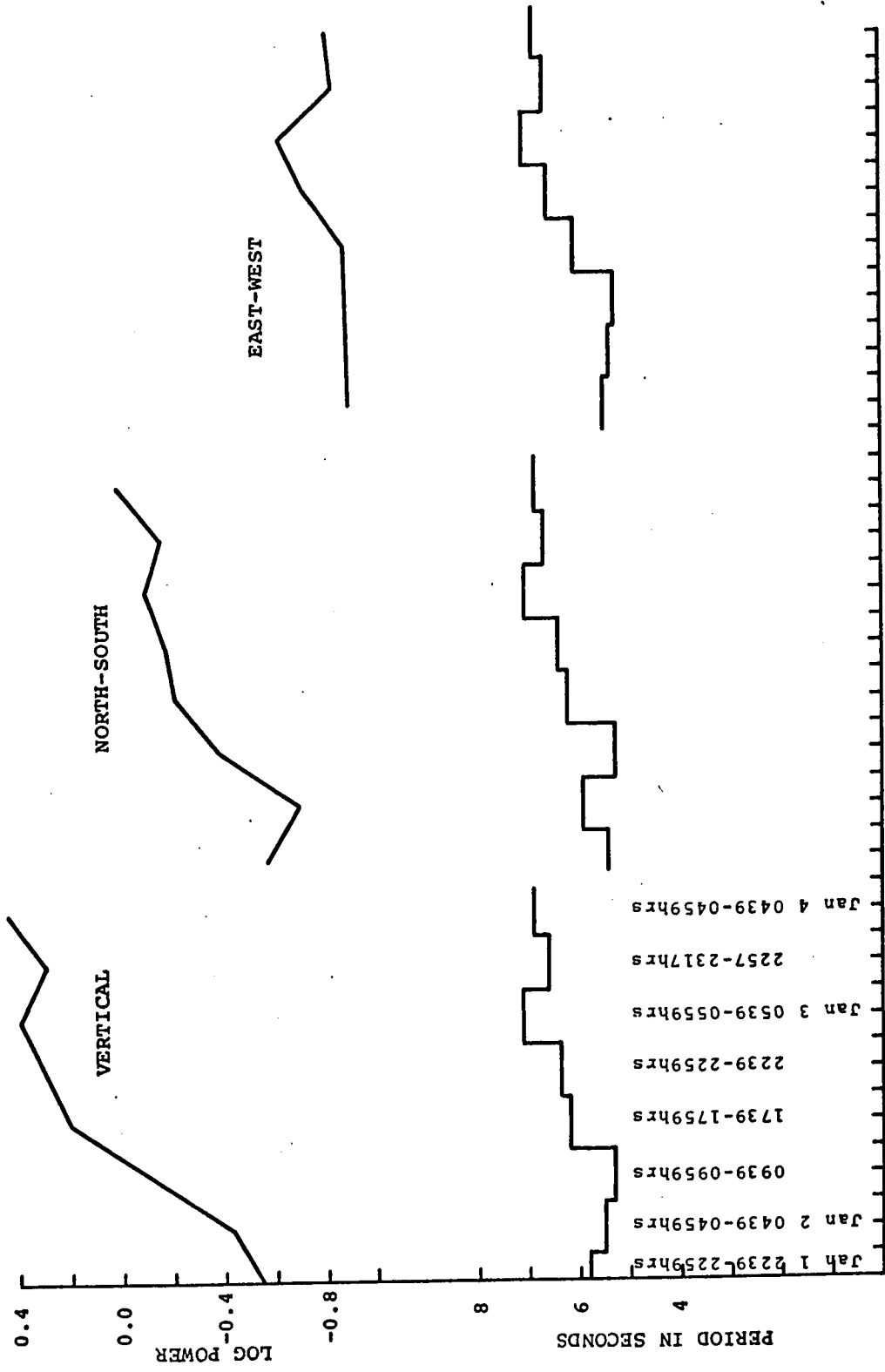


FIG III.7

AUTO-POWER PEAKS AT RESOLUTE

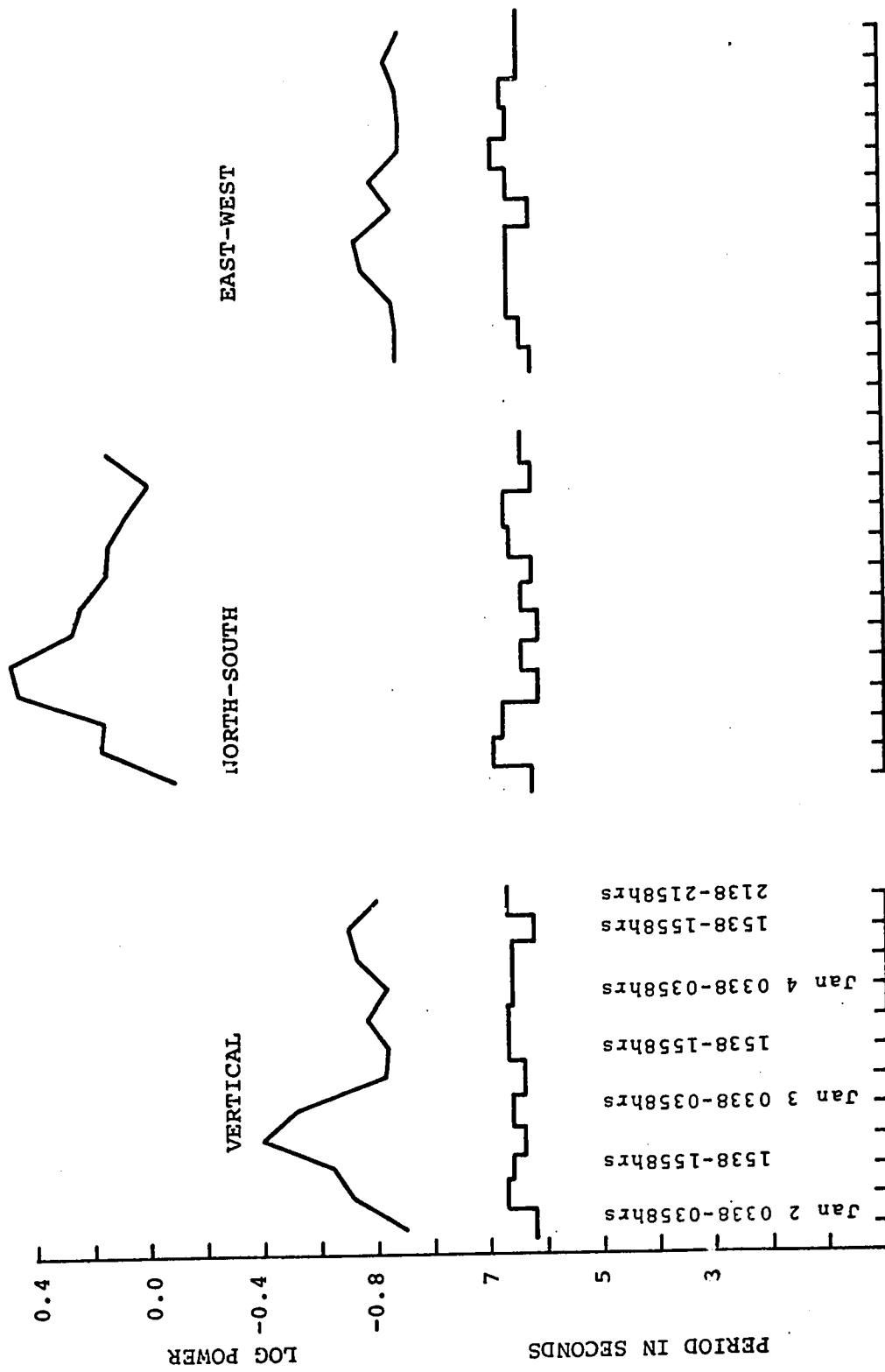


FIG III.8

variation of period in time. The table III.1 shows the minimum and maximum values of period at different stations and their geometric mean. Not much statistical importance can be attached to this mean value, but it is useful as a preliminary guide line for identifying the event. If we now take the following relationship between the period and velocity viz.  $T = 0.4V$  (Defant, 1961),  $V$  being the velocity of the wind in the ocean storm center we can easily calculate the high and low values this velocity attains and a mean value of this can be taken. The mean velocity as calculated from the known value of the period varies between 15.5 and 17 knots. As can be seen from meteorological charts, this is in good agreement with the value of wind velocity.

Table III.2 now lists the periods at which there exists an autopower peak for each component and also the periods at which there exists a crosspower peak between two given components at each station. The values in this table are actually the mean values calculated before as shown in table III.1.

III.3 Some salient features of the histograms and curves shown in figures III.2-8 can be cited as follows:

1. There are random changes in the period with time.
2. At a given time and a given site the period at which peak is observed in the power spectrum of one component does not always correspond to the period at which a peak is observed on another component. This discrepancy varies from a fraction of a second to as much as 3 seconds.

TABLE III.1  
 AUTOPOWER AND CROSS POWER PEAK  
 RANGES IN TERMS OF PERIOD IN SECONDS  
 AND WIND VELOCITIES IN KNOTS

Station	Component	Period (Sec)			Velocity (Knots)			
		Max	Min	Mean	High	Low	Mean	
VICTORIA	Auto Power	Z	6.7	5.5	5.9	17	14	15.5
		N	6.9	5.4	6.1	17	14	15.5
		E	6.6	5.3	5.8	16.5	13	15
	Cross Power	ZN	6.9	5.6	6.2	17	14	15.5
		NE	6.7	6.1	6.4	17	15	16
		EZ	7.3	5.9	6.4	18	15	16.5
PENTICTON	Auto Power	Z	6.4	6.0	6.2	16	15	15.5
		N	6.6	5.8	6.2	16.5	14.5	15.5
		E	6.4	6.1	6.2	16	15	15.5
	Cross Power	ZN	6.6	6.1	6.3	16.5	15	16
		NE	6.6	5.7	6.2	16.5	14	15.5
		EZ	6.7	6.1	6.3	17	15	16
EDMONTON	Auto Power	Z	8.0	5.2	6.8	20	13	16.5
		N	8.0	5.2	6.8	20	13	16.5
		E	8.8	4.8	6.2	22	12	17
	Cross Power	ZN	8.0	4.5	6.0	20	11	15.5
		NE	8.0	5.2	6.8	20	13	16.5
		EZ	8.0	5.3	6.8	20	13	16.5

Station	Component	Period (Sec)			Velocity (knots)			
		Max	Min	Mean	High	Low	Mean	
RESOLUTE	Auto Power	Z	6.7	6.2	6.3	18	15.5	17
		N	6.9	6.1	6.4	18	15	16.5
		E	6.9	6.2	6.5	18	15.5	17
	Cross Power	ZN	6.9	6.0	6.4	17	15	16
		NE	6.9	5.8	6.3	17	14.5	16
		EZ	6.9	6.2	6.5	17	15.5	16
OTTAWA	Auto Power	Z	7.1	6.3	6.7	18	16	17
		N	7.1	6.4	6.7	18	16	17
		E	7.1	6.2	6.6	18	15.5	16.5
	Cross Power	ZN	7.1	5.4	6.1	18	13.5	16
		NE	7.1	5.8	6.4	18	14.5	16
		EZ	7.1	5.9	6.4	18	15	16.5

TABLE III.2

MICROSEISMIC PERIODS AT WHICH  
THERE IS PEAK IN THE POWER SPECTRUM

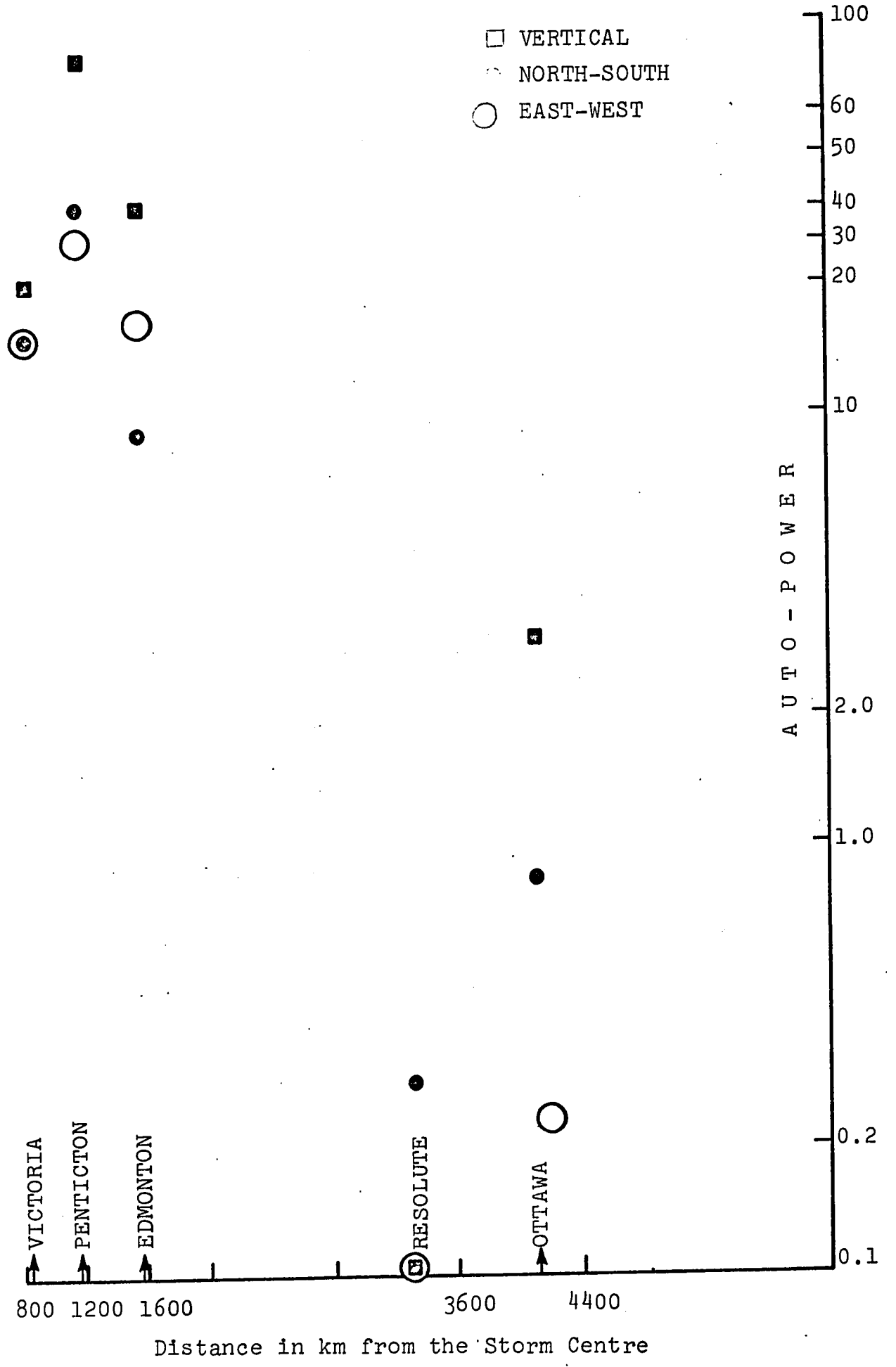
Component	Z	N	E	ZN	NE	EZ
Station						
Victoria	5.9	6.1	5.8	6.2	6.4	6.4
Penticton	6.2	6.2	6.2	6.3	6.2	6.3
Resolute	6.3	6.4	6.5	6.4	6.3	6.5
Edmonton	6.8	6.8	6.2	6.0	6.8	6.8
Ottawa	6.7	6.7	6.6	6.1	6.4	6.4



3. The periods can not be correlated spatially to better than about one or two seconds.
4. At some stations only, there is a rough correlation between changes in the period of maximum microseism power and the changes in the wind velocity in the ocean storm.
5. The variations in period are remarkably large at Edmonton compared to the other stations. The variation of magnitude of power is almost oscillatory in time. No straightforward explanation is available for this phenomenon.
6. The power reaches a maximum value and then decreases at Victoria, Penticton and Resolute.
7. At Edmonton no such systematic variation is evident.
8. At Ottawa the variation in period with time and the variation in the magnitude of the autopower with time have a general trend of increase throughout the time interval sampled by the data sets, suggesting that stable storm conditions have not yet been reached. This may be due to another storm approaching the East Coast at the same time the storm under consideration is receding away from the West Coast.

III.4 At all recording sites except at Edmonton the power reaches a maximum value on all three components at approximately the same time. The behavior of power as a function of time is very similar for all three components at these four stations. This shows that the mechanism of propagation of microseisms is in general very similar in the portions of the crust separated by these four sites. If the microseisms contain both Rayleigh and Love waves, which seems probable from the power recorded on the three components, then both these wave types seem to arrive simultaneously at these four sites.

# VARIATION OF AUTO-POWER WITH DISTANCE



Distance in km from the Storm Centre

Fig. III.9

This feature is borne out by the statement made in the first sentence of this section. No such conclusion can be reached on Edmonton data because there is a marked irregularity at this location from component to component in the variation of power as function of time.

There is more power in the vertical component at Victoria, Penticton and Ottawa than is present in the two horizontal components. At Resolute the north-south component registers more power than the vertical and the east-west components. This presumably has something to do with the crustal structure at these sites. For a Rayleigh wave travelling in a homogeneous, isotropic half-space the amplitude ratio between the vertical component and the radial component should be 1.5 and hence the power ratio between these two components should be 2.25. Table III.3 shows the source is neither east-west nor north-south for any recording site if we assume this particular power ratio to be true. The situation is further complicated by the fact that Rayleigh wave motion is not the same for a multi-layered medium as it is for a half-space, and the crustal layering at the various sites is markedly different, and by the probable presence of body waves in the data.

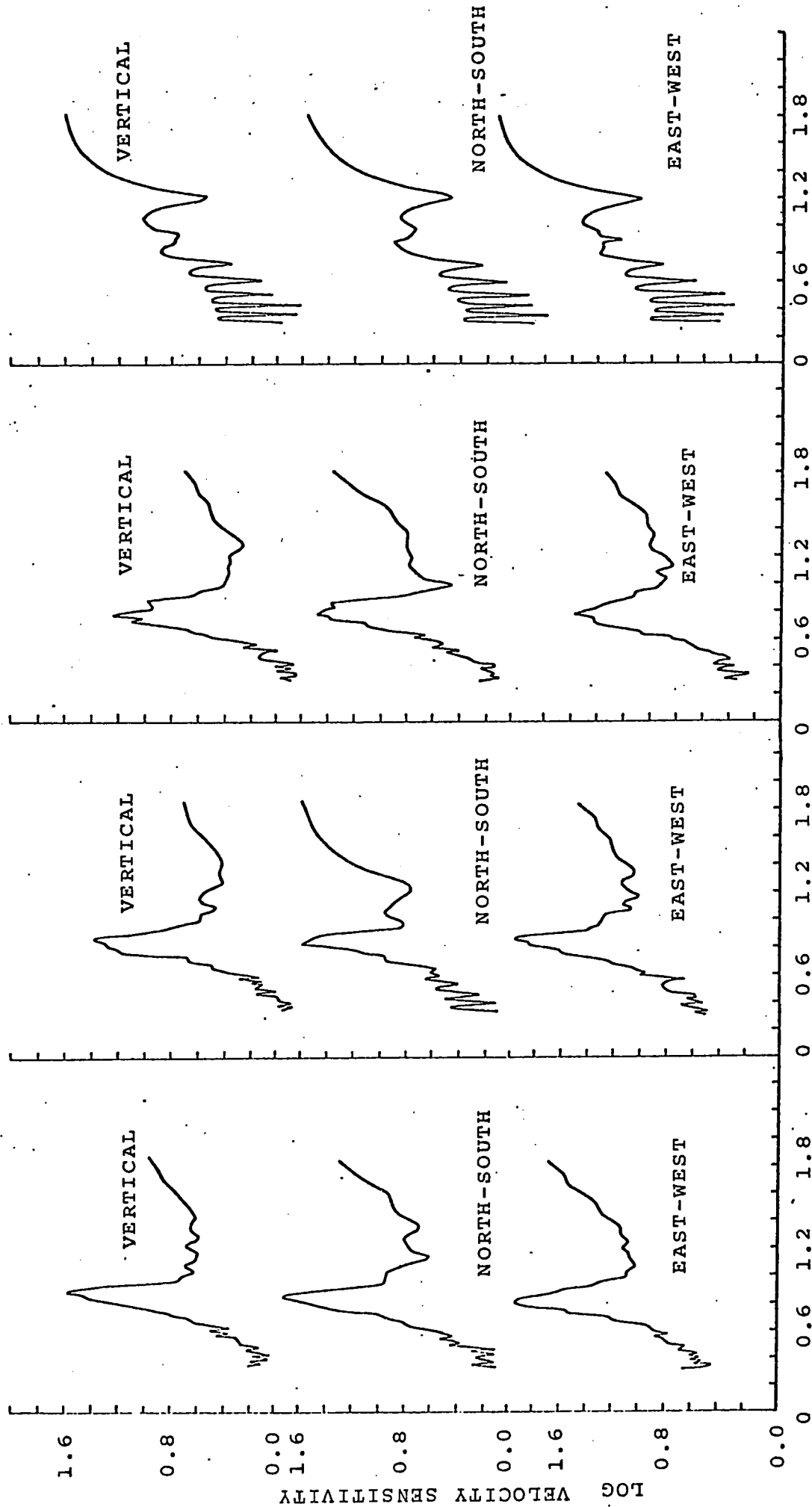
III.5 Figure III.9 shows the spatial variation of the peak value of the autopower. There is a maximum value of power at Penticton but a decrease on either side of this station. Why the power at Victoria is smaller than that at Penticton can

not be answered at all if we assume that main microseism signal has an amplitude which decreases as  $\frac{1}{r^n}$  and that the source is to the west of these two locations. The value of  $n$ , however, can be calculated from the power recorded at Penticton, Edmonton and Ottawa sites. Mean value of  $n$  so calculated is 2.1 for the vertical component, 2.6 for the north-south component and also 2.6 for the east-west component. The autopower on the vertical component thus varies as  $\frac{1}{r^{2.1}}$  and hence the amplitude varies as  $\frac{1}{r}$  approximately, as would be expected for a simple surface wave. If one were to take the actual figures, one would observe that the amplitude varies as  $\frac{1}{r^n}$  where  $n$  is between 1 (for surface waves) and 2 (for body waves), indicating some kind of a quasi-surface wave (perhaps a leaking mode).

III.6 The velocity sensitivity spectra for three stations Victoria, Penticton and Edmonton are shown in Figures III.10, 11 and 12. At all these sites these spectra show sequential peaks.

Andrianova et al. (1967) in a treatise published in Seismic Love waves (p.45) point out that for foci located at the depth of 30-40 km it is possible to record in a crust of 30-40 km not only the first, but the second and third modes of Love waves for periods less than 7-8 sec. The dispersion curves for second and third modes in a crust with a sedimentary layer are marked by maxima and minima. (p. 39, Fig. 15b, Model 8, Andrianova, op. cit.) According to the same authors specific vibrations with quasi-stationary periods (less than

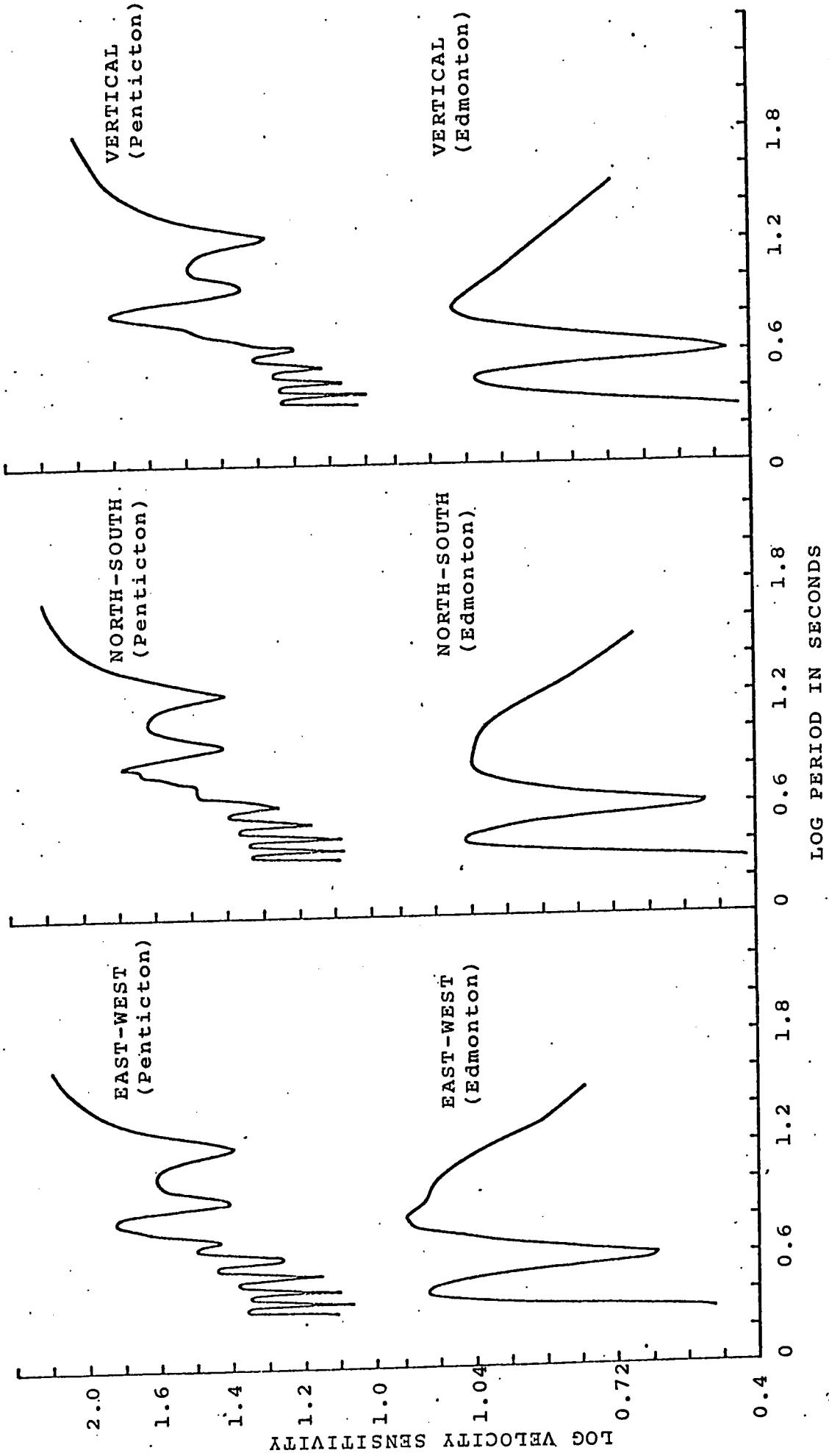
VELOCITY SENSITIVITY SPECTRA AT VICTORIA



LOG PERIOD IN SECONDS

FIG III.10

VELOCITY SENSITIVITY SPECTRA AT PENTICTON AND EDMONTON



FIGS III.11-12

2 secs) and long duration can be generated corresponding to resonance in the system consisting of a surface layer and a wave guide in the crust. If we now assume that the Longuet-Higgins theory is true to the extent that the ocean water would excite elastic waves in the ocean bottom and that the oceanic crust acts as a waveguide for the seismic waves to be propagated to the continent and thence along a higher velocity wave guide beneath the granitic layer then we satisfy the first condition in Andrianova's theory, that the source is at a depth of around 30-40 km, by the time we observe the waves on the continent. Observe that the crustal thickness at Victoria is in excess of 40 km.

Thus in terms of Andrianova's theory Victoria data could be interpreted as consisting of higher modes of Love and perhaps of Rayleigh Waves, since the vertical component also shows sequential peaks in the velocity sensitivity spectra. It would be however impossible to interpret Penticton and Edmonton data in terms of higher modes of surface waves as these modes would attenuate at larger distances. In addition to this, a sedimentary layer of thickness 5 kms with a transverse wave velocity of 2.6 km/sec is required for the 2 sec microseisms to be recorded at Victoria. In view of the fact that such layer is absent at Victoria, and in view of the difficulty of interpreting Penticton and Edmonton data in terms of higher modes of surface waves, one would have to look for a different interpretation of these spectra.

Phinney (1964) working on earthquake body waves of periods 5-50 secs, obtained curves for spectral ratios vs frequency in which "characteristically the spectral response,  $T_p$ , shows sequence of peaks due to resonance effects in the crust." Phinney (1961) also mentions in a theoretical consideration on leaking modes " . . . pressure variations, . . . due to standing water waves, will excite this mode (late arriving quasi-standing mode) at least as efficiently as they excite undamped Rayleigh waves. The noise may then leave the source region either by horizontal propagation in the layer or by means of the P waves leaking into the bottom. The former must be regarded as short-range mechanism where as the latter would carry the energy to appreciable distances as body waves." We merely mention these two statements from Phinney to suggest that body waves, perhaps leaky modes, are present in the data.

III.7 Figures III.13-19 show the crosspower spectral abundances at each station. These histograms show exactly the same features as those mentioned under the autopower spectra. The peak shifts in period from record to record at a given station, the shift being as small as a fraction of a second and as large as 3 seconds. The following features can be recognized from these histogram:

1. On Victoria records the range of variation for the period at which the crosspower peaks is 5.6-6.9 seconds for the vertical and North-South components, 6.1-6.7 seconds for the North-South and East-West components and 5.9-



CROSS-POWER PEAKS AT VICTORIA

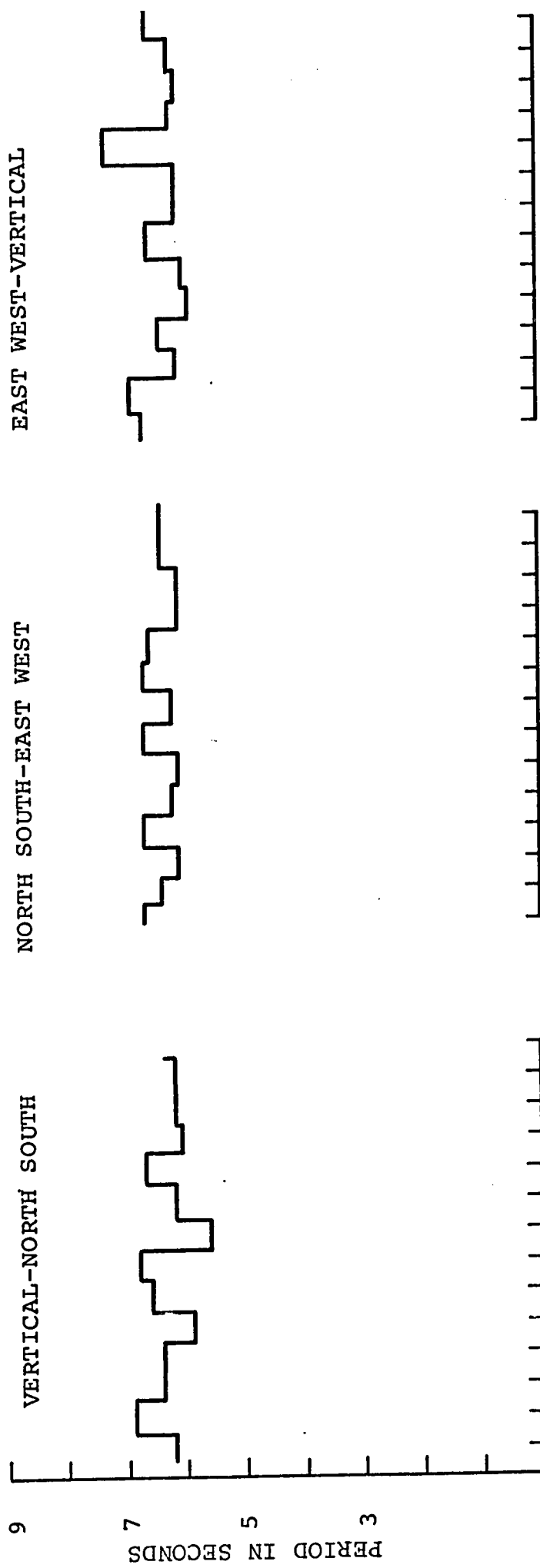


FIG III.13

CROSS-POWER PEAKS AT PENTICTON

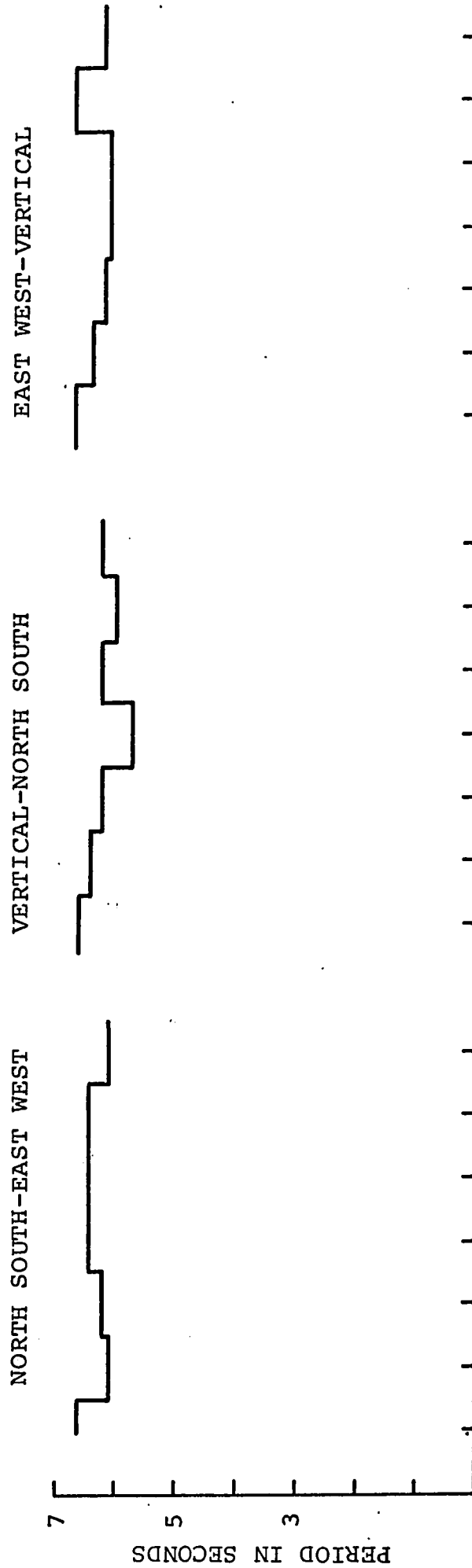


FIG III.14

CROSS-POWER PEAKS BETWEEN VERTICAL AND NORTH-SOUTH COMPONENTS AT EDMONTON

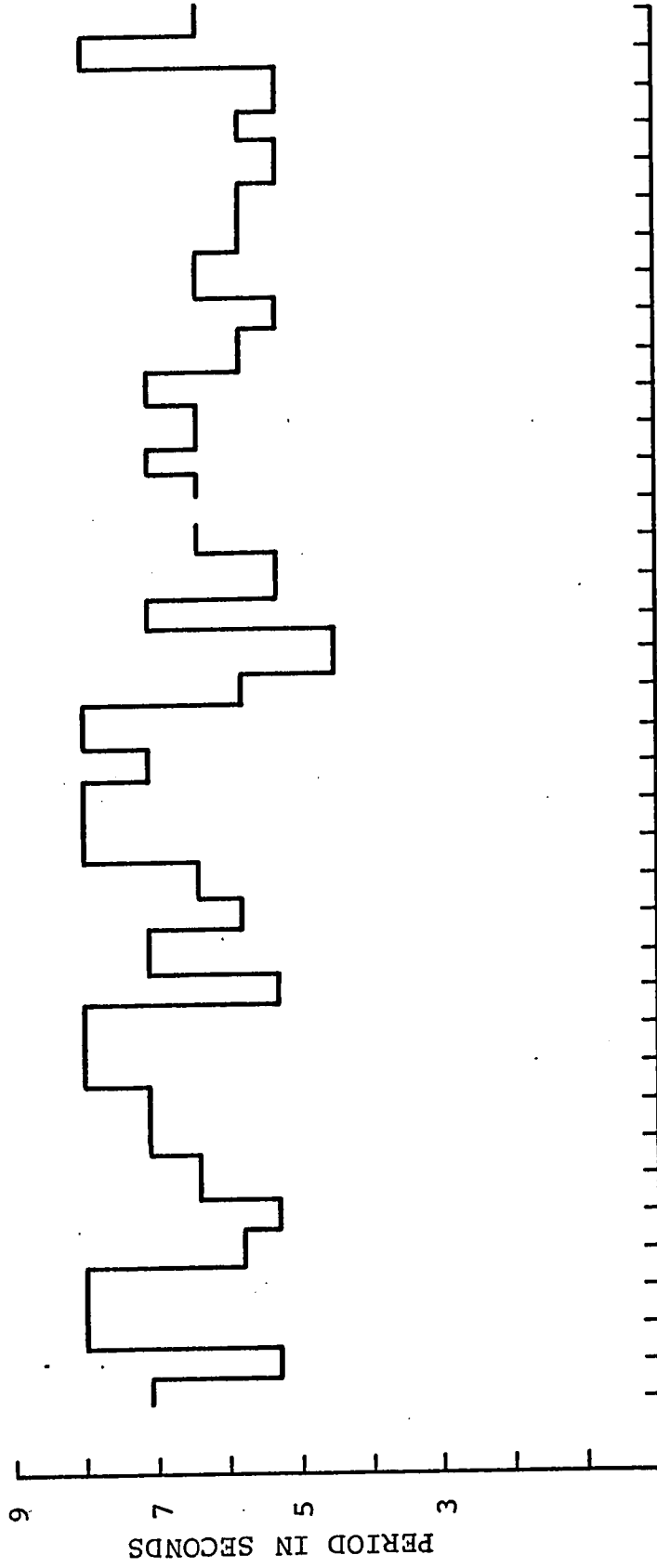


FIG III.15

CROSS-POWER PEAKS BETWEEN NORTH-SOUTH AND EAST-WEST COMPONENTS AT EDMONTON

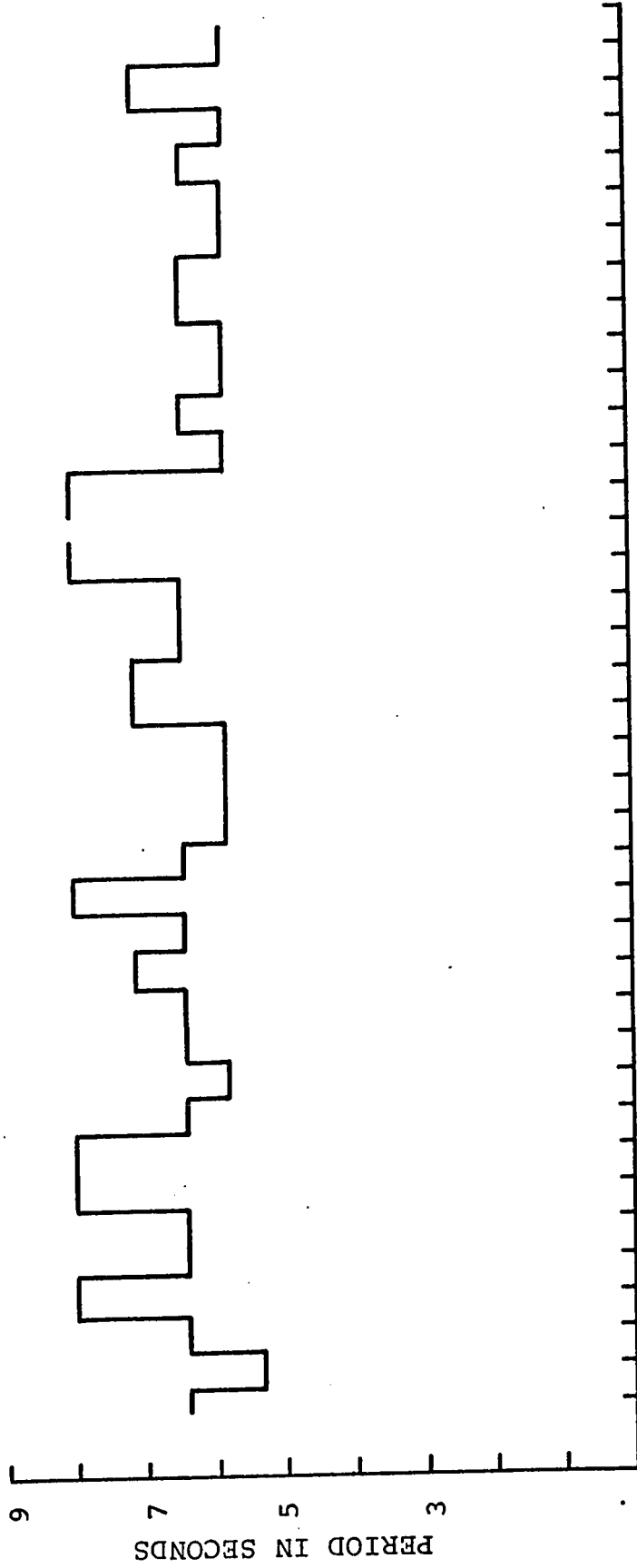


FIG III.16

CROSS-POWER PEAKS BETWEEN EAST-WEST AND VERTICAL COMPONENTS AT EDMONTON

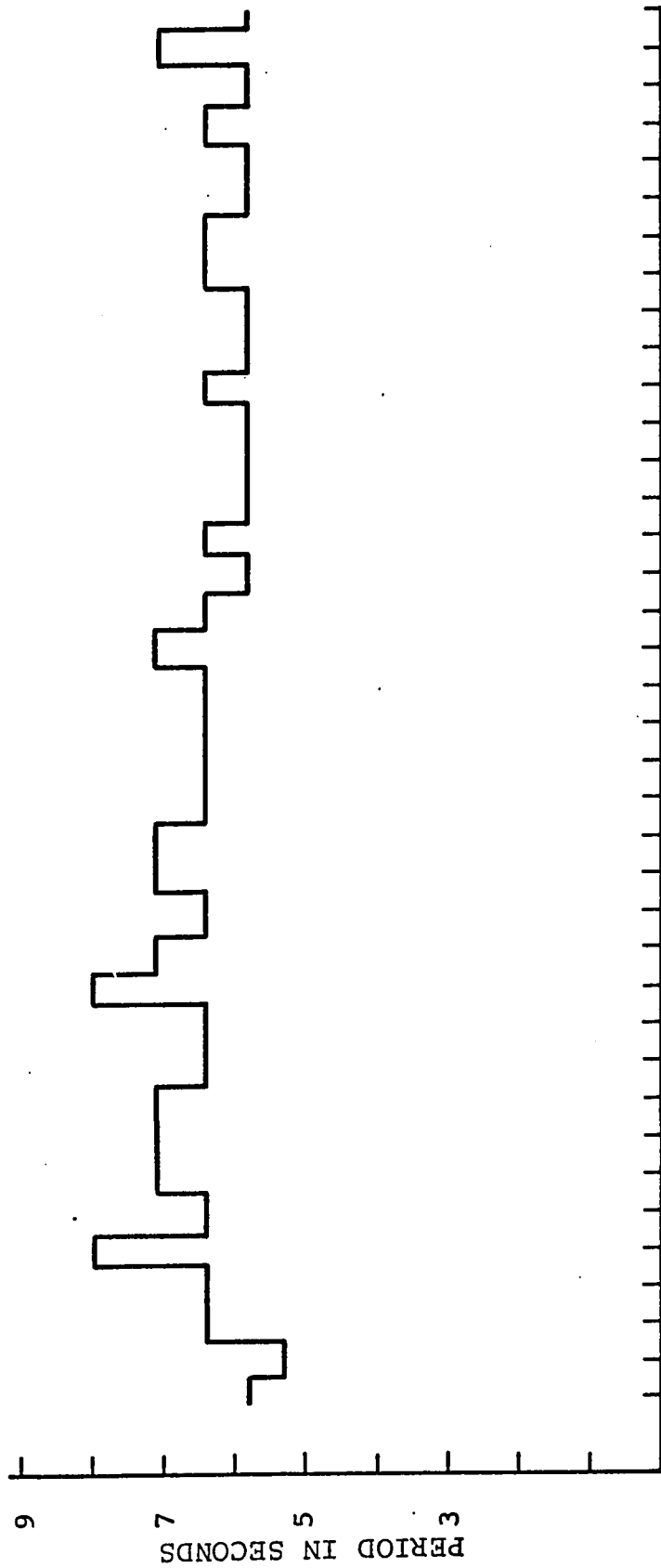


FIG III.17

CROSS-POWER PEAKS AT RESOLUTE

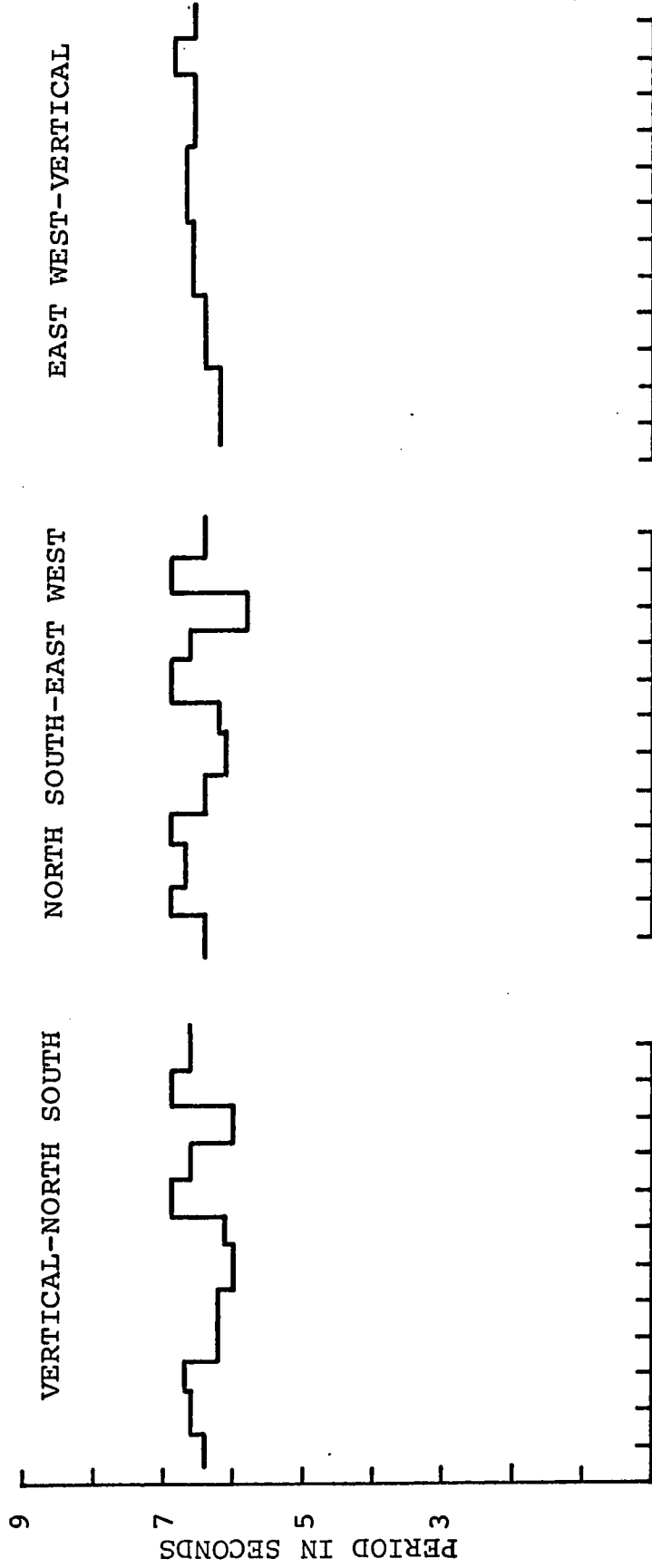


FIG III.18

CROSS-POWER PEAKS AT OTTAWA

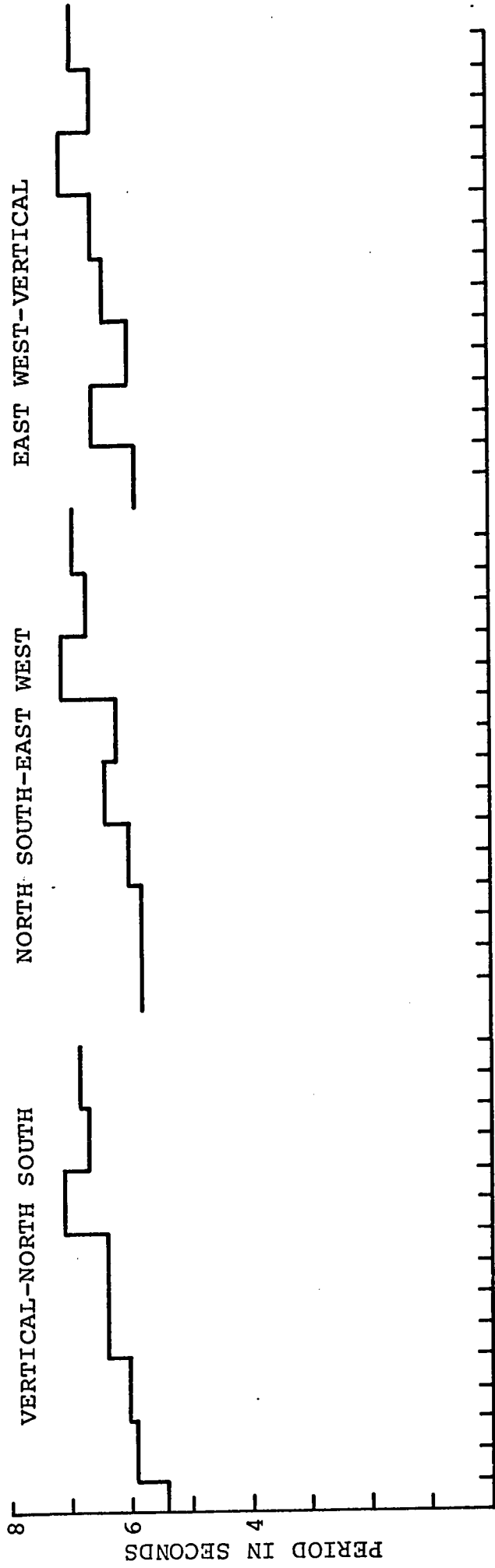


FIG III.19

TABLE III.3

## RATIOS OF VERTICAL TO HORIZONTAL POWERS

Station	Z Power	EW Power	Ratio	NS Power	Ratio
Victoria	20	15	1.3	15	1.3
Penticton	63	25	2.5	40	1.5
Edmonton	40	16	2.5	9	4.5
Resolute	0.4	0.18	2.2	2.5	0.16
Ottawa	2.5	0.7	3.5	0.22	10

TABLE III.4

POWER VS DISTANCE (POWER  $\frac{1}{r^n}$ )

Station	Distance in km	Power			n for Z	n for NS	n for EW
		Z	N	E			
Penticton	1111	66	40	25	1.6	2.1	1.3
Edmonton	1534	40	9	16	2.7	2.3	3.4
Ottawa	4344	2.5	.84	.23	2.2	4.4	4.1
			Mean		2.1	2.6	2.6



- 7.3 seconds for the east-west and vertical components.
2. On Penticton records the respective figures are 6.1-6.6 seconds, 5.7-6.6 seconds and 6.1-6.7 seconds.
  3. On Edmonton records the peaks are more scattered in period, the variation being 5-8 seconds, a spread of three seconds for the long period event.
  4. On Resolute records the corresponding figures are 6.0-6.9 seconds, 5.8-6.9 seconds and 6.2-6.9 seconds.
  5. On Ottawa records they are 5.6-7.1 seconds, 5.8-7.1 seconds, and 5.9-7.1 seconds respectively.

The crosspower spectra thus do not conclusively point toward a well defined wave type occurring within a range of fraction of second in period. The data is scattered from trace to trace at almost all stations, and there is a scattering from station to station. This is not due to the recording but due to the arriving microseisms themselves as can be seen from the following remarks and the later discussion of synthetic microseisms in chapter IV. The coherency values rarely exceed 0.7 at these peak values, especially where the vertical component is involved. The phase between the vertical and a horizontal component is rarely  $-90$  as would be expected of a Rayleigh wave recorded on these two components. The phase between the two horizontals is also rarely  $0^{\circ}$  or  $180^{\circ}$  as would be expected of a Love wave that would be recorded on the two horizontal components. Fig. III.20 shows a typical example for an Edmonton trace of a plot of phase vs period and coher-

PHASE AND COHERENCY BETWEEN  
VERTICAL AND EAST-WEST COMPONENTS

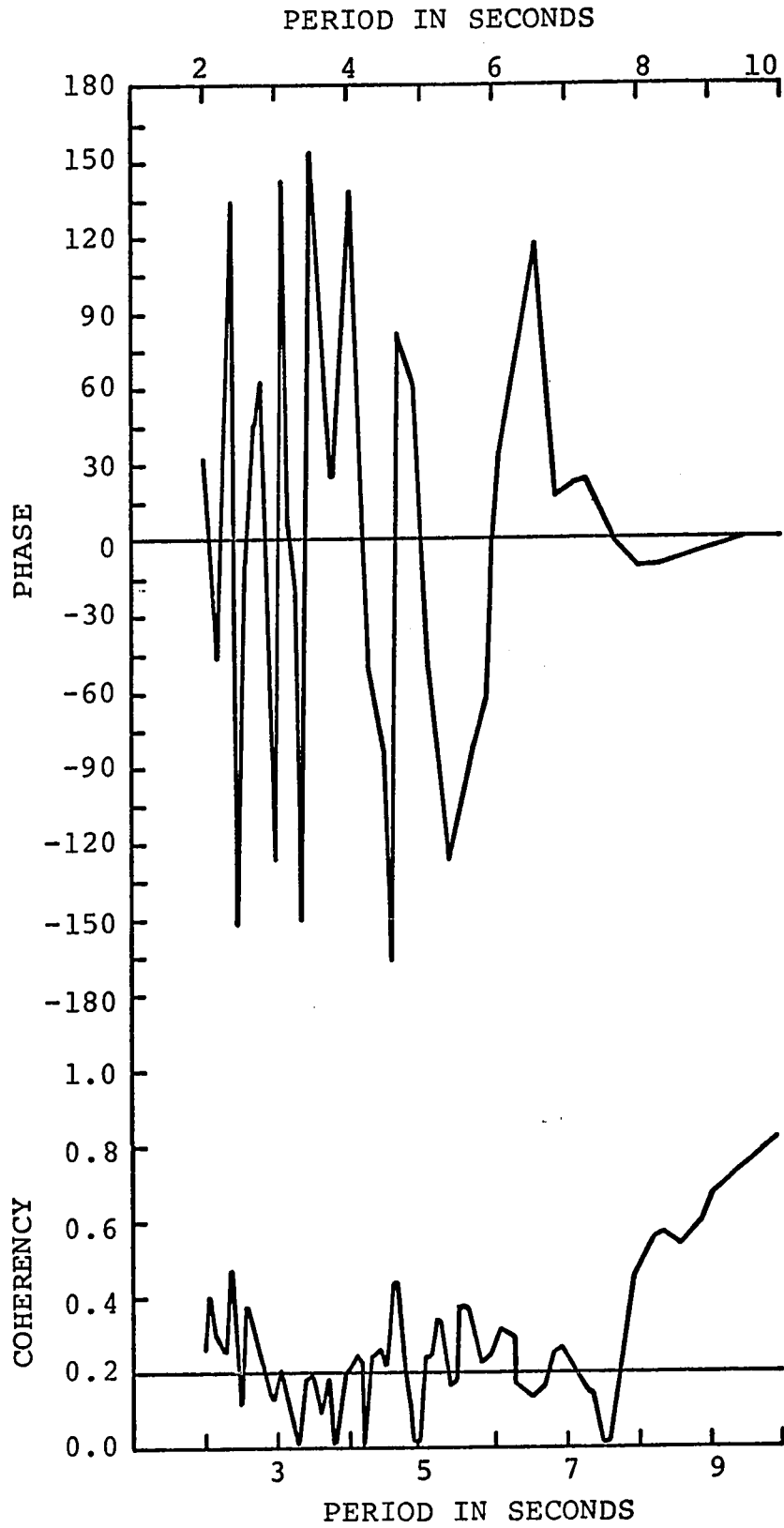


FIG III.20

ency vs period. Phase changes rapidly from one frequency to the other. In addition, the peaks on crosspower vs period, and coherency vs period are not at all correlated. Not one trace at all these stations could be found which would show all the three quantities correlated. Coherencies are low because of the lack of correlation on the autopower peaks for various components. In general the phase also varies in a random way and seldom takes on consistent values related to any simple wave type. There are only a few examples of well defined Rayleigh and Love wave recordings at these stations and they will be discussed in the next chapter.

## CHAPTER IV

### WAVE TYPES IN MICROSEISMS

IV.1 In tables IV.1-5 are listed some of the more important events recorded. In these tables are shown the period at which either there is a peak in coherency or in crosspower, and the values of the coherency, phase and the components involved. For a Rayleigh wave coming from the west, the coherency between the east-west and vertical components has to be high, the phase between the two has to be  $-90^{\circ}$  for the simplest wave type, and there should be a clear cut peak on the crosspower spectra between these components. For a Rayleigh wave arriving from the north the two components involved are vertical and north-south. In the last column of these tables an attempt is made to identify the wave type on this basis.

It is quite obvious that many spectral peaks could not be readily identified as to wave type. Some of these events were identified as Rayleigh or Love or the first mode of Rayleigh on the basis of phase and/or coherency and/or peak on the crosspower spectrum. An event with a peak on coherency and crosspower, and a phase of  $-90^{\circ} \pm 20^{\circ}$  between the vertical and a horizontal component could be identified as Rayleigh. In this case when occasionally the phase is approximately  $-90^{\circ}$ , the other two criteria are seldom sat-

## VICTORIA

Trace #	Per- iod	Coher- ency	Phase	Comp- onent	Peak Coh.	Peak Cross- power	Type
3	5.8	0.45	-72	EZ	Yes	Yes	Rayleigh
4	6.7	0.18	-81	EZ	No	Yes	
	5.1	0.52	148	EZ	Yes	Yes	
	4.4	0.47	-73	EZ	Yes	No	
5	6.1	0.41	18.0	NE	Yes	Yes	Love
	6.6	0.29	107	EZ	No	Yes	Rayleigh (First Mode)
	4.1	0.43	-3.9	NE	Yes	Yes	Love
6	6.4	0.16	104	EZ	Yes	Yes	Rayleigh (First Mode)
	4.5	0.47	-103	ZN	Yes	Yes	Rayleigh (First Mode)
	6.7	0.55	-49	NE	Yes	Yes	Love (?)
7	6.0	0.36	-102	ZN	Yes	Yes	Rayleigh
	5.8	0.24	-70	NE	Yes	Yes	
	6.1	0.22	104	EZ	Yes	Yes	
	4.2	0.34	-120	ZN	Yes	Yes	
8	6.0	0.16	-92	EZ	Yes	Yes	Rayleigh
	4.5	0.39	180	ZN	Yes	Yes	
	6.1	0.12	8.2	NE	Yes	Yes	Love (?)
	5.6	0.24	135	NE	Yes	Yes	Love (?)
9	6.6	0.40	-131	EZ	Yes	Yes	
	6.0	0.51	7.0	EZ	Yes	Yes	
	5.7	0.49	-10	ZN	Yes	Yes	
	6.7	0.47	17	NE	Yes	Yes	Love (?)

Trace #	Period	Coherency	Phase	Component	Peak Coh.	Peak Cross-power	Type
10	6.1	0.37	11	EZ	Yes	Yes	
	5.2	0.62	82	EZ	Yes	Yes	
	6.2	0.28	-17	NE	Yes	Yes	
11	6.1	0.34	1.8	EZ	Yes	Yes	
	6.1	0.35	100	NE	Yes	Yes	
	5.7	0.59	-0.9	ZN	Yes	Yes	
12	5.8	0.23	8.7	EZ	Yes	Yes	
	6.6	0.35	155	NE	Yes	Yes	Love
	6.6	0.47	9	EZ	Yes	Yes	
	4.9	0.41	-111	EZ	Yes	Yes	Rayleigh
13	6.1	0.78	4.4	NE	Yes	Yes	Love
	6.1	.88	-10	EZ	Yes	Yes	
	4.5	.92	4	NE	Yes	Yes	Love
	4.6	.94	-8.6	EZ	Yes	Yes	
	4.6	.90	-3.5	ZN	Yes	Yes	
14	6.1	0.80	-1.3	NE	Yes	Yes	Love
	6.1	0.86	-0.3	EZ	Yes	Yes	
	6.2	0.90	1.0	ZN	Yes	Yes	
	4.6	0.93	12.0	ZN	Yes	Yes	
	4.6	0.94	4.0	NE	Yes	Yes	Love
	4.6	0.93	-5.1	EZ	Yes	Yes	
15	6.4	0.73	167	NE	Yes	Yes	Love
	6.2	0.75	-28	EZ	Yes	Yes	
	6.1	0.75	20				
	4.6	0.85	20.5	ZN	Yes	Yes	
	4.6	0.91	-5.7	NE	Yes	Yes	Love
	4.6	0.95	-17	EZ	Yes	Yes	

Trace #	Per- iod	Coher- ency	Phase	Comp- onent	Peak Coh.	Peak Cro- ss-power	Type
16	6.4	0.69	-32	EZ	Yes	Yes	
	5.8	0.81	2.2	NE	Yes	Yes	Love

## PENTICTON

Trace #	Period	Coherency	Phase	Component	Peak Coh.	Peak Cross-power	Type
18	6.7	0.45	-76	EZ	Yes	Yes	Rayleigh
	6.7	0.44	10	NE	No	Yes	Love
	4.4	0.83	-1.7	NE	Yes	Yes	Love
19	6.6	0.62	9.9	EZ	Yes	No	
	7.1	0.50	-5.5	NE	Yes	No	Love
	6.1	0.41	6.3	NE	Yes	Yes	Love
	4.6	0.88	-5.8	NE	Yes	Yes	Love
	6.6	0.65	-13	EZ	Yes	Yes	
20	6.2	0.48	-111	EZ	Yes	Yes	Rayleigh
	6.2	0.38	-20	NE	Yes	Yes	
	4.6	0.85	0	NE	Yes	Yes	Love
21	6.1	0.65	15	EZ	Yes	Yes	
	6.4	0.50	-43	NE	Yes	Yes	
	4.5	0.85	5	NE	Yes	Yes	Love
22	6.1	0.21	-50	EZ	Yes	Yes	
	6.4	0.55	-6	NE	Yes	Yes	Love
	4.6	0.85	11	NE	Yes	Yes	Love
	4.7	0.51	-76	EZ	No	No	Rayleigh
23	6.4	0.64	-3	NE	Yes	Yes	Love
	4.6	0.91	0.1	NE	Yes	Yes	Love
	4.9	0.62	-82	EZ	Yes	Yes	Rayleigh
24	6.0	0.68	-1	NE	Yes	Yes	Love
	4.5	0.92	-3	NE	Yes	Yes	Love



TABLE IV.3

Trace #	RESOLUTE						
	Per iod	Coher- ency	Phase	Comp- onent	Peak Coh.	Peak ss.-power	Type
49	7.1	.81	0.5	ZN	Yes	No	
	6.9	0.79	40	EZ	Yes	No	
	6.9	0.70	-35	NE	Yes	No	
	5.6	0.56	-55	ZN	Yes	Yes	
	4.3	0.88	-3	NE	Yes	Yes	Love
50	6.9	0.74	6.7	NE	Yes	Yes	Love
	6.6	.34	-104	ZN	Yes	Yes	Rayleigh
	4.3	.80	2.0	NE	Yes	Yes	Love
	4.7	189	16	EZ	Yes	Yes	
51	6.4	.52	111	EZ	Yes	Yes	
	6.0	.45	25	NE	Yes	Yes	Love (?)
52	4.1	0.71	-88	EZ	Yes	No	Rayleigh
	5.6	.42	-105	EZ	Yes	Yes	Rayleigh
	4.8	0.71	0.7	NE	Yes	Yes	Love
	6.9	0.50	3.4	NE	Yes	Yes	Love
53	6.2	.47	-83	ZN	Yes	Yes	Rayleigh
	6.4	.41	4.3	NE	Yes	Yes	Love
	4.7	189	-10	NE	Yes	Yes	
54	6.1	.43	-95	ZN	Yes	Yes	Rayleigh
	4.4	189	1.8	NE	Yes	Yes	Love
	6.4	.53	16	NE	Yes	Yes	Love
55	6.6	.60	96	NE	Yes	Yes	
	4.9	187	-104	EZ	Yes	Yes	Rayleigh

Trace #	Per- iod	Coher- ency	Phase	Comp- onent	Peak	Peak ss	Cro- -power	Type
56	4.7	.84	-86	ZN	Yes	Yes		Love
57	6.6	.63	-5.3	NE	Yes	Yes		Love
	4.8	.75	93	EZ	Yes	Yes		
	6.6	.55	46	EZ	Yes	Yes		
58	6.6	.80	15	EZ	Yes	Yes		Love
	5.8	.80	3.9	NE	Yes	Yes		
59	6.2	.70	-8	EZ	Yes	Yes		Love
	4.9	.90	0.5	NE	Yes	Yes		
60	4.3	.92	1.1	NE				Love

## OTTAWA

Trace #	Period	Coherency	Phase	Component	Peak Coh.	Peak Cross power	Type
40	7.3	.60	-110	EZ	Yes	Yes	Rayleigh
41	6.6	.43	-80	EZ	Yes	Yes	Rayleigh
	6.6	.68	49	NE	Yes	Yes	
	4.5	.70	-95	EZ	Yes	Yes	Rayleigh
	5.8	.37	2.6	NE	Yes	Yes	Love
	4.5	.51	2.5	NE	Yes	Yes	Love
42	6.0	.64	-37	EZ	Yes	Yes	
	6.6	.61	52	NE	Yes	Yes	
43	5.7	.42	-72	EZ	Yes	Yes	Rayleigh
	7.1	.50	-16	NE	Yes	Yes	Love
	4.2	.59	-1.2	NE	Yes	Yes	Love
44.5	6.6	.56	29	EZ	Yes	Yes	
	5.6	.48	75	EZ	Yes	Yes	Rayleigh (First Mode)
	4.6	.62	-15	NE	Yes	Yes	Love
45	7.1	.74	96	ZN	Yes	Yes	
	7.1	.57	119	EZ	Yes	Yes	
	7.1	.42	134	NE	Yes	Yes	Love (?)
46	6.6	.51	166	EZ	Yes	Yes	
	6.6	.65	167	ZN	Yes	Yes	
	6.6	.44	8.4	NE	Yes	Yes	Love
	5.2	.76	-92	EZ	Yes	Yes	Rayleigh
	5.2	.44	156	NE	Yes	Yes	Love

Trace #	Per- iod	Coher- ency	Phase	Comp- onent	Peak Coh.	Peak Cro- ss -power	Type
47	4.9	.66	-100	EZ	Yes	Yes	Rayleigh
	5.3	.44	-92	ZN	Yes	Yes	Rayleigh (?)
	6.9	.60	47	EZ	Yes	Yes	
	6.9	.57	14	NE	Yes	Yes	Love

TABLE IV.5

EDMONTON							
Trace #	Period	Coherency	Phase	Component	Peak Coh.	Peak Cross-power	Type
1	7.1	.87	-3.3	NE	No	Yes	Love
	3.8	.92	-3.0	NE	Yes	Yes	Love
2							
3	5.3	.87	1.5	NE	Yes	Yes	Love
	7.1	.32	-119	EZ	No	Yes	
4	7.1	.53	108	EZ	Yes	Yes	
5	4.0	.74	154	NE	Yes	No	
	4.0	.96	-173	EZ	Yes	No	
6	5.8	.55	-100	ZN	Yes	Yes	
	6.4	.45	74	NE	Yes	Yes	Love (?)
7	7.1	0.49	-83	EZ	Yes	No	Rayleigh
8	5.3	.75	1.9	NE	Yes	Yes	Love
	4.0	.71	-160	EZ	Yes	Yes	
9	3.2	.98	-3.1	NE	Yes	Yes	Love
	4.0	.81	164	EZ	Yes	Yes	
10	3.8	.87	-174	NE	Yes	Yes	Love
	4.3	.89	-11	ZN	Yes	Yes	
11	4.3	.69	-112	EZ	No	Yes	Rayleigh
	5.8	.60	-43	NE	Yes	Yes	Love
	5.8	.35	-109	ZN	Yes	Yes	Rayleigh

Trace #	Per- iod	Coher- ency	Phase	Comp- onent	Peak Coh.	Peak Cro- ss-power	Type
12	6.4	.46	-12	NE	Yes	Yes	Love
	6.4	.50	33	EZ	Yes	Yes	
13	8.0	.53	-6.7	NE	Yes	Yes	Love
14	3.2	.99	0.9	NE	Yes	Yes	Love
15							
16	8.0	.82	3	NE	No	Yes	Love
17	4.0	.97	-169	EZ	Yes	Yes	
	2.5	.53	-102	EZ	Yes	Yes	Rayleigh
18	5.3	.59	-15	NE	Yes	Yes	Love (?)
	2.5	.55	-77	EZ	Yes	Yes	Rayleigh
	4.6	.89	-164	EZ	Yes	Yes	
19	4.9	.62	-95	EZ	Yes	Yes	Rayleigh
	3.8	.90	8.6	NE	Yes	Yes	Love
20	6.4	.43	100	EZ	Yes	Yes	Rayleigh (?) (First-Mode)
21	6.4	.50	-91	EZ	Yes	Yes	Rayleigh
	5.3	.52	163	NE	Yes	Yes	Love
22	7.1	.62	-117	EZ	Yes	Yes	Rayleigh
	7.1	.77	-13	NE	No	Yes	Love
	3.2	.90	1.9	NE	Yes	Yes	Love
23	6.4	.49	-13	NE	Yes	Yes	Love
	2.6	.95	-1.0	NE	Yes	Yes	Love

Trace #	Per- iod	Coher- ency	Phase	Comp- onent	Peak Coh.	Peak SS-power	Cro- power	Type
24	5.8	.48	-46	EZ	Yes	Yes		
25	6.4	.58	-70	EZ	Yes	Yes		Rayleigh
28	5.3	.70	17	NE	Yes	Yes		Love
31	5.8	.36	-63	EZ	Yes	Yes		Rayleigh (?)
	5.8	.38	7	NE	Yes	Yes		Love
32	6.4	.57	13	NE	Yes	Yes		Love
33	6.4	.81	-3	NE	Yes	Yes		Love
	6.4	.36	-85	EZ	Yes	Yes		Rayleigh
38	8.0	.34	-103	EZ	Yes	Yes		Rayleigh
	7.1	.62	3	NE	No	Yes		Love (?)

isfied. An event with a peak on coherency and cross-power, and a phase of  $0^\circ$  or  $180^\circ \pm 20^\circ$  between two horizontal components could be tentatively identified as a Love wave if no vertical peak were present. First mode of Rayleigh waves could be identified with a peak on coherency and crosspower, and a phase of  $+90^\circ \pm 20^\circ$  between the vertical and a horizontal component. Since all the three criteria are seldom satisfied simultaneously, use was made of either two or one of the criteria. When only one criterion was used, care was taken to see that the other two were nearly satisfied, and the instances where only one criterion was used are sparse.

In all the cases where a Rayleigh wave was identified the coherency between the vertical and a horizontal component rarely exceeds 0.7 but is often around 0.5 where as in most cases when a Love was identified the coherencies generally exceed 0.7 and more often they are around 0.9. This again shows the complex nature of the microseisms. A large amount of noise on the vertical component could be the reason for such low coherency. The word "noise" has to be understood here as any energy interfering with the Rayleigh wave signal. A body wave (for example a long period leaking P-mode) registered on the vertical component with the same period would definitely have a low coherence with the horizontal component when other wave types are present at the same time. Theoretically, for an LP-mode the vertical leads the horizontal



component by  $180^{\circ}$  but for a Rayleigh mode it lags behind the horizontal component by  $+90^{\circ}$ . So depending on the path difference, the phase between the vertical component and the horizontal component would vary between these two limits if the signal was composed of LP-mode and Rayleigh mode with approximately the same period. Thus the low coherency between these two components or a lack of peak on the crosspower between them or a wrong phase value between them is neither due to the recording nor due to the method of calculation, but is certainly due to the arriving microseisms themselves. As will be shown by the studies on the synthetic microseisms, a large amount of white noise would be required to lower the coherency and change the phase to the observed values. In addition to these factors, low values of coherency between the vertical and horizontal component in question could also be attributed to the fact that the autopower peaks at slightly different periods on these two instruments. The latter is a further evidence which reinforces the idea that body waves of periods around 6 sec are indeed present in the microseisms. Even though the problem of identification of a wave type is beset with tremendous amounts of difficulty, and because of this not all wave types could be properly identified, unmistakable Rayleigh and Love wave examples are not entirely lacking in the data.

IV.2 Five examples of Rayleigh wave can be cited at

Victoria at the periods of 5.8, 4.5, 6.0, 6.0, and 4.9 sec. The maximum value the coherency reaches at these periods is 0.47. Out of the five, three are the events involving east-west and vertical components. Two correspond to the recordings on north-south component and the vertical. This suggests that the Rayleigh waves are arriving at Victoria from at least two directions roughly perpendicular to each other, i.e. from north and west. Excellent examples of Love waves occur at 6.1 and 4.5 secs on the record #13, at 6.1 and 4.6 secs on record #14, 6.4 and 4.6 secs on record #15, and 5.8 secs on record #16. The coherencies are high, usually greater than 0.8 between east and north with phases close to  $0^{\circ}$  or  $180^{\circ}$ . There are certain cases where the coherency between EW and vertical is very high (.90) but the phase is only  $-0.3^{\circ}$ . This wave is tentatively identified as some kind of a body wave. Few cases of first mode of Rayleigh wave could be clearly identified. Some important conclusions can be drawn from this analysis.

1. Surface waves occur at two periods, one around 6.0 seconds and the other around 4.5 seconds.
2. Rayleigh and Love waves arrive at the station in the same time segment having the same frequency.
3. High coherency between the two horizontals shows the Love wave is recorded almost without any interference. Low coherency between the horizontal and vertical indicates some kind of interference for the Rayleigh type

of wave. It could be different modes of of Raleigh wave or in addition there could be an LP-type of motion as the phase values suggest.

4. Direction of approach is not very clear from this analysis, but westerly direction seems to be predominant.

IV.3 Rayleigh wave with periods of 6.7, 6.2, and 4.7 seconds with coherencies between east-west and vertical .48, .45, and .51 and phases -76, -111, and -76 respectively is recorded at Penticton. At this station Love waves have periods of 6.7, 7.1, 6.1, 4.6, 4.5, 6.4, 4.6, 6.4, 4.6, 6.0, 4.5 seconds with high coherencies between north-south and east-west components and right order of magnitude for the phases. The coherencies are as high as .93 and phases are very approximately either zero or  $180^{\circ}$ . Thus we have:

1. Both types of surface waves are again present at two periods, one ranging between 6.0-7.0 and the other around 4.5 seconds.
2. They occur in the same time segment.
3. There is a low coherency between vertical and horizontal for Rayleigh waves and high coherency between the two horizontals for Love waves. Phase values for Rayleigh are out by -15 to  $-21^{\circ}$ ; phase values for Love are of right order.
4. Direction of approach seems to be somewhere in the north-west quadrant.

IV.4 The best example of Rayleigh wave at Resolute occurs at 4.7 secs with a coherency of .84 between vertical and north-south with a phase difference of  $-86^{\circ}$ . Another example is that of a 4.1 sec event with a coherency of 0.71 and

phase of  $-88^{\circ}$  for the east-west and vertical. Rayleigh wave with a period of 6.2 sec with a coherency of .47 and phase of  $-83^{\circ}$  between north-south and vertical is also recorded. There is however no evidence for a 6.0 second Rayleigh wave coming from west or east. Love waves of 6.9, 6.4, 6.1, and 4.5 seconds are also recorded at Resolute. They have expected phase relationships between the two horizontals.

IV.5 Two events, one around 6.5 sec and the other around 4.6 sec are found on Ottawa records. Rayleigh waves have an east-west direction of approach. One excellent example occurs on record #46 at the period of 5.2 sec with a coherency of 0.76 and phase of  $-92^{\circ}$  between the vertical and east-west. Love and Rayleigh waves have approximately the same order of coherency. There is one instance of a northerly approaching Rayleigh wave.

IV.6 The best example of Rayleigh wave occurrence at Edmonton is on record #21 at period of 6.4 sec with a coherency of .50 between east-west and vertical components and a phase of  $-91^{\circ}$ . In addition to the event with a period of 4.9 sec., another event at 2.5 sec can be easily seen at this station. Surface wave period changes with time and the range of variation is 5.3-8.0 sec and 4.0-5.0 sec and the third one occurring around 2.5 sec. This wide range is probably due to the crustal layering at Edmonton. The 2.5 sec event

is likely due to the unconsolidated sediments overlying the Precambrian. The relatively larger amplitudes of the short period peak at Edmonton compared to stations at both greater and lesser distances from the presumed source suggests that the effect cannot be due solely to differing attenuations with distance but must be related in some way to the unconsolidated sediments overlying the Precambrian at Edmonton.

In summary then:

1. Rayleigh and Love waves arrive at the station simultaneously.
2. They have approximately the same periods.
3. Two predominant periods can be recognized for these waves. One train of waves has a period around 6.5 sec and the other around 4.5 sec. Yet another event of 2.5 sec could be identified only at Edmonton.
4. There seems to be more than one direction from which the waves are approaching the recording site.
5. The coherency between the two horizontals is high indicating a coherent propagation of Love waves in the crust. The coherency between the vertical and any one horizontal component rarely exceeds 0.70 suggesting an interference of fundamental and higher Rayleigh modes and LP-modes.
6. The phases are in most cases correct for a Love wave but vary by approximately  $20^\circ$  for the Rayleigh wave, a circumstance supporting the interference above.
7. Certain wave types with a coherency of as high as .90 between the vertical and a horizontal component but phase of  $0^\circ$  or  $180^\circ$  were conspicuous in the spectral analysis. These wave

types have a period also around 6.5 sec. and strongly suggest the existence of long period body waves in microseisms.

8. One or two examples of first mode of Rayleigh wave could be identified.

IV.7 Wherever there was a good example of Rayleigh wave, the vertical to radial ratio was calculated (radial being the EW component) for both events of 6.5 secs and 4.5 secs and the results are listed in Table IV.6. The crustal structure at all these stations is approximately known from the literature. From the known crustal structure Rayleigh wave dispersion curves were calculated and the vertical to horizontal ratio computed. These theoretically calculated ratios are compared with the observed ones in Table IV.7. The crustal models used are shown in Table IV.8. The models at Victoria and Penticton are taken from White et al (1965), that at Edmonton from Cumming et al (1966), at Ottawa from Brune et al (1963) and finally at Resolute from Sander et al (1965). The method used in computing the dispersion curves is that described by Thomson (1950) and later generalized by Haskell (1953) and subsequently known as the Haskell-Thomson method. A program earlier described by Press et al (1961) and later expanded by Harkrider and Anderson (1962) was used to calculate the dispersion. An isotropic model was used for all locations.

For the longer period event the agreement between

## VERTICAL-HORIZONTAL AMPLITUDE RATIOS FOR RAYLEIGH WAVE

Site	Vertical <sup>2</sup>		Horizontal <sup>2</sup>		V <sup>2</sup> /H <sup>2</sup>		V/H	
	6.5	4.5	6.5	4.5	6.5	4.5	6.5	4.5
Period in Secs	6.5	4.5	6.5	4.5	6.5	4.5	6.5	4.5
Victoria	8.6	.55	15.2	2.2	.57	.25	.75	.5
Penticton	6.6	5.5	2.5	6.0	2.6	.92	1.6	.96
Edmonton	3.1	.74	2.7	1.8	1.1	.41	.10	.64
Resolute	.09	.096	.10	.11	.9	.87	.95	.93
Ottawa	.05	.20	.09	.08	.56	215	.75	1.6

TABLE IV.7

## COMPARISON WITH THEORETICAL VALUES

Site	6.5 sec		4.5 sec	
	Exper	Theo	Exper	Theo
Victoria	0.75	0.90	0.50	0.80
Penticton	1.6	0.98	0.96	0.98
Edmonton	1.01	1.1	0.64	0.91
Resolute	0.95	0.69	0.93	0.70
Ottawa	0.75	0.72	1.6	0.66

TABLE IV.8

## CRUSTAL MODELS

	Thickness	P-wave Velocity
1. Victoria	2.5 km	4.4 km/sec
	6.2 km	6.0 km/sec
	45.0 km	6.73 km/sec
		7.74 km/sec
2. Penticton	1 km sediments	
	20 km	5.91 km/sec
	5 km	6.8 km/sec
		7.8 km/sec
3. Edmonton	2.0 km	3.0 km/sec
	3.0 km	5.2 km/sec
	10.0 km	6.1 km/sec
	20.0 km	6.5 km/sec
	11.0 km	7.2 km/sec
		8.2 km/sec
4. Resolute	20.0 km	6.0 km/sec
	20.0 km	7.3 km/sec
		8.2 km/sec
5. Ottawa	6.0 km	5.64 km/sec
	10.5 km	6.15 km/sec
	18.7 km	6.6 km/sec
		8.1 km/sec

Comments

1. Victoria: Travel time curves of White and Savage (op.cit.) all indicate that a thin layer of low velocity material is present. Values used are estimated from this data.
2. Penticton: Negligible low velocity surface material is present. (White, Bone and Milne, 1968).
3. Edmonton: This model is based on Cumming and Kanasewich (op.cit.) Ellis and Basham (op. cit.) indicate thinner second layer.



observed and calculated values is good at all stations except at Penticton. For the shorter period event the agreement is good only at Penticton and Resolute. Major discrepancies occur for the long period event at Penticton. For the shorter period event the agreement is good only at Penticton and Resolute. Major discrepancies occur for the long period event at Penticton and short period event at Ottawa. If we assume microseisms contain body waves and surface waves, this discrepancy could be attributed to a major contribution from LP-waves which would reflect in the larger value of amplitude on the vertical component. Observe that the values cited in Table IV.6 pertain to only one record where Rayleigh wave was identified on the basis of correct phase and coherency values. Discrepancy could then be ascribed to the lack of knowledge of crustal layering at Penticton. However the discrepancy at Ottawa for the 4.5 sec event can not be readily explained. These results at least partly confirm that the radial direction is approximately EW at every station for the record chosen with the waves approaching the sites from a westerly direction.

IV.8 All the results enumerated so far point out that the arriving microseisms are very complex in their nature. They arrive from different directions; they are not simple Rayleigh and Love waves, but are a mixture of fundamental and higher modes; the wave types even include some body waves. Since

the coherency is usually less than 0.7 (especially for Rayleigh waves), there appears to be considerable random noise contained in the records. It is this randomness that seems to be the crux of the problem.

An attempt was made to combine a signal with random numbers and calculate the crosspower, coherency and phase between two components simulating a Rayleigh wave, with  $-90^\circ$  phase difference, and between a second set of two components with  $180^\circ$  phase difference simulating a Love-type of wave. Random numbers were generated and added to these signals in different proportions. Five cases were tested.

The signal to (white) noise ratio in these five cases is 1) 1/1, 2)  $1/\sqrt{2}$ , 3) 1/5, 4) 1/10, and 5) 1/20.

Table IV.9 lists the phase and coherency values between the two traces for these five cases for the two wave types considered. The following features stand out of these investigations:

1. Coherency falls to less than one half for both wave types only in the case when the noise is 20 times the signal.
2. Phase changes by  $10^\circ$  for the Rayleigh type of motion and  $16^\circ$  for the Love type of motion in the fifth case when the noise is 20 times the signal.
3. The values obtained for coherency in the fifth case (a signal to white noise ratio of 1/20) are comparable to the experimentally obtained values for the Rayleigh type of motion.
4. The comparison of the experimental values with the ones obtained in Table IV.9 for coherency

## SYNTHETIC MICROSEISMS AND RANDOM NOISE

S/N	Rayleigh Type		Love Type	
	Coherency	Phase	Coherency	Phase
1	1.0	-89	1.0	179.0
1/√2	0.99	-88.0	.99	178.4
1/5	0.84	-84.0	.90	176.0
1/10	0.78	-82.0	.86	170.0
1/20	0.44	-80.9	.49	164.8

of Love type motion indicates that in the case of Love wave the signal to noise ratio is somewhere between  $1/\sqrt{2}$  and  $1/5$ .

5. The comparison of phase values would put the signal to noise ratio even lower for both wave types. Even a considerable amount of white noise by itself is not capable of changing the phase by more than  $20^\circ$ .
6. The microseisms as observed on the records exhibit a clear sinusoidal motion with beat phenomenon superimposed on them. A signal to noise ratio of  $1/20$  can not produce the type of sinusoids seen on the records and hence this type of noise clearly does not model the observed records.
7. In order to explain the low coherency observed for Rayleigh waves, and at the same time the high coherency observed for Love waves, one has to concede that white noise in any proportion is not an adequate explanation of the observed data. The phase values suggest that other types of motion must be present in the microseisms but associated with Rayleigh and Love waves. That these spurious phase values are not introduced by the method of analysis is clear from the fact that even though the data on all the components are subjected to the same mathematical operations, the phase between horizontal components is often appropriate for Love waves, while results including vertical motion are seldom reasonable for simple Rayleigh waves.
8. Since the "randomness" or "noise" is not solely due to 1) white noise which is incapable of producing the observed coherency and phase values while preserving the general appearance of the records, 2) the method of analysis, and 3) the recording instruments; it must be associated with the nature of the arriving microseisms themselves.
9. In tables IV.1-5, one can observe some wave types which have a phase relationship of  $0^\circ$  or  $180^\circ$  between the vertical and horizontal components with a coherency as high as 0.9. If this is some kind of a leaking LP-mode, then the interference of Rayleigh motion and

LP-motion may be responsible for the low coherencies observed between the vertical and horizontal components for the majority of the data.

## CHAPTER V

### JENSEN'S DIAGRAMS AND PARTICLE MOTION TRAJECTORIES

V.1 A brief description of the method of plotting Jensen's diagrams was given in I.6. The first derivatives of the two horizontal components with respect to time are calculated at the points of maxima on the vertical component. These two are then plotted against each other and this plot would then describe the velocity of the particle. An average of several velocity vectors would give the direction of approach. All the points would lie on the half plane away from the source for a fundamental Rayleigh mode, because of the retrograde nature of the particle motion. For a first Rayleigh mode they would lie on a half plane towards the source. All these points tend to cluster around the line along which the pure Rayleigh wave is propagated. For a combination of fundamental Rayleigh mode and Love wave the points still fall on a half plane away from the source but in this case the points are widely dispersed from the line representing the direction of approach. For a combination of first Rayleigh mode and Love wave the points still lie on a half plane towards the source but they are widely dispersed around the line along which the waves are propagated. For an SV-type or SH-type of motion these points representing the velocity vectors would fall on the half plane towards the source, but

form a straight line. In the former case there is no appreciable horizontal motion and in the latter case there is no appreciable vertical motion.

If the points are spread around the centre (point of intersection of the two axes representing slopes of two horizontal components) it would indicate i) either the waves are approaching the site from different directions, or ii) the signal is composed of different wave types.

It is desirable to suppress the noise as much as possible in order to draw any meaningful Jensen's diagrams so a Butterworth band pass filter was used on the data before plotting. The band pass was centered at around 6.0 sec which is the most prevalent period in the microseisms. The filter designed by Butterworth (1930) is fully described by Weinberg (1962). A brief outline is given here.

## V.2 The function

$$|Y(\bar{\omega})|^2 = \frac{1}{1 + \bar{\omega}^{2n}} \quad (1)$$

describes the low pass Butterworth filter, where  $\bar{\omega}$  is normalized frequency,  $\bar{\omega} = \omega / \omega_c$ ,  $\omega_c$  being the cut off of frequency. The function does not tend to oscillate in the band pass and this property is exploited to design a maximally flat curve, which falls off rapidly outside the pass band as  $n$  is increased. Poles of the low pass filter are obtained by taking the Laplace transform of (1).

$$\text{Thus } |Y_L(p)|^2 = \frac{1}{1 + (-1)^n p^{2n}} \quad (2)$$

where  $p = \rho + i\bar{\omega}$  and  $\rho = 0$ . There are no zeroes in a low pass filter except at infinity and the poles are given by

$$1 + (-1)^n p^{2n} = 0 \quad (3)$$

In general  $|Y_L(p)|^2$  can be represented as

$$[Y_L(p)]^2 = \frac{1}{B_n(p)B_n^*(p)} \quad (4)$$

$B_n(p)$  being known as Butterworth polynomial. In the  $p$  plane  $B_n(p)$  can be shown to be

$$B_n(p) = \prod_{v=0}^{n-1} \left( p - e^{\frac{in}{2n}(2v+1+n)} \right) \quad (5)$$

For a high pass filter the frequency transformation is given by  $S = \bar{\omega} + i\omega$  where  $\bar{\omega} = \omega/\omega_H$ ,  $\omega_H$  is cut off frequency.

For a band pass filter the normalized frequency transformation is  $p = S + \frac{1}{S}$  (6)

The normalized relations must be generalized to the desired band pass filter with unnormalized upper and lower frequency limits  $\omega_1$  and  $\omega_2$ . The geometric mean is sometimes called the center frequency. Any other frequency with a particular attenuation is related to a higher frequency,  $\omega_k$  by the relation

$$\omega_0 = \sqrt{\omega_\ell \omega_k} \quad (7)$$

The band width  $\Delta\omega$  is obviously  $\omega_k - \omega_\ell$ . The band width will be rescaled by dividing by the geometric mean



$$\Omega_1 = \frac{\omega_2 - \omega_1}{\omega_0}$$

Any frequency in general can be given by

$$\Omega = \frac{\omega}{\omega_0} - \frac{\omega_0}{\omega}$$

Normalized frequency is then

$$\bar{\Omega} = \frac{\Omega}{\Omega_1} = \frac{\omega^2 - \omega_1\omega_2}{\omega(\omega_2 - \omega_1)}$$

Since  $p = i\bar{\Omega}$  and  $S = i\omega$ , we obtain

$$S^2 - p(\omega_2 - \omega_1)S + \omega_1\omega_2 = 0 \quad (8)$$

is a quadratic in  $S$ .

The transfer function has the form

$$Y_L(p) = \frac{1}{(p-p_1)(p-p_2)(p-p_3)(p-p_4)} \quad (9)$$

for a fourth order Butterworth polynomial, if we consider a band pass filter,  $p = S + \frac{1}{S}$ . Equation (9) can be reduced to

$$Y_{BP}(S) = \left(\frac{S}{S^2+b_1S+c_1}\right) \left(\frac{S}{S^2+b_2S+c_2}\right) \left(\frac{S}{S^2+b_3S+c_3}\right) \left(\frac{S}{S^2+b_4S+c_4}\right) \quad (10)$$

The coefficients  $b_j$  and  $c_j$  are obtained from the pole positions, which occur in complex conjugate pairs to make each of the above terms in brackets real.

$$(S - S_j)(S - S_j^*) = S^2 + b_jS + c_j \quad (11)$$

The continuous  $S$  plane representation has now to be modified to a digital  $Z$  - plane. The standard  $Z \leftarrow$  transform is

is 
$$z = e^{-S(\Delta t)} \quad (12)$$

( $\Delta t$ ) being the digitizing interval. In order to eliminate the aliasing errors present in the standard  $z$  - transform, one uses a bilinear  $Z$  - transform following Golden and Kaiser (1964). The desired transformation is then

$$S_d = (2/\Delta t) (1-Z)/(1+Z) \quad (13)$$

$$S_d = 2/\Delta t \tanh 1/2\Delta t \text{ because of (12)}$$

In the frequency domain  $S_d = i\omega_d$  and using  $\tanh x = -i \tan ix$ , we have 
$$\omega_d = \frac{2}{\Delta t} \tan \frac{\Delta t}{2} \quad (14)$$

From (10) then

$$\begin{aligned} \frac{S_d}{S_d^2 + b_j S_d + c_j} &= \frac{\frac{1}{a_j}(1 - z^2)}{1 + \frac{z}{a_j}(c_j \Delta t - \frac{4}{\Delta t}) + \frac{z^2}{a_j}(\frac{2}{\Delta t} - b_j + c_j \frac{\Delta t}{2})} \\ &= \frac{\frac{1}{a_j}(1 - z^2)}{B_j} \end{aligned} \quad (15)$$

where 
$$a_j = \frac{2}{\Delta t} + b_j + c_j \frac{\Delta t}{2}$$

$$B_j = 1 - D_{1j}z + D_{2j}z^2$$

$Z$  - transform of a Butterworth band pass filter with eight poles is given by

$$W(Z) = \frac{(1-Z^2)^4}{B_1(Z)B_2(Z)B_3(Z)B_4(Z)} \quad (16)$$

The  $Z$  - transform thus has both singularities and poles.

Equation (16) can be modified to give a  $Z$  - transform for a band pass filter with four poles.

$$W(Z) = \frac{(1-Z^2)^2}{B_1(Z)B_2(Z)} \quad (17)$$

where  $B_1 (Z) = 1 - 1.307476Z + 0.450190Z^2$

$$B_2 (Z) = 1 - 1.494986Z + 0.724783Z^2$$

In equation (10)

$$b_1 = 94.10519; c_1 = 2882.33984$$

$$b_2 = 40.34528; c_2 = 3975.04687$$

The singularities in equation (17) are given by

$$z_1 = 1.452137 \pm i 0.335533$$

$$z_2 = 1.031333 \pm i 0.562206$$

A programme was in operation previously (Alpaslan, M.Sc Thesis 1968) for an eight pole transfer function for a Butterworth band pass filter. The filter was thought to be too severe for microseisms and the programme was modified for a four pole transfer function. The programme can be manipulated to give a zero phase-shift response. The amplitude response is fairly flat with sharp cut offs at the two limits of frequency.

The operation of this filter on microseisms is illustrated in Figures V.1-3. In Figure V.1 is shown the autopower spectrum of vertical component of a particular record (from Ottawa) on which two peaks at around 6 seconds and 16 seconds were found. The autopower spectrum was calculated for this trace after it was band pass filtered for two bands .10 - .05 and .20 - .10, and the results are shown in Figures V.2 and V.3. The filter is obviously very effective in rejecting signal outside the

POWER SPECTRUM OF THE UNFILTERED DATA

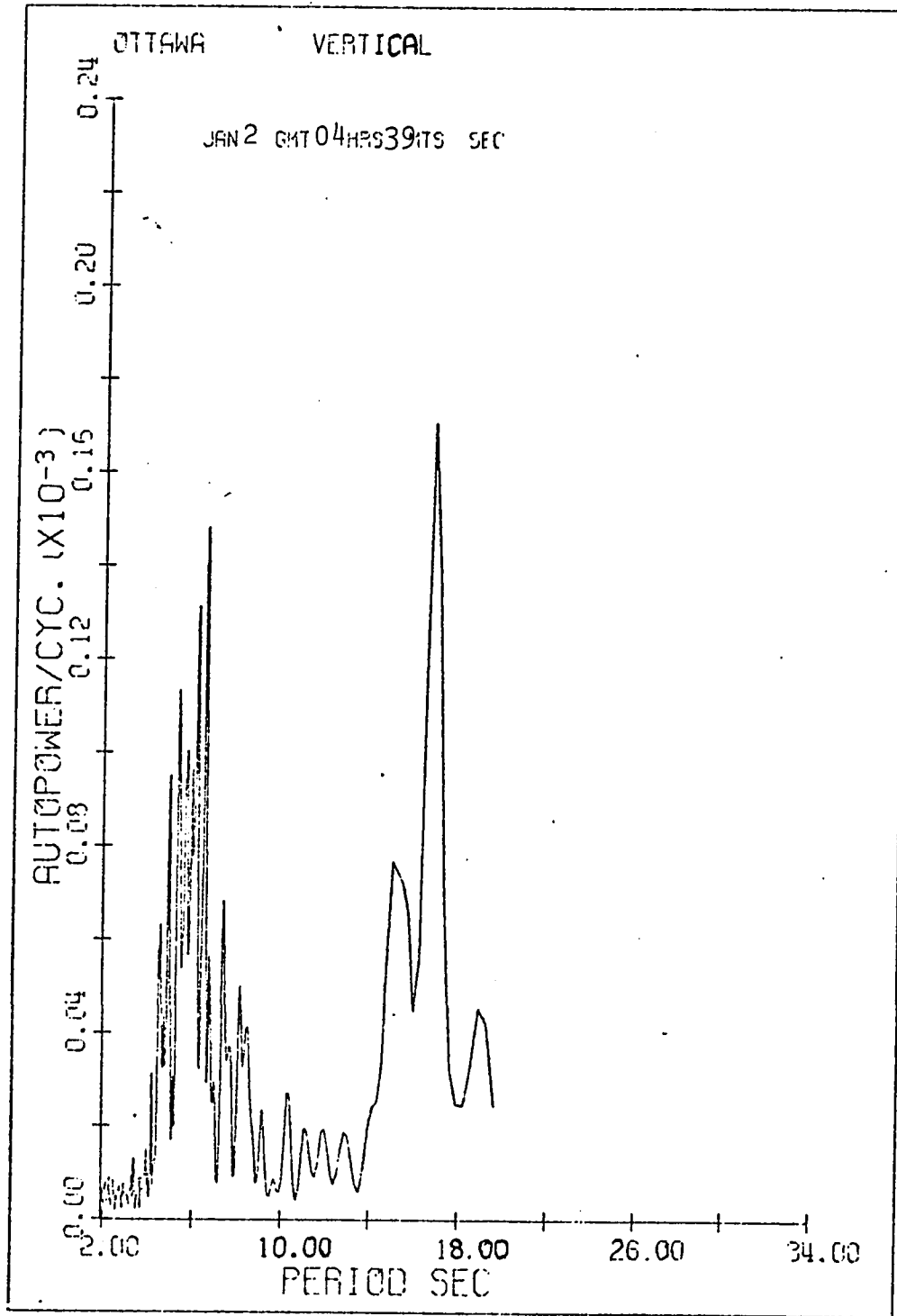


FIG V.1

POWER SPECTRUM OF THE FILTERED DATA  
BAND PASS 0.05-0.10 hz

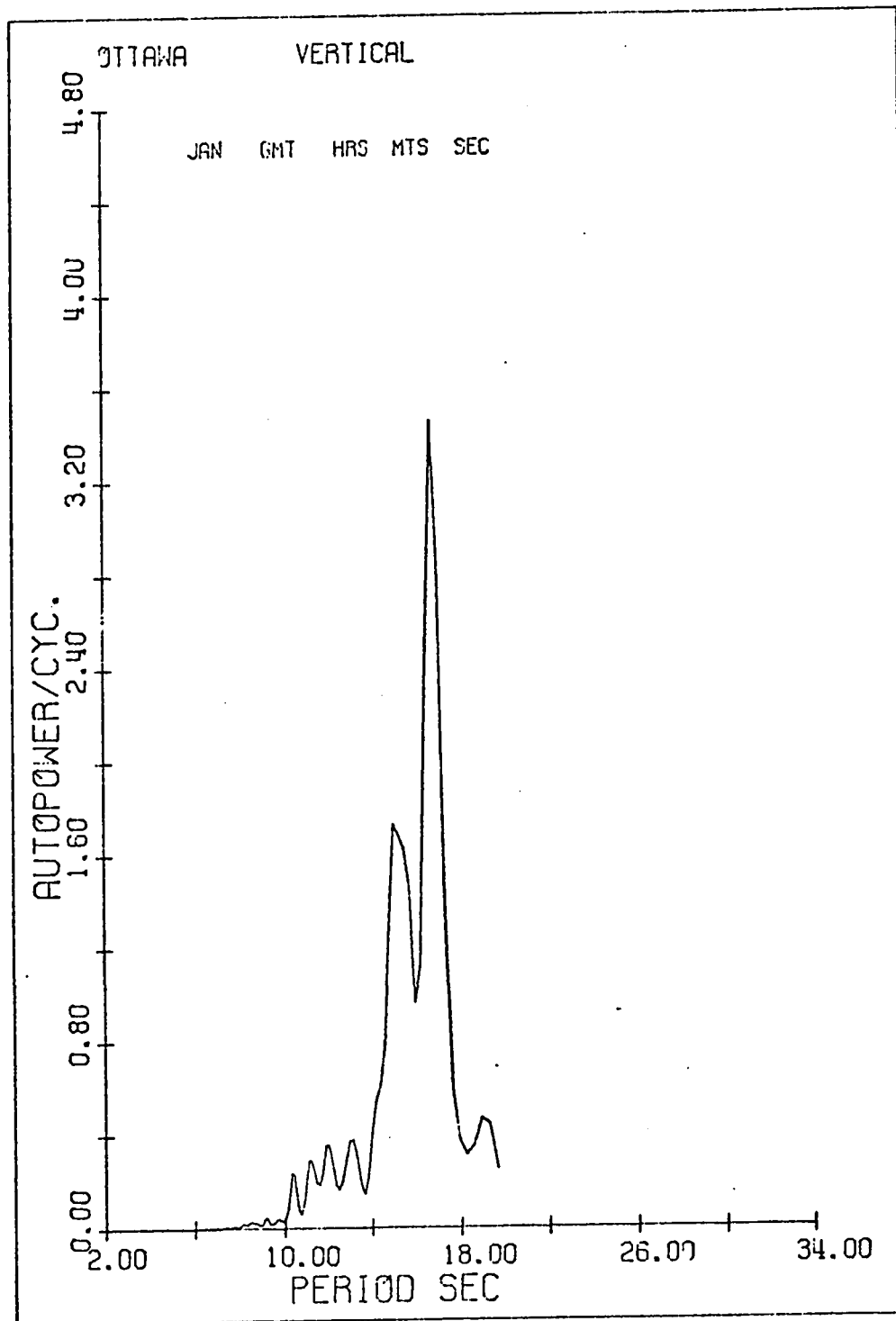


FIG V.2

POWER SPECTRUM OF THE FILTERED DATA

BAND PASS 0.10-0.20 hz

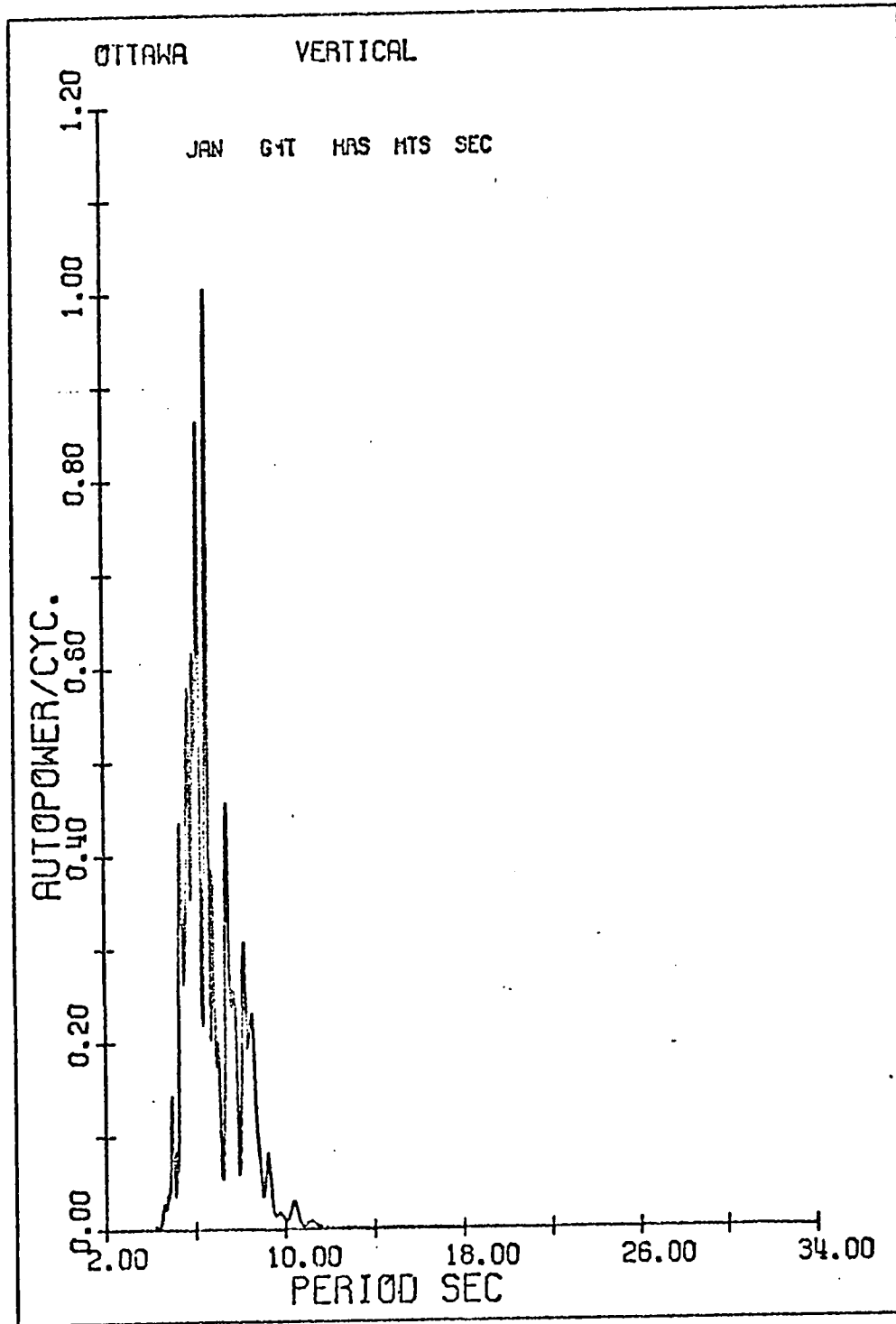
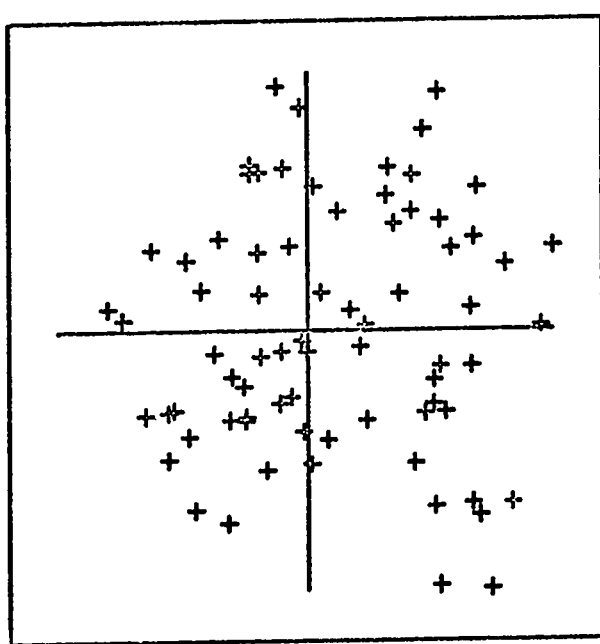


FIG V.3

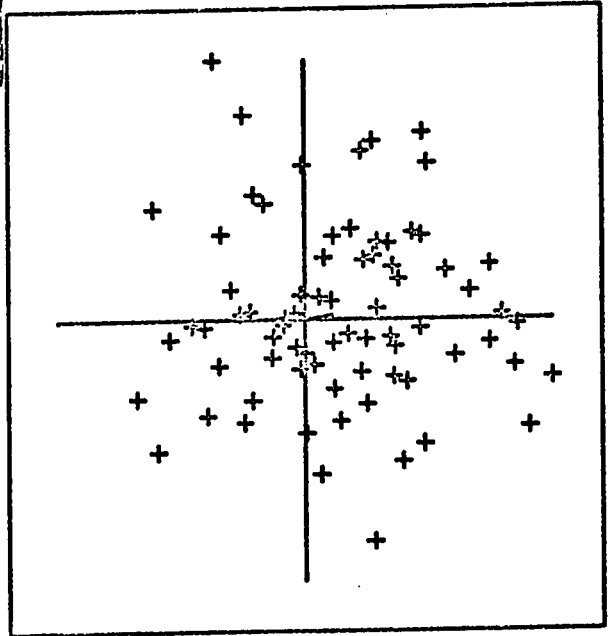
desired pass band.

V.3 The microseismic data were Butterworth band pass filtered and Jensen's diagrams were drawn for several cases. These diagrams did not show any encouraging results. Since the filter did not introduce any undesirable frequencies or phases (note that the filter was manipulated to give a zero phase-shift response), the lack of any coherent direction of approach is attributed to the arriving microseisms themselves. In Figures V.4-5 are shown some typical Jensen's diagrams for the three stations Victoria, Pen-ticton and Edmonton. In almost all these diagrams the points are not confined to one half plane, thus indicating that the microseisms recorded at these sites are indeed composed of different types of surface waves superimposed in a complex fashion. As will be shown in the next chapter on the rotated crosspower, it is possible to find in several cases a direction of approach correct to plus or minus ten degrees. Since this magnitude of error is not solely capable of producing the large amounts of scattering observed in the Jensen's diagrams, it is believed that microseisms are very complex in their content of physical wave types. If it were possible to separate the different wave types, perhaps using an array of tripartite stations, then meaningful diagrams might be drawn, but with the present data it appears that this technique is not capable of producing useful results.

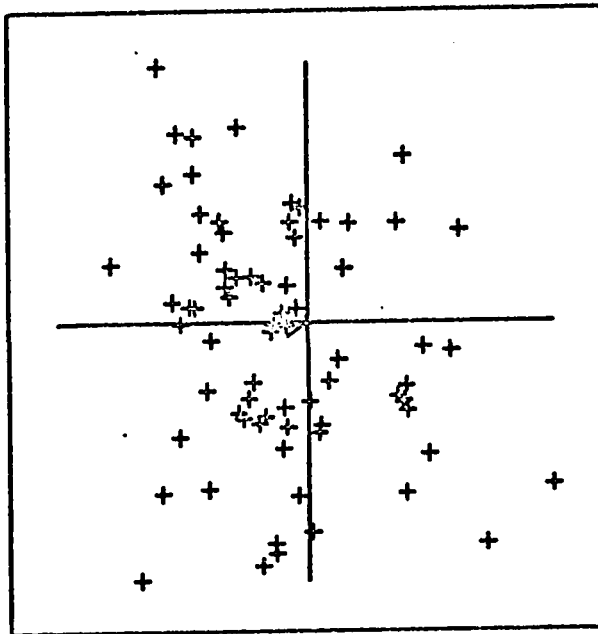
JENSEN'S DIAGRAMS AT VICTORIA



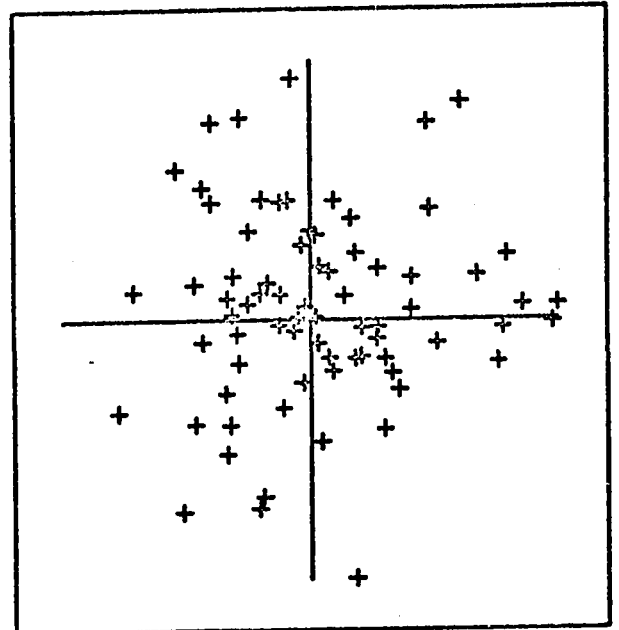
Record #5



Record #9



Record #4



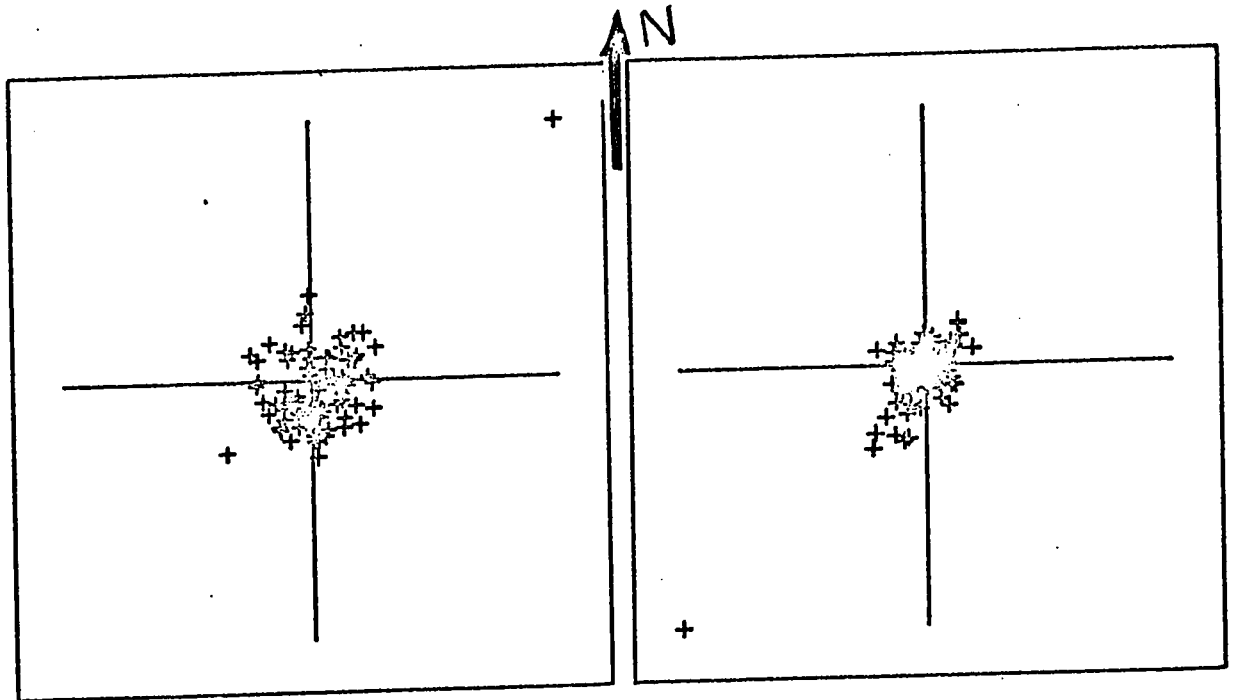
Record #8

(All record numbers as on T00472)

FIG V.4

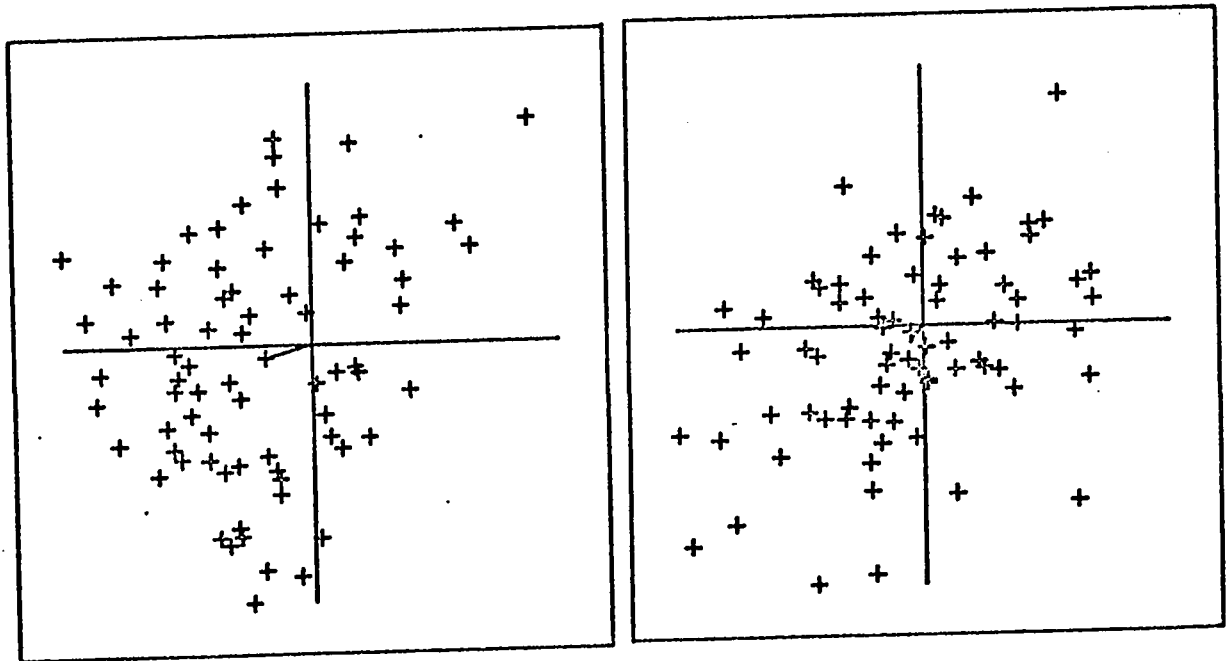


JENSEN'S DIAGRAMS AT PENTICTON



Record #19

Record #23



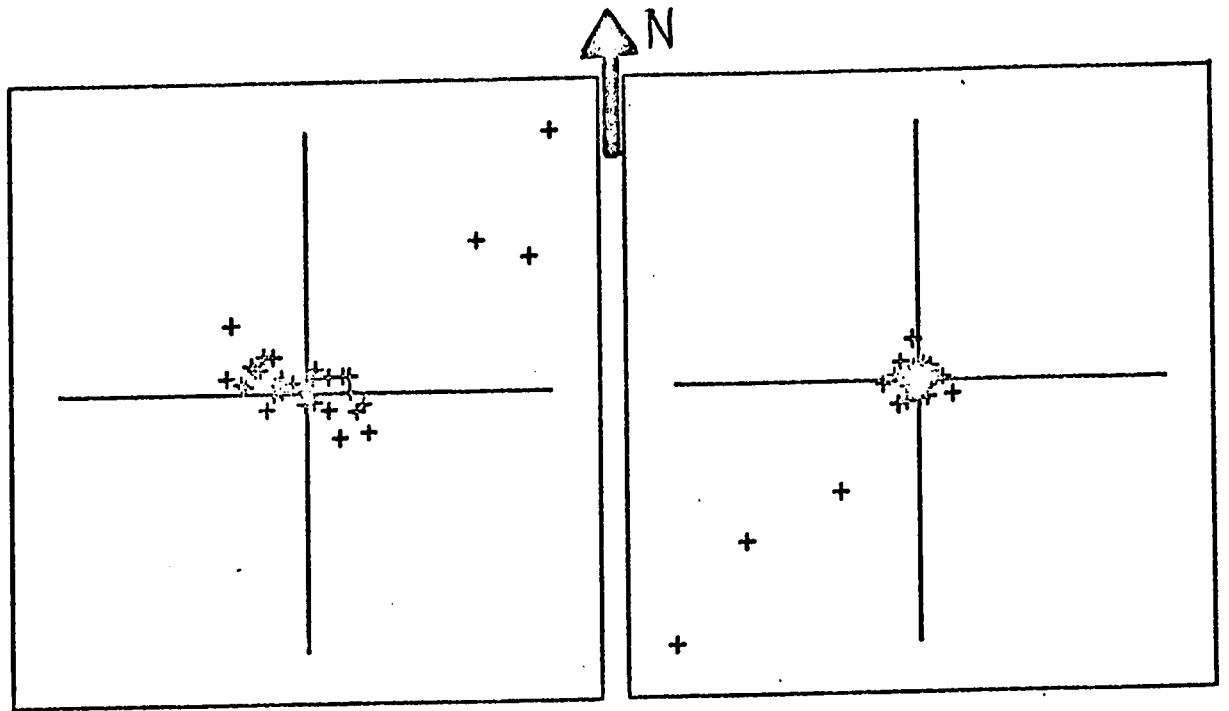
Record #18

Record #22

(All record numbers as on T00472)

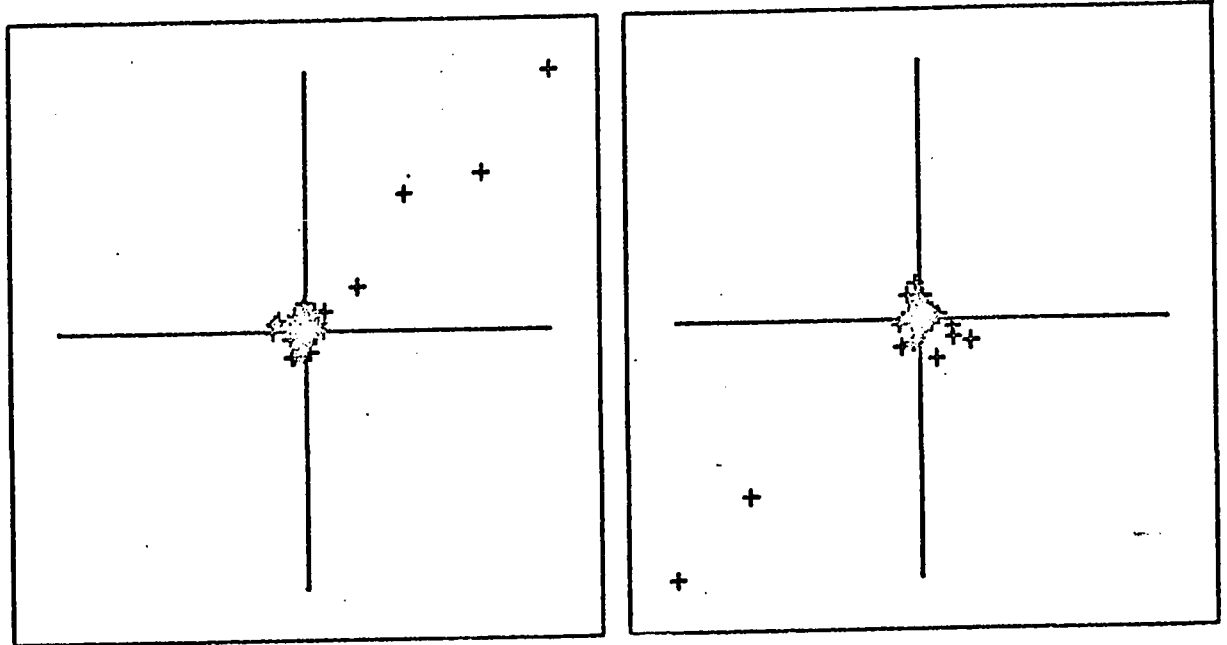
FIG V.5

JENSEN'S DIAGRAMS AT EDMONTON



Record #33

Record #29



Record #32

Record #28

(All record numbers as on T00472)

FIG V.6

V.4 It is also possible to draw particle motion trajectories using the filter traces. Two such sets of diagrams can be drawn; one of them between the vertical component and the horizontal component rotated into the approximate direction of approach of the waves, and the second between the two horizontal components again rotated so that the radial direction corresponds to the approximate direction of source. The former should be a Rayleigh wave trajectory and the latter a Love wave trajectory with respectively elliptical and linear particle motions.

In figures V.6-7 are illustrated the particle trajectories drawn between

- 1) the vertical and the radial components (for Rayleigh wave)

- 2) the radial and the transverse components (for Love wave) at Victoria and Penticton. The examples shown were chosen from among several such diagrams. Although particularly in Fig. V.7 there is some indication of polarization of the trajectories, if one were to examine similar diagrams constructed at slightly different times the plane of polarization would be seen to have rotated to a new direction and in general there does not seem to be any clear cut particle motion.

It may also be noted that for the vertical-radial plot

- 1) the axis of the trajectory is inclined to the

PARTICLE TRAJECTORIES AT VICTORIA

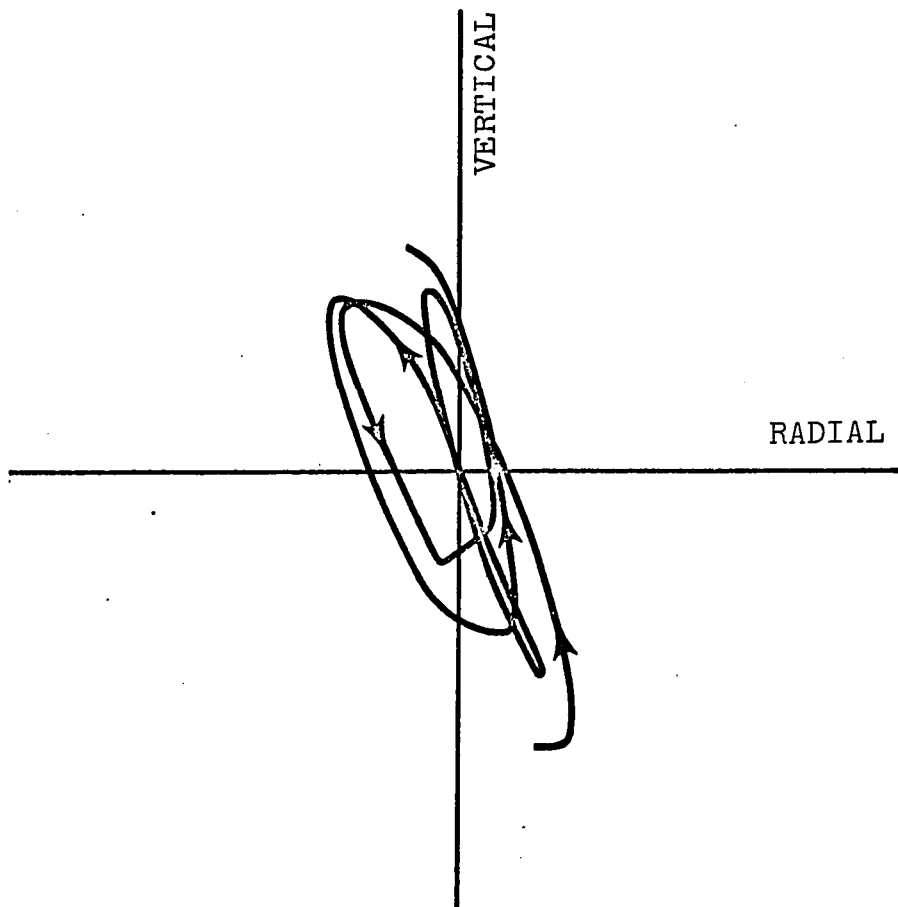
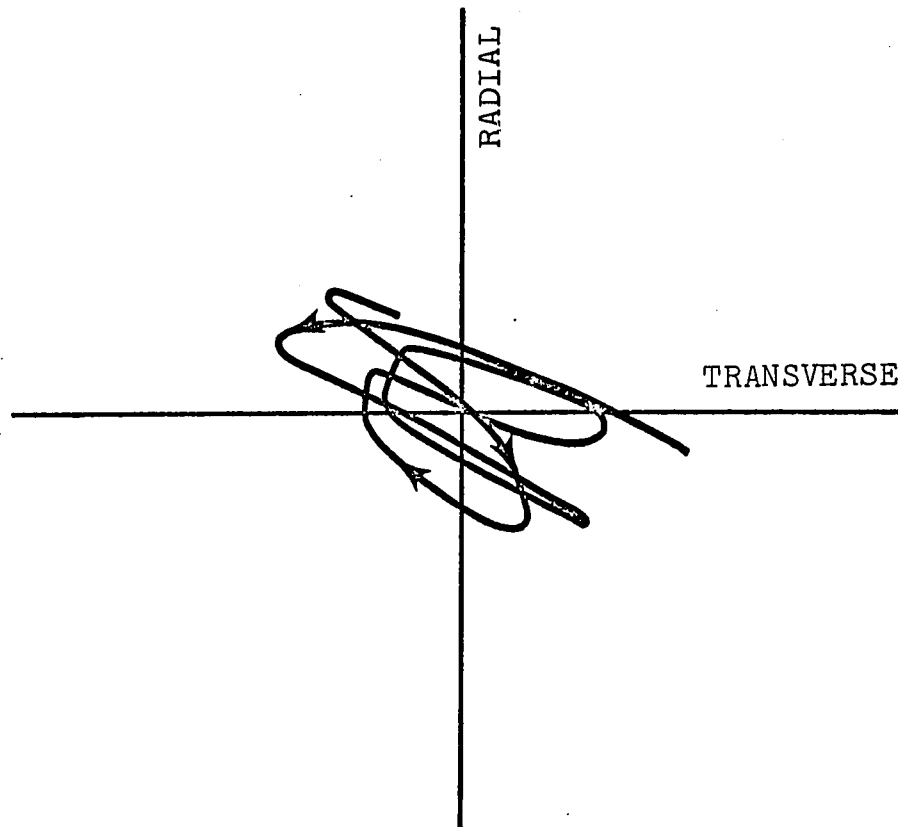


FIG V.7

PARTICLE TRAJECTORIES AT PENTICTON

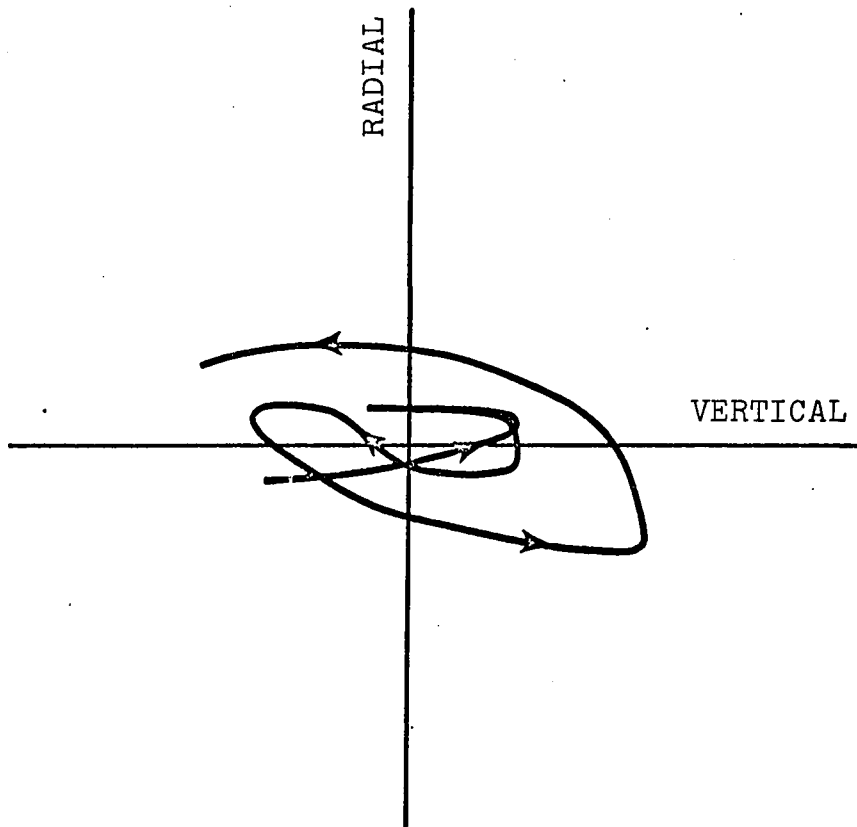
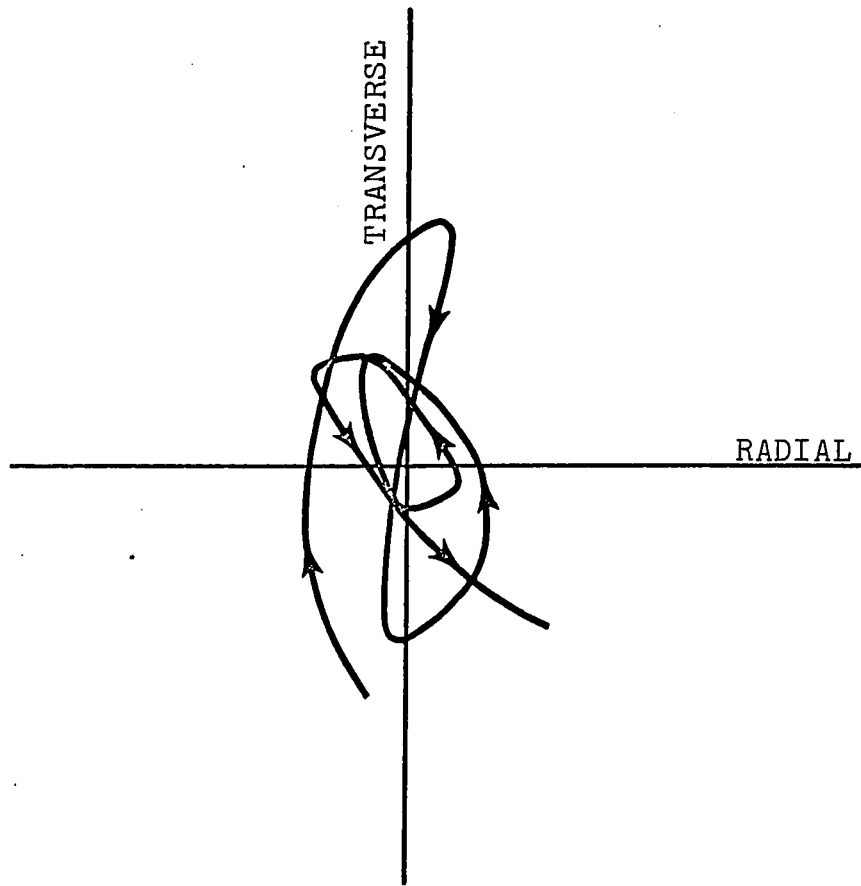


FIG V.8

vertical;

- 2) the motion is retrograde at the start, but it switches to prograde later in this particular time segment; this can be especially seen in Fig. V.8.

and 3) there is a large "vertical" to "horizontal" ratio (almost three to one)

## CHAPTER VI

### DIRECTIONAL SPECTRA

VI.1 It is clear from what has been said so far that the determination of such a simple property as the direction of approach of the surface waves is a difficult problem when one has available only single three-component stations. It is even more difficult in most cases to determine with any degree of certainty what types of waves are present in the data. In some cases one can assume that the source is roughly in the direction of one of the horizontal components and thus get some idea of the possible wave types from the relations between crosspower, coherency and phase but a more detailed analysis is obviously desirable.

The approach taken here is to first compute the resultant horizontal motions at various azimuths starting in a westerly direction and rotating the axes clockwise at  $10^\circ$  intervals to a maximum of  $180^\circ$  at which point the data then repeats with the phase reversed. For convenience the initial west component is referred to as "radial" and the orthogonal component as "transverse", and this terminology is maintained throughout the rotation.

The data were then used to calculate the crosspower, coherency and phase between the vertical and the radial components, and between the radial and the transverse components, for each rotation. These quantities were written on a grid as functions of two variables, azimuth and period and then contoured. Four such maps, two for crosspower and two for coherency were prepared at each station. In addition to coherency and crosspower, the phase between the two components involved was also written on the grid as a function of two variables, azimuth and period. No contour diagrams for phase values was drawn as they varied in an extremely random fashion from period to period.

VI.2 Some properties of these contour maps can be enumerated as follows:

1. Maxima and minima in the crosspower and coherency of the original data will now be reflected in the contour map as high and low closures.
2. From the properties of the rotation and the crosspower calculations, it can be seen that, when dealing with vertical-horizontal power, the value will repeat after  $180^\circ$  (one full rotation) and any high will have a corresponding low separated from it by  $90^\circ$  (one half rotation).
3. The values of crosspower and coherency between the two resolved horizontal components will be repeated every  $90^\circ$  and the highs and lows will be separated by  $45^\circ$ .
4. For vertical-radial data a single direction of propagation of the wave will result in a high, sharply defined in azimuth, whereas a diffuse source will result in a broad peak and the half-power width can be used as a measure of the angular size of the source region.
5. For radial-transverse power a Rayleigh wave coming from a single direction will result in a sharply defined high as above, but the maximum will occur  $45^\circ$  away from the direction of approach. The presence of Love waves in the data will result in departures from this relationship and the position of maxima and minima will be a function of the magnitude and direction of the Love component. If, for example, the Love and Rayleigh waves approach from the same direction and are coherent the maximum in the horizontal crosspower will occur at the same direction as that for vertical-radial crosspower and the coherency will be high.
6. The crosspower  $90^\circ$  from a maximum represents noise from that azimuth and if we make the reasonable assumption that the noise is isotropic we can use the ratio between high and low crosspower as a measure of microseismic signal to noise ratio.



7. The ratio of the magnitude ( $A^2$ ) of the vertical autopower spectrum to the cross-power(AB) between vertical and radial at the same period is the ratio of vertical to radial amplitudes and this may then be compared with Rayleigh wave values calculated from dispersion curves for layered media.

VI.3      A sample of these contour maps for each station is shown in Figures VI.1-5. It should be mentioned here that the samples chosen correspond to those times at which there is a maximum peak value on the autopower spectrum of the vertical. This maximum is reached at different times at different sites. As a result these samples also differ in time and the position of the storm center is therefore different for the various examples. On these grids the angles of rotation are given in columns and the periods as rows. By the side of the contour map is given a plot of the autopower spectrum of the vertical component. This plot is given only on those maps where vertical component is involved either in the crosspower or in the coherency calculation.

At Victoria there is one peak at 6.56 seconds on the autopower spectrum of the vertical component. A high at this period can be seen on both contour maps, for coherency and crosspower between the vertical and the radial components at the directions of  $60^\circ$  and  $65^\circ$  measured clockwise from West. (Note that all directions mentioned here are measured in this manner.) Phase for this event is  $90^\circ$  a possible indication of prograde Rayleigh motion. On

CROSS-POWER BETWEEN VERTICAL AND HORIZONTAL COMPONENTS AT VICTORIA

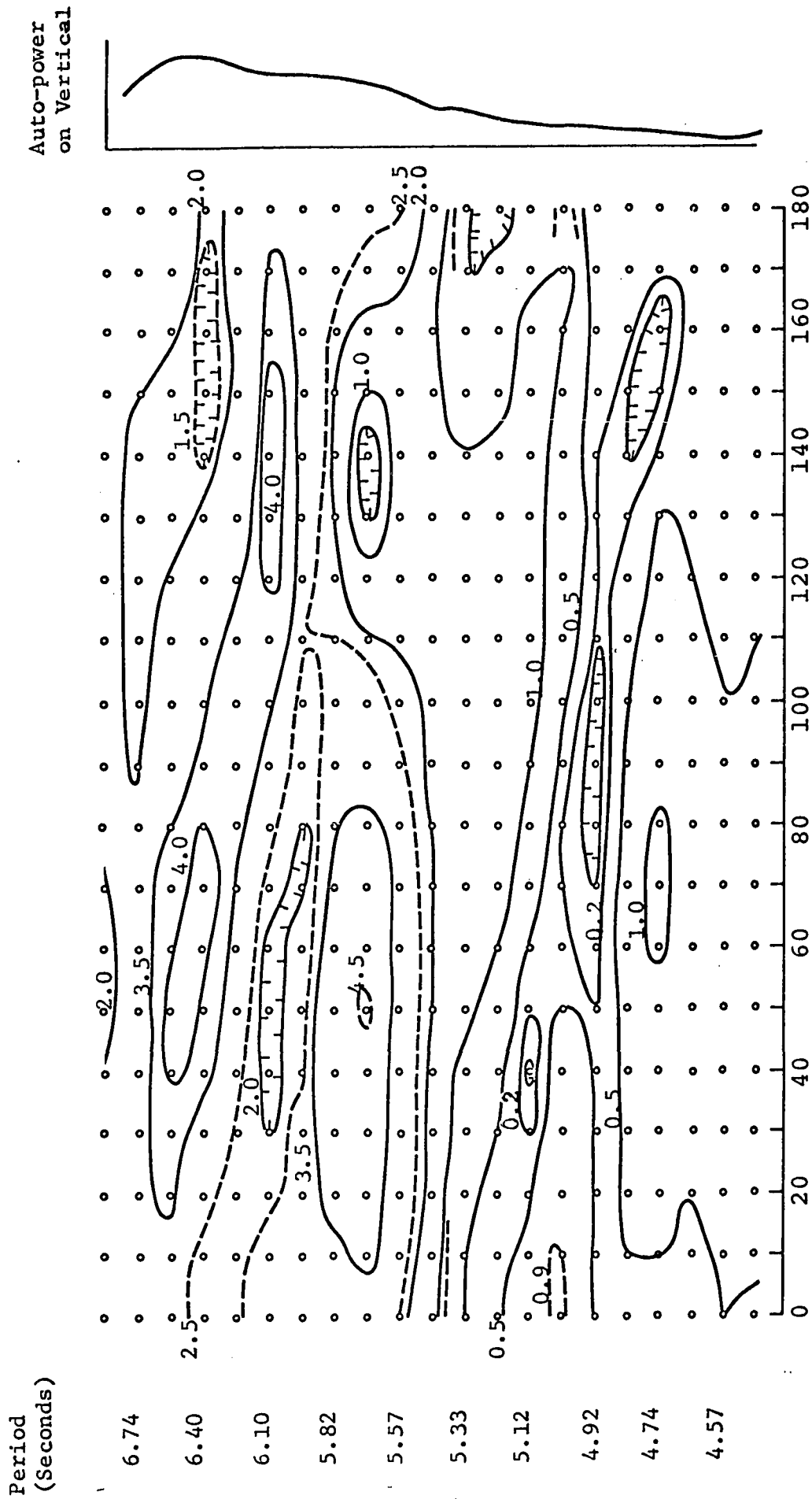


Fig. VI.1.a

COHERENCY BETWEEN VERTICAL AND HORIZONTAL COMPONENTS AT VICTORIA

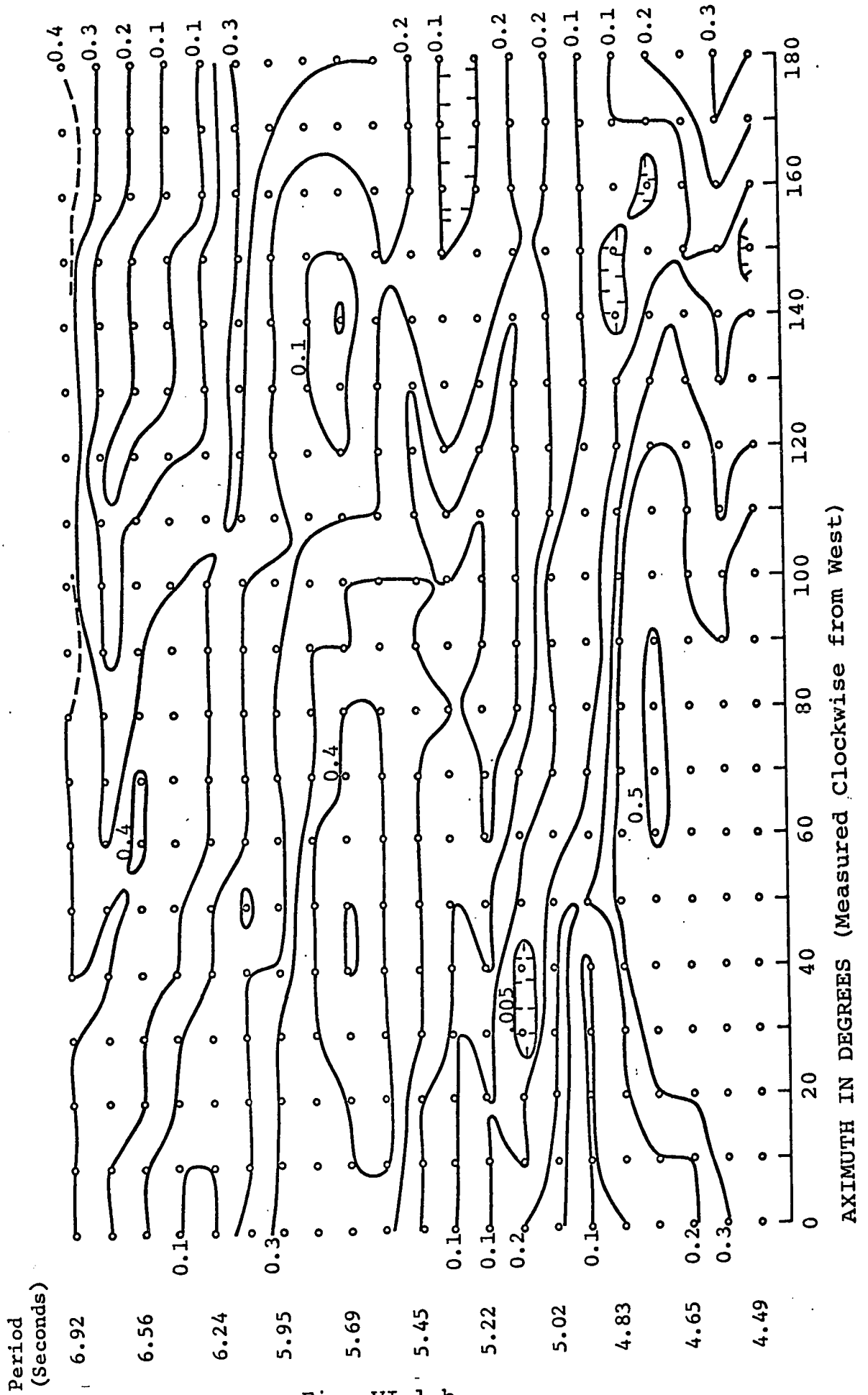


Fig. VI.1.b

CROSS-POWER BETWEEN THE HORIZONTAL COMPONENTS AT VICTORIA

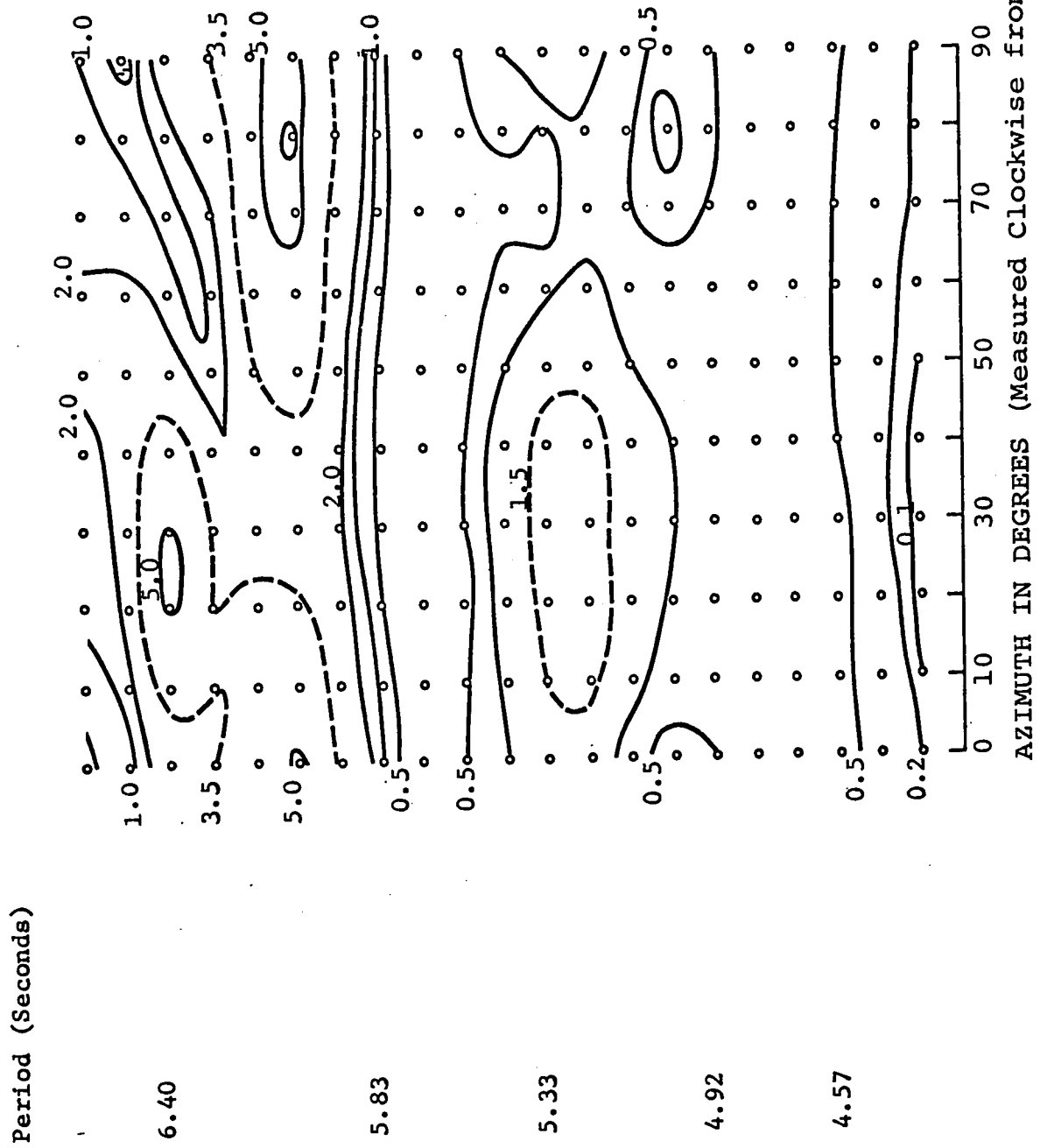


Fig. VI.1.c

COHERENCY BETWEEN THE HORIZONTAL COMPONENTS AT VICTORIA

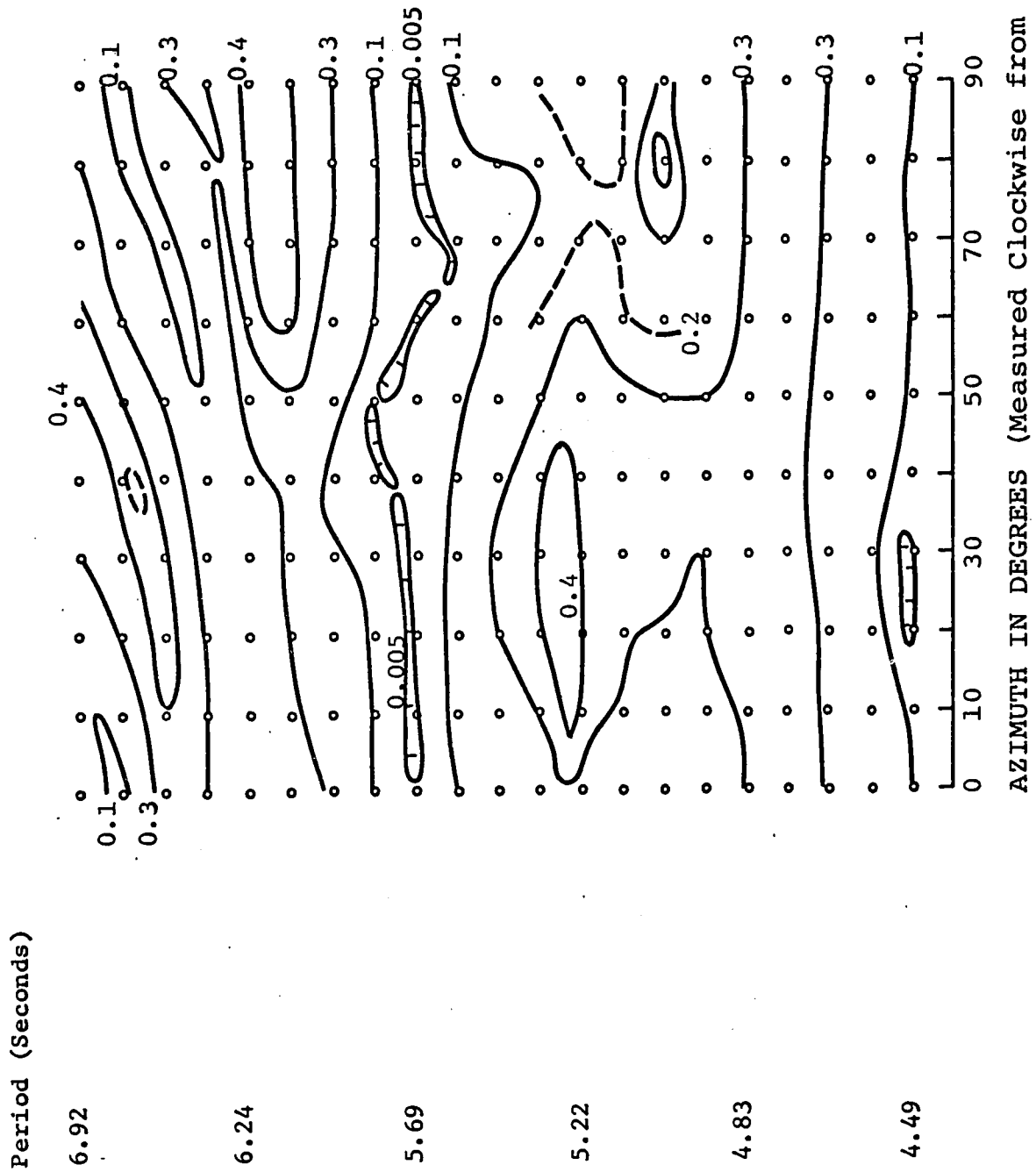
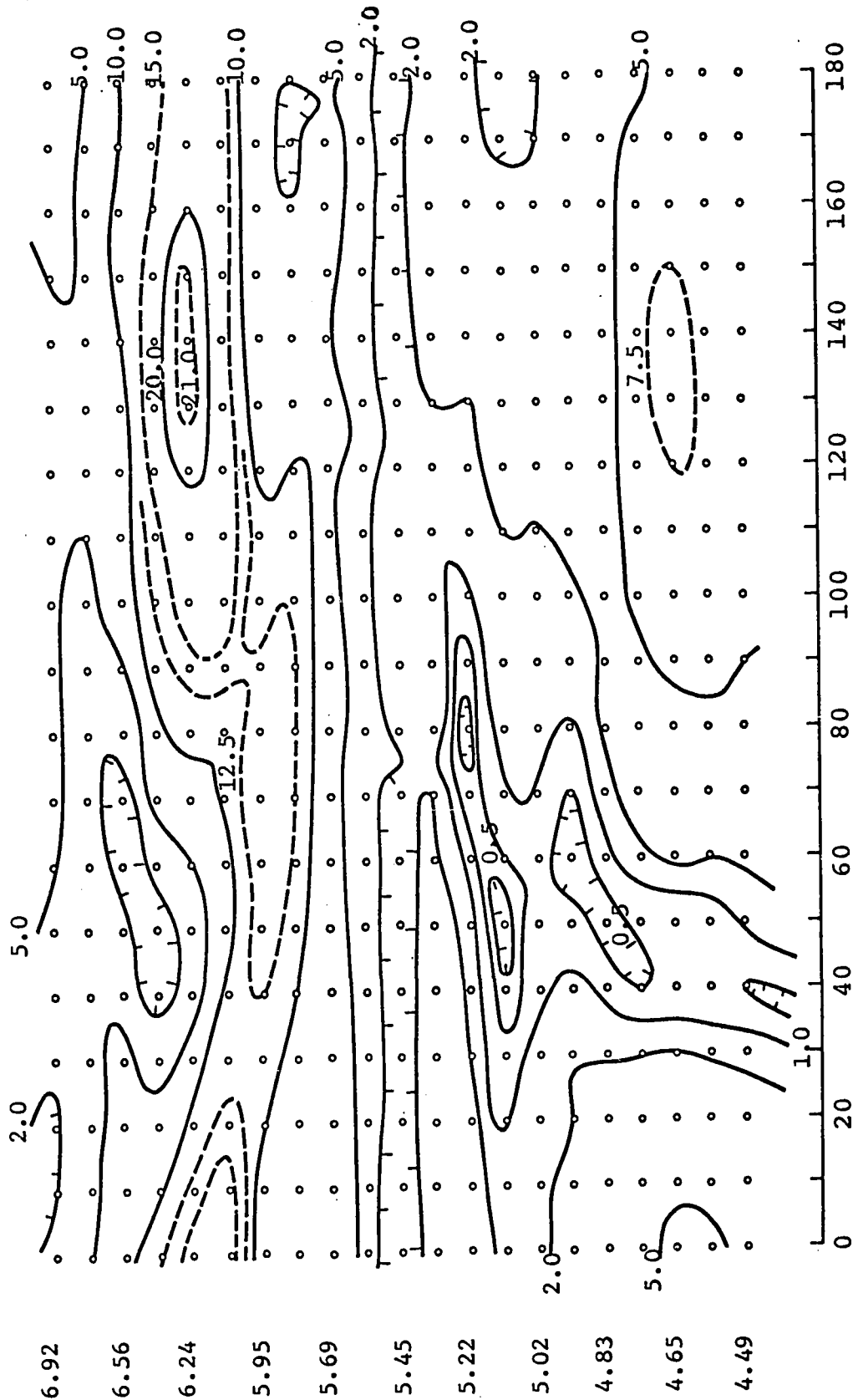


Fig. VI.1.d

CROSS-POWER BETWEEN VERTICAL AND HORIZONTAL COMPONENTS AT PENTICTON

Period  
(Seconds)



AZIMUTH IN DEGREES (Measured clockwise from West)

Fig. VI.2.a

COHERENCY BETWEEN VERTICAL AND HORIZONTAL COMPONENTS AT PENTICTON

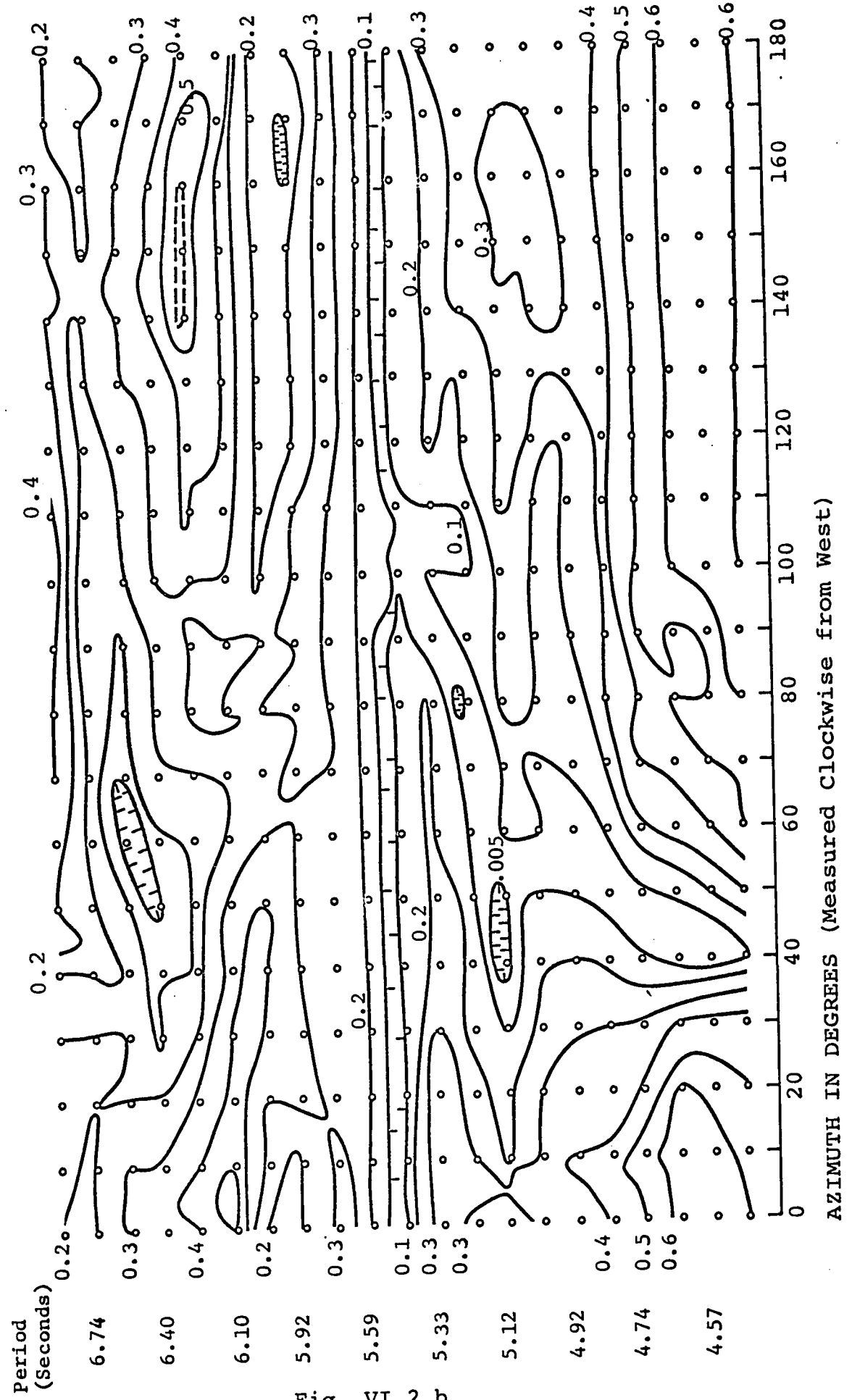


Fig. VI.2.b

CROSS-POWER BETWEEN THE HORIZONTAL COMPONENTS AT PENTICTON

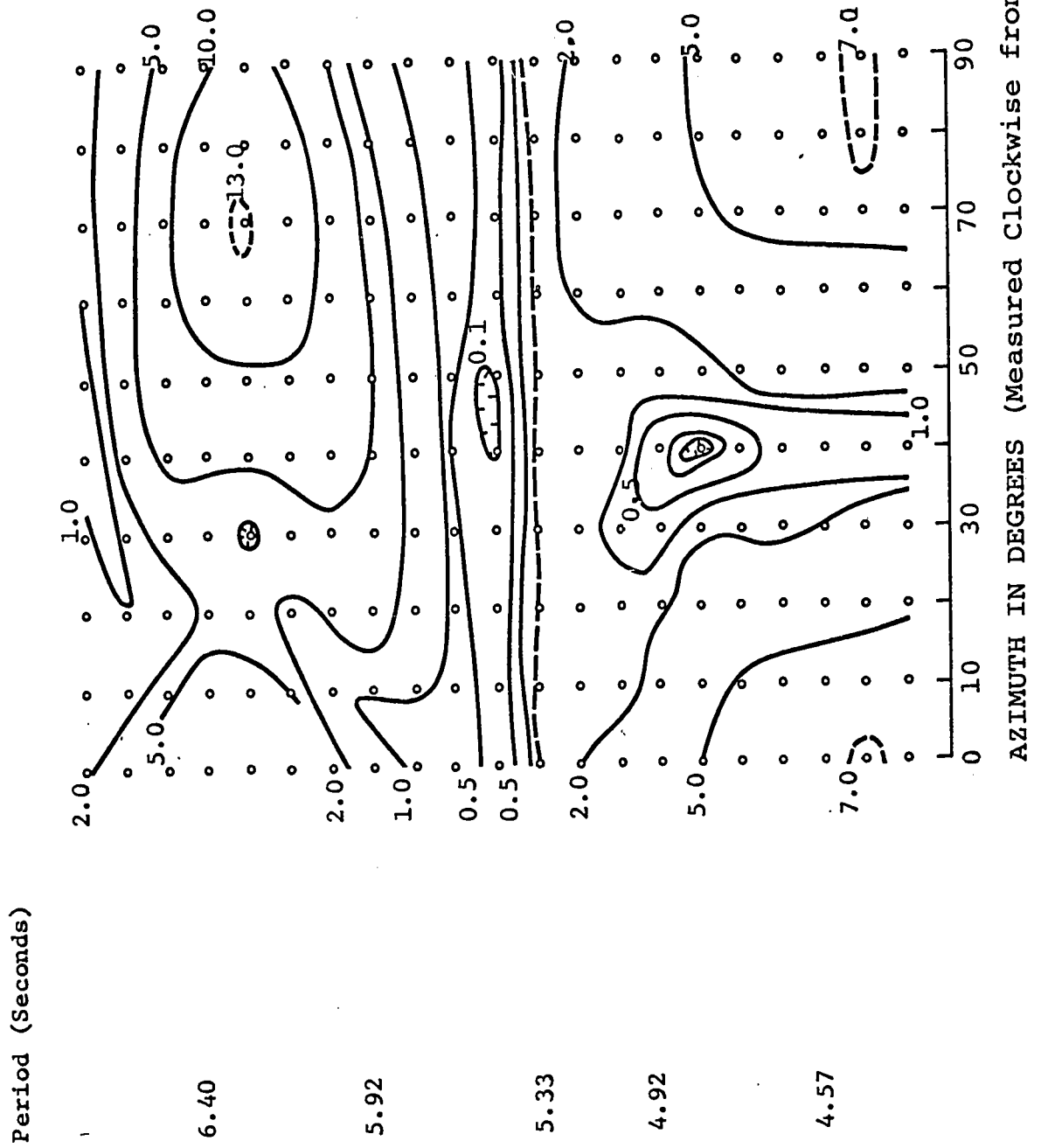


Fig. VI.2.c



COHERENCY BETWEEN THE HORIZONTAL COMPONENTS AT PENTICTON

Period (Seconds)

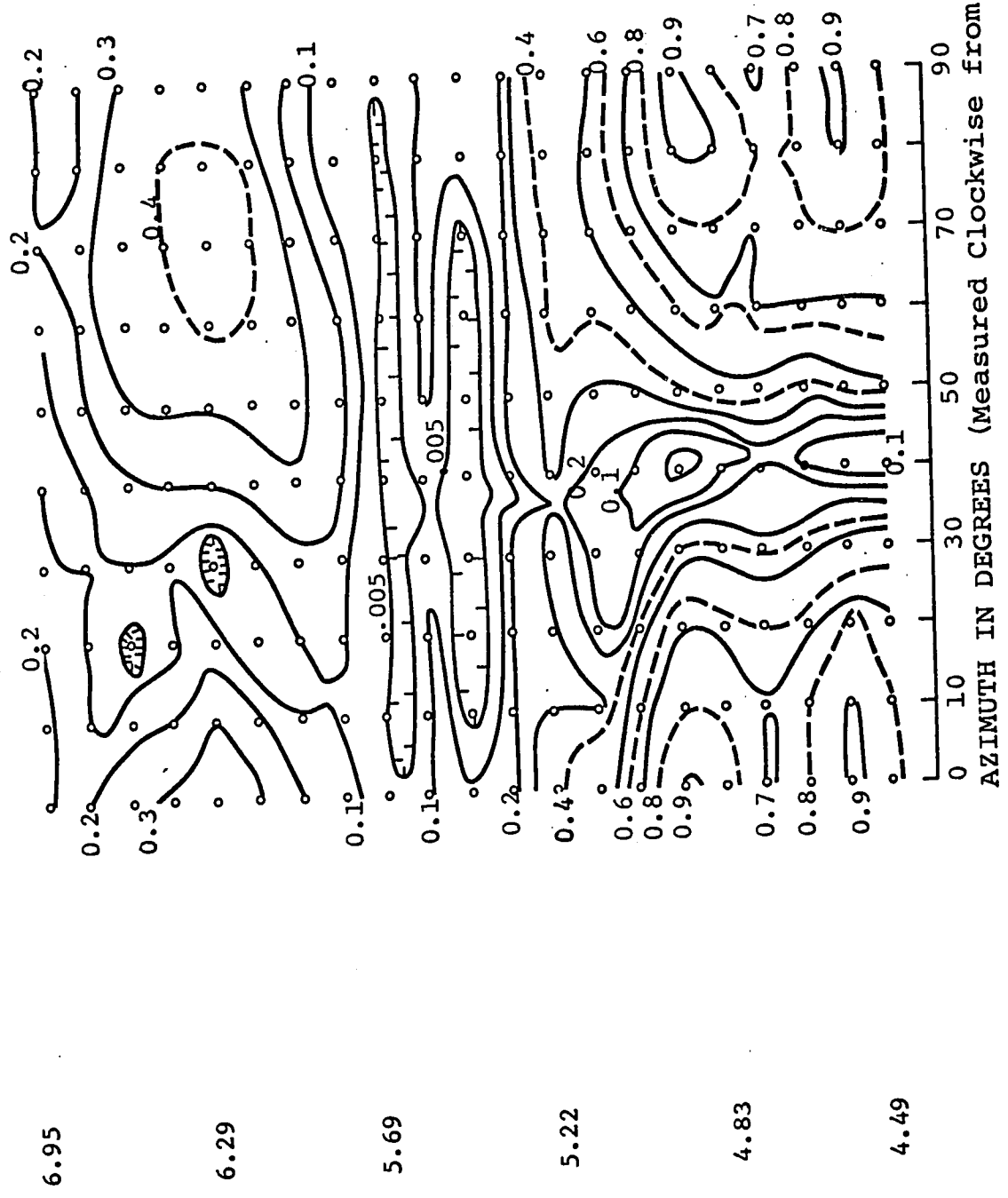


Fig. VI.2.d

CROSS-POWER BETWEEN VERTICAL AND HORIZONTAL COMPONENTS AT EDMONTON

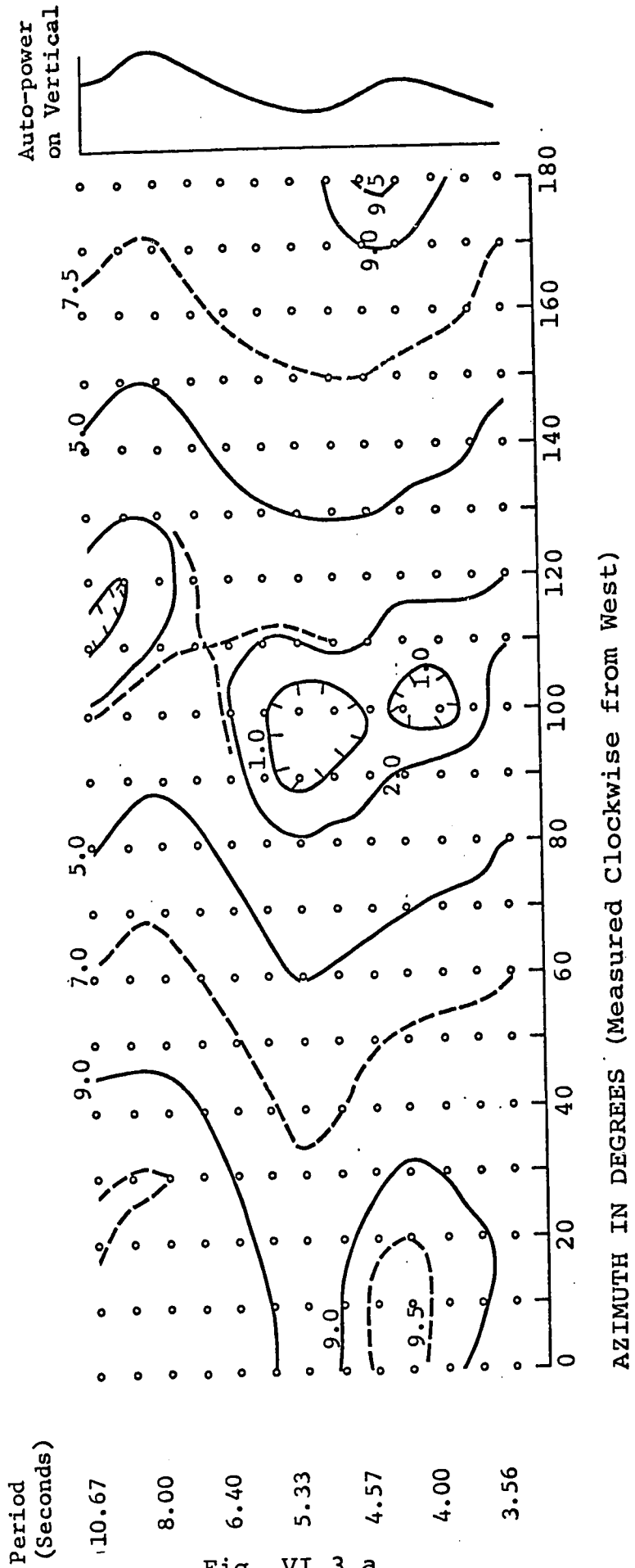


Fig. VI.3.a

COHERENCY BETWEEN VERTICAL AND HORIZONTAL COMPONENTS AT EDMONTON

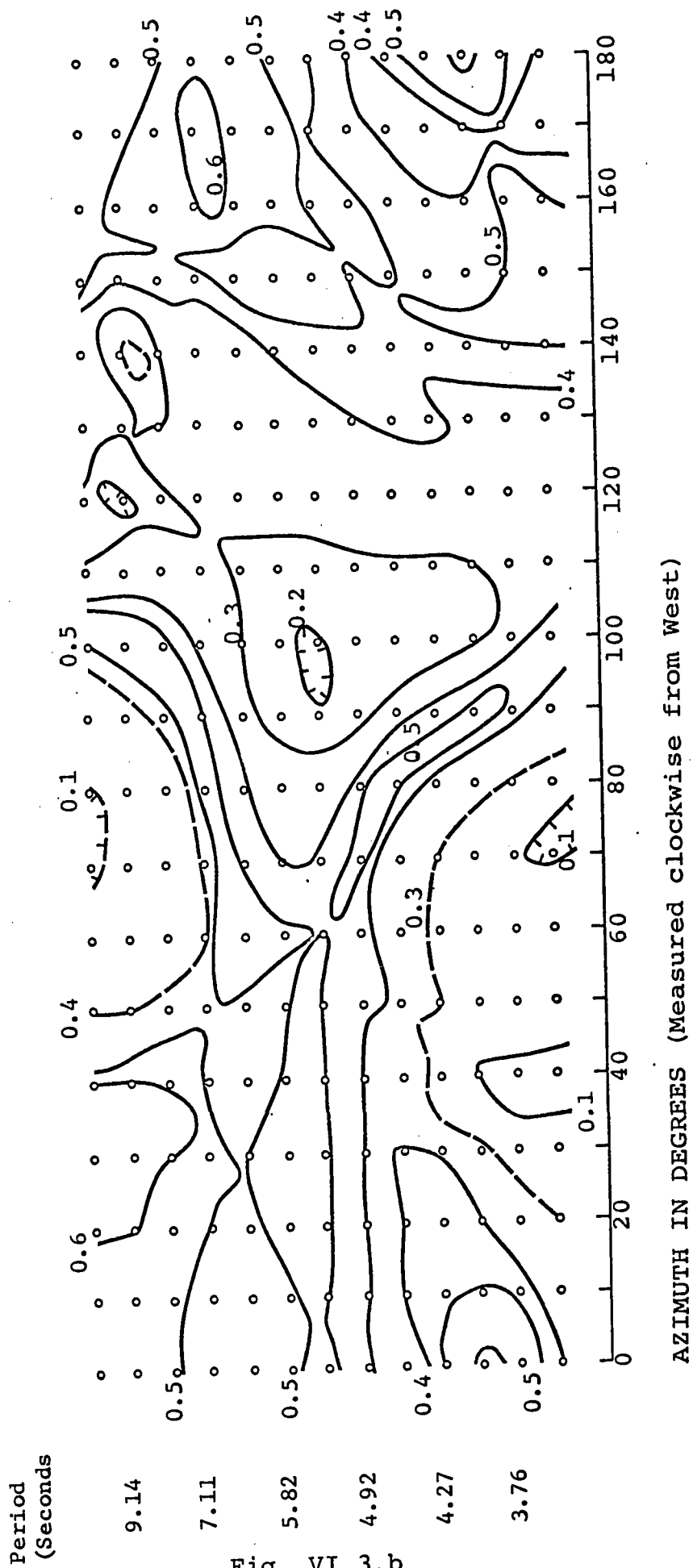


Fig. VI.3.b

CROSS-POWER BETWEEN THE HORIZONTAL COMPONENTS AT EDMONTON

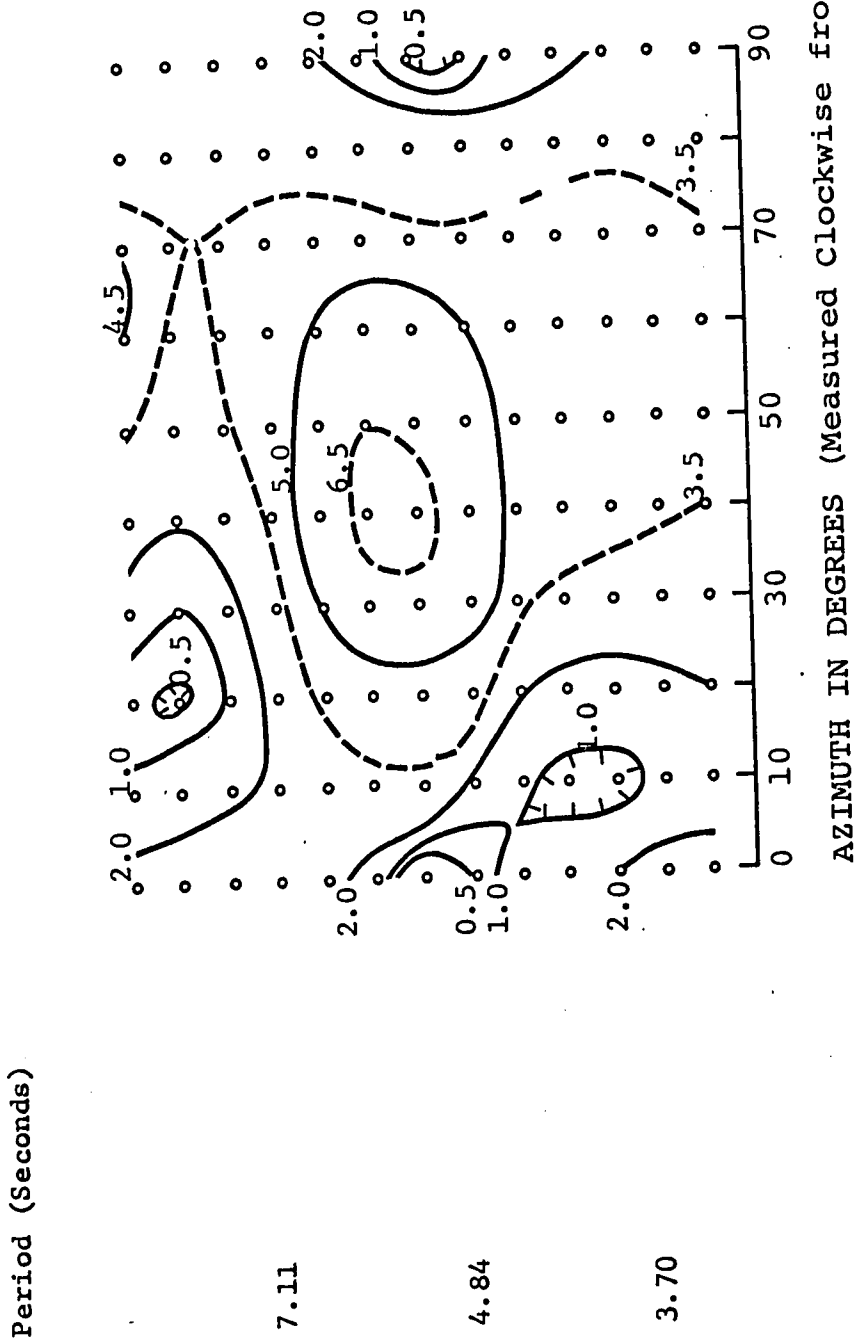


Fig. VI.3.c

COHERENCY BETWEEN THE HORIZONTAL COMPONENTS AT EDMONTON

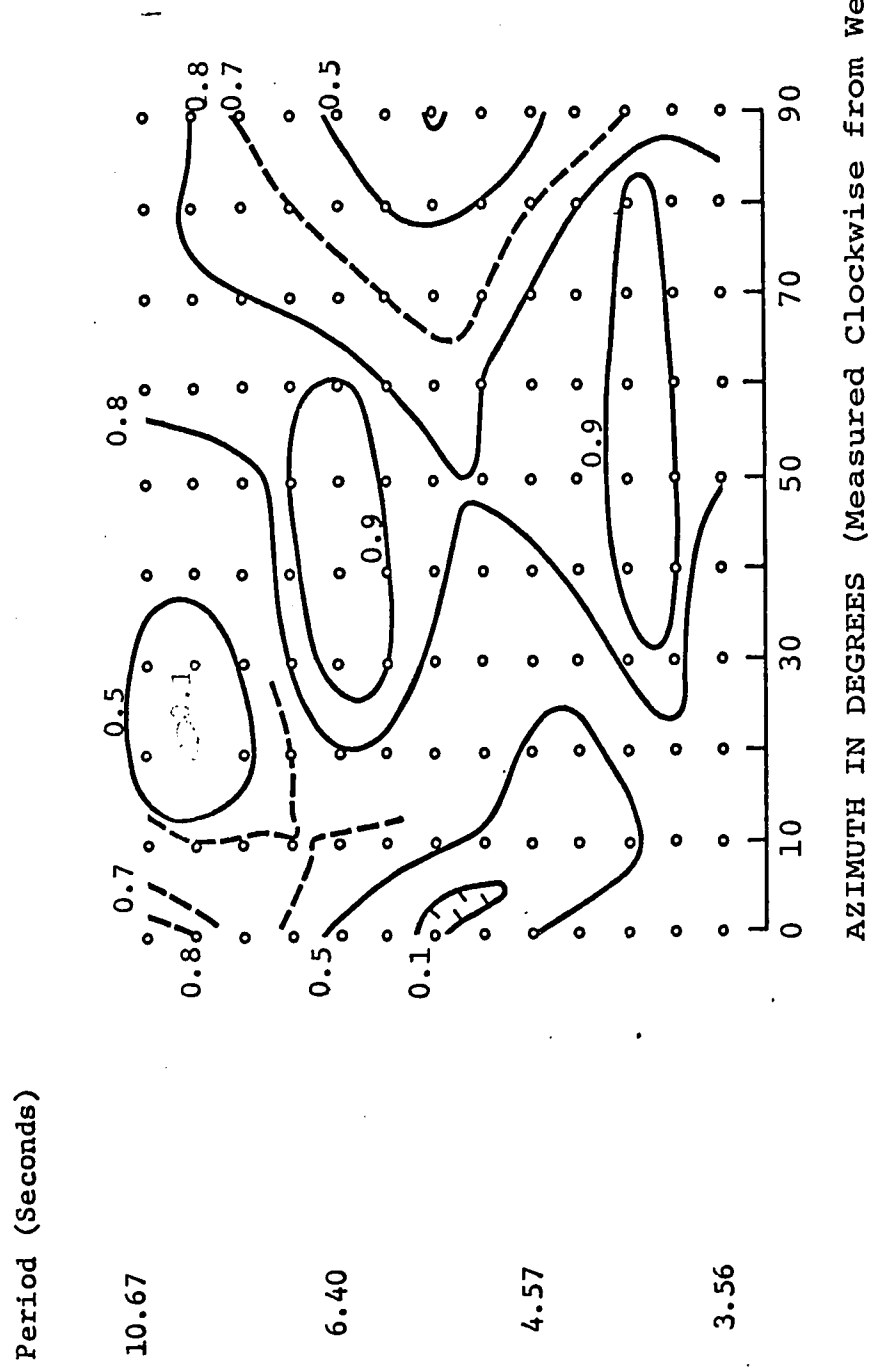


Fig. VI.3.d

CROSS-POWER BETWEEN VERTICAL AND HORIZONTAL COMPONENTS AT RESOLUTE

Period  
(Seconds)

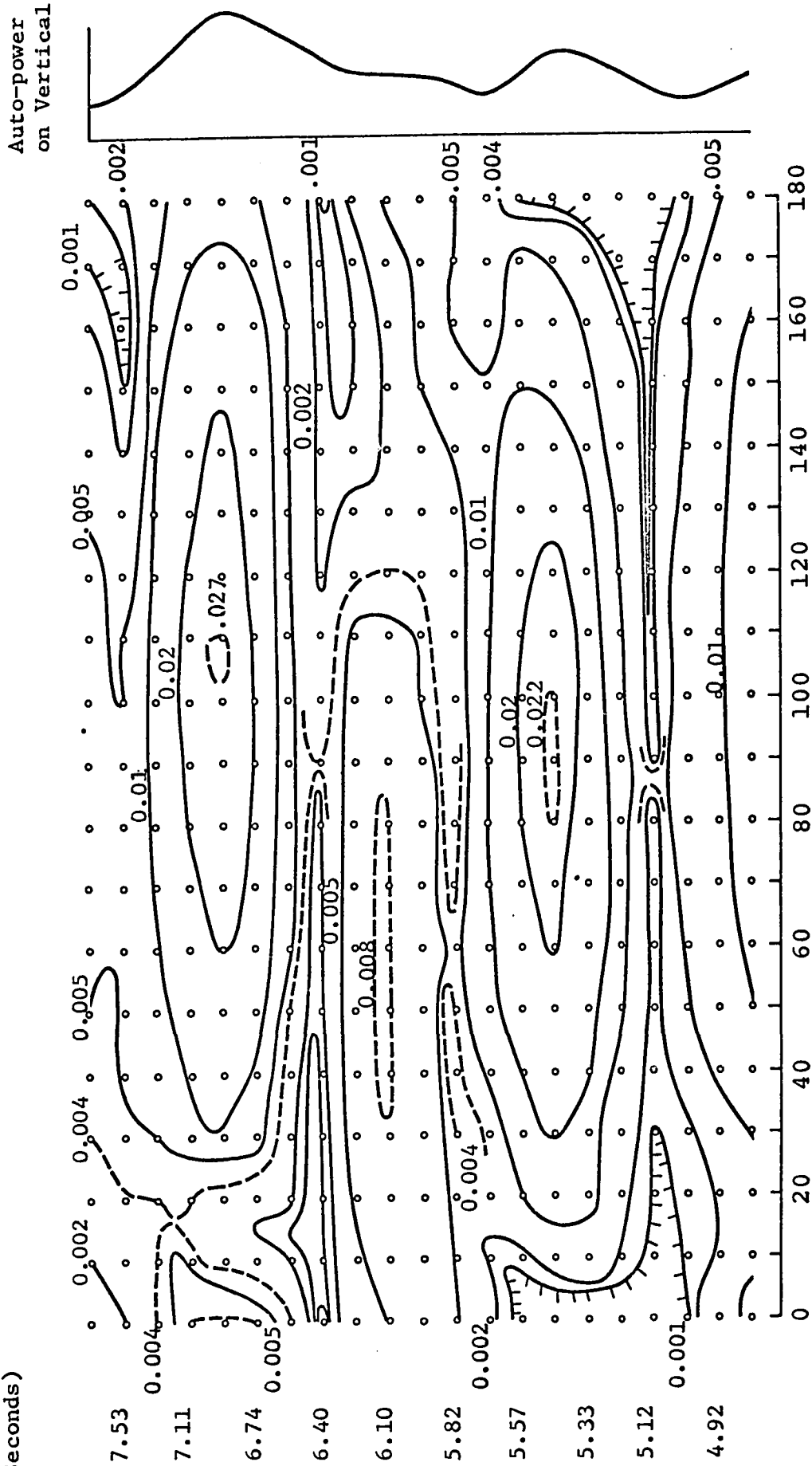


Fig. VI.4.a

# COHERENCY BETWEEN VERTICAL AND HORIZONTAL COMPONENTS AT RESOLUTE

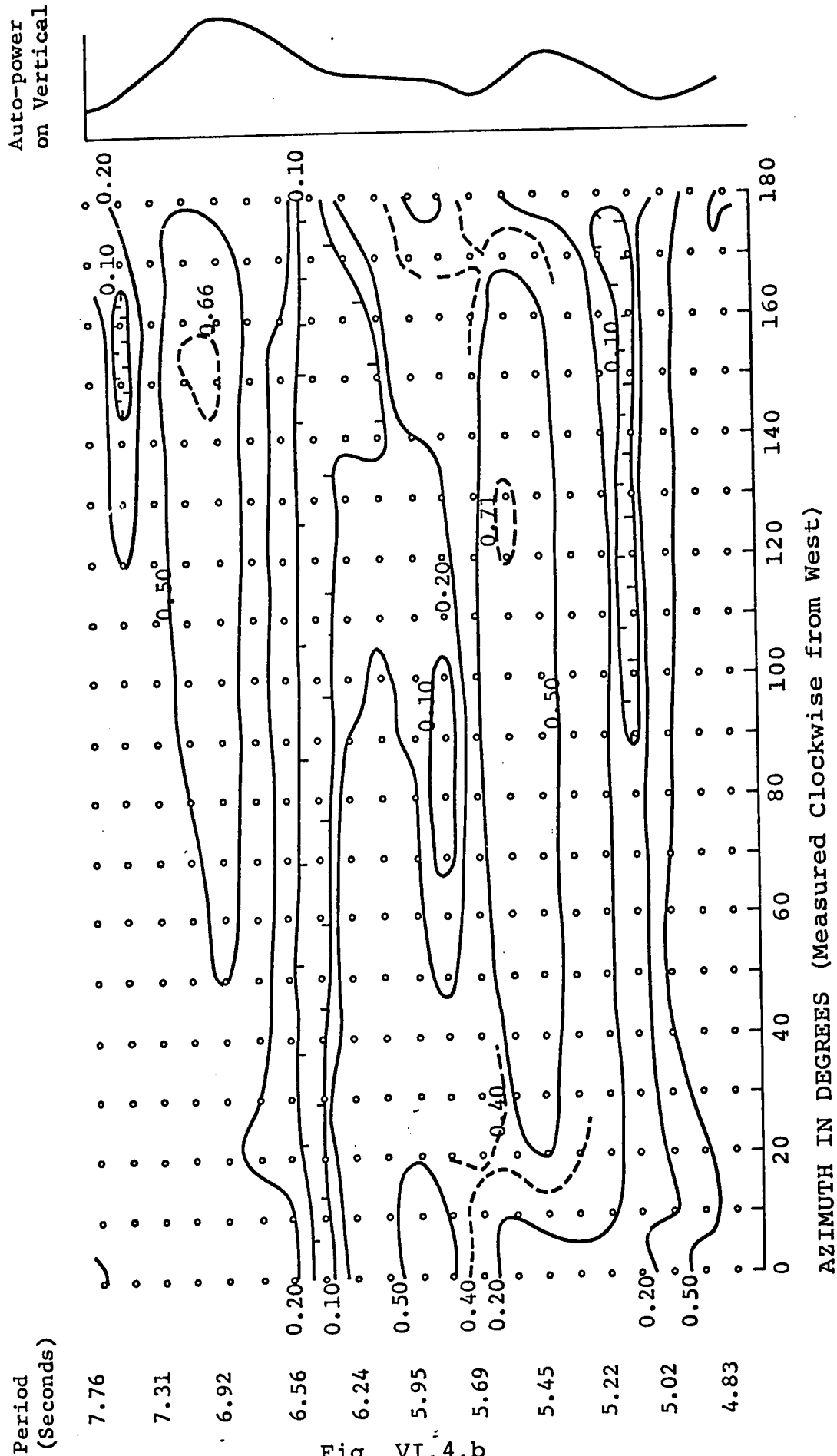


Fig. VI.4.b

CROSS-POWER BETWEEN THE HORIZONTAL COMPONENTS AT RESOLUTE

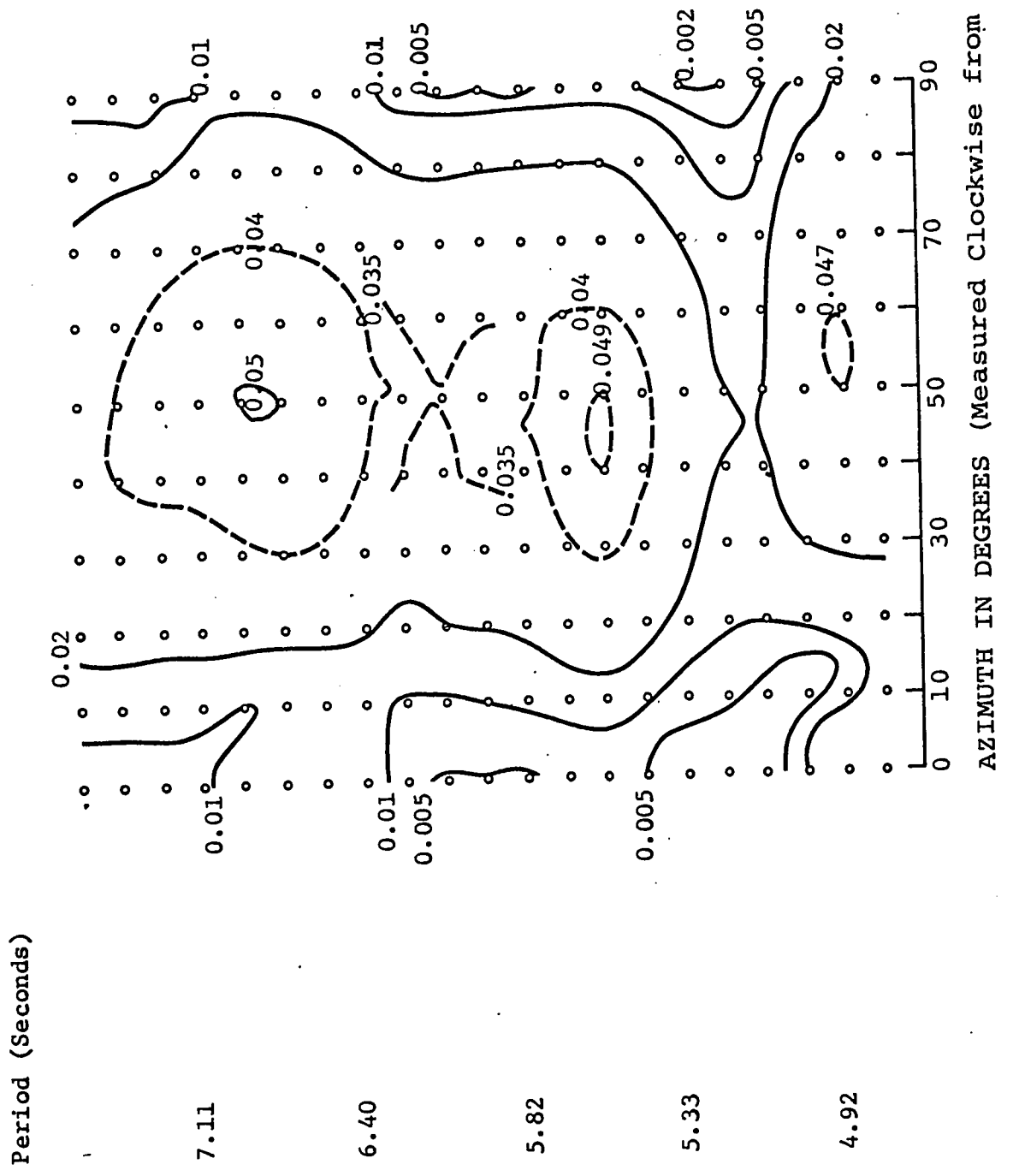


Fig. VI.4.c





CROSS-POWER BETWEEN VERTICAL AND HORIZONTAL COMPONENTS AT OTTAWA

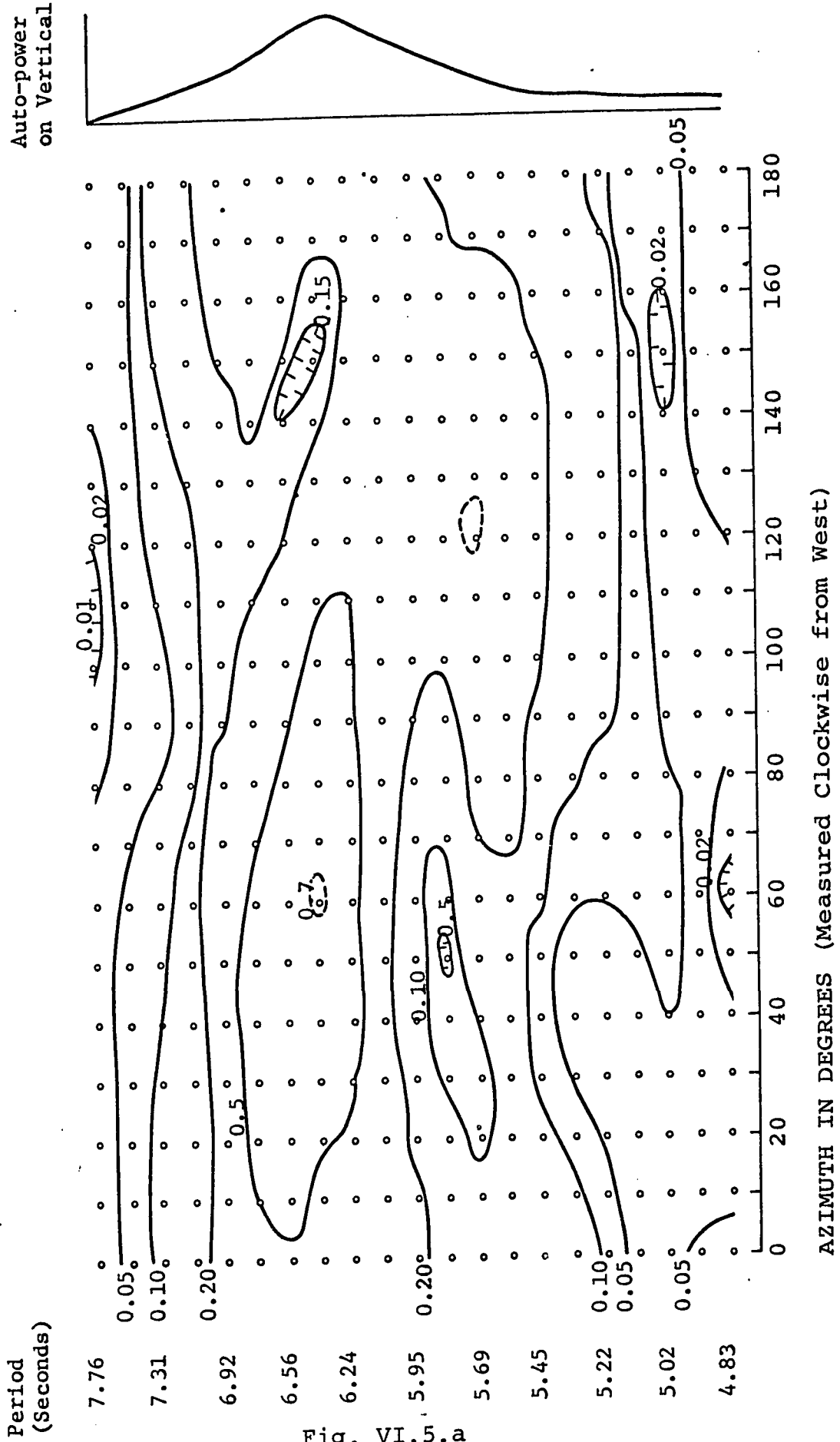


Fig. VI. 5. a

COHERENCY BETWEEN VERTICAL AND HORIZONTAL COMPONENTS AT OTTAWA

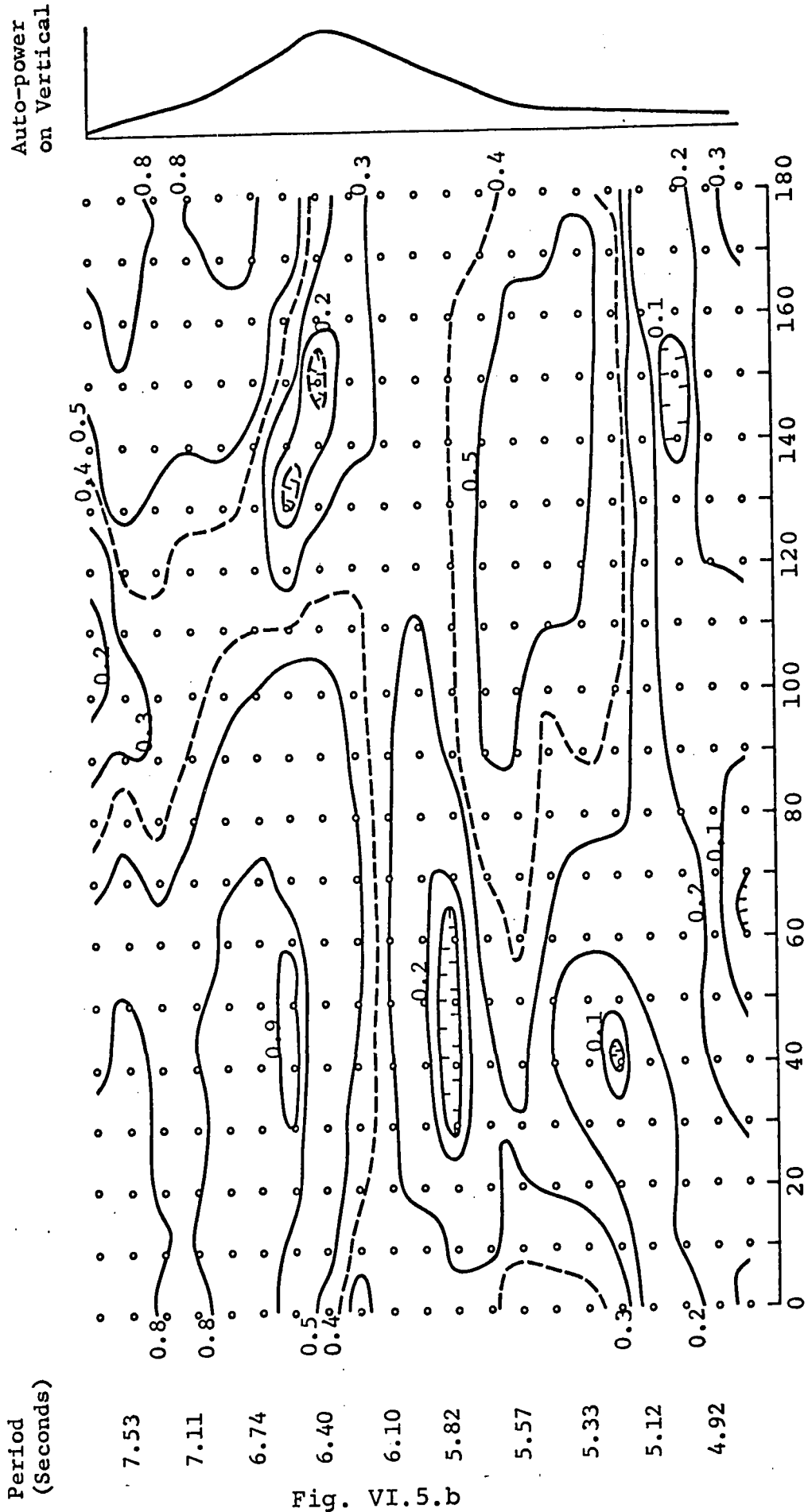


Fig. VI. 5. b

CROSS-POWER BETWEEN THE HORIZONTAL COMPONENTS AT OTTAWA

Period (Seconds)

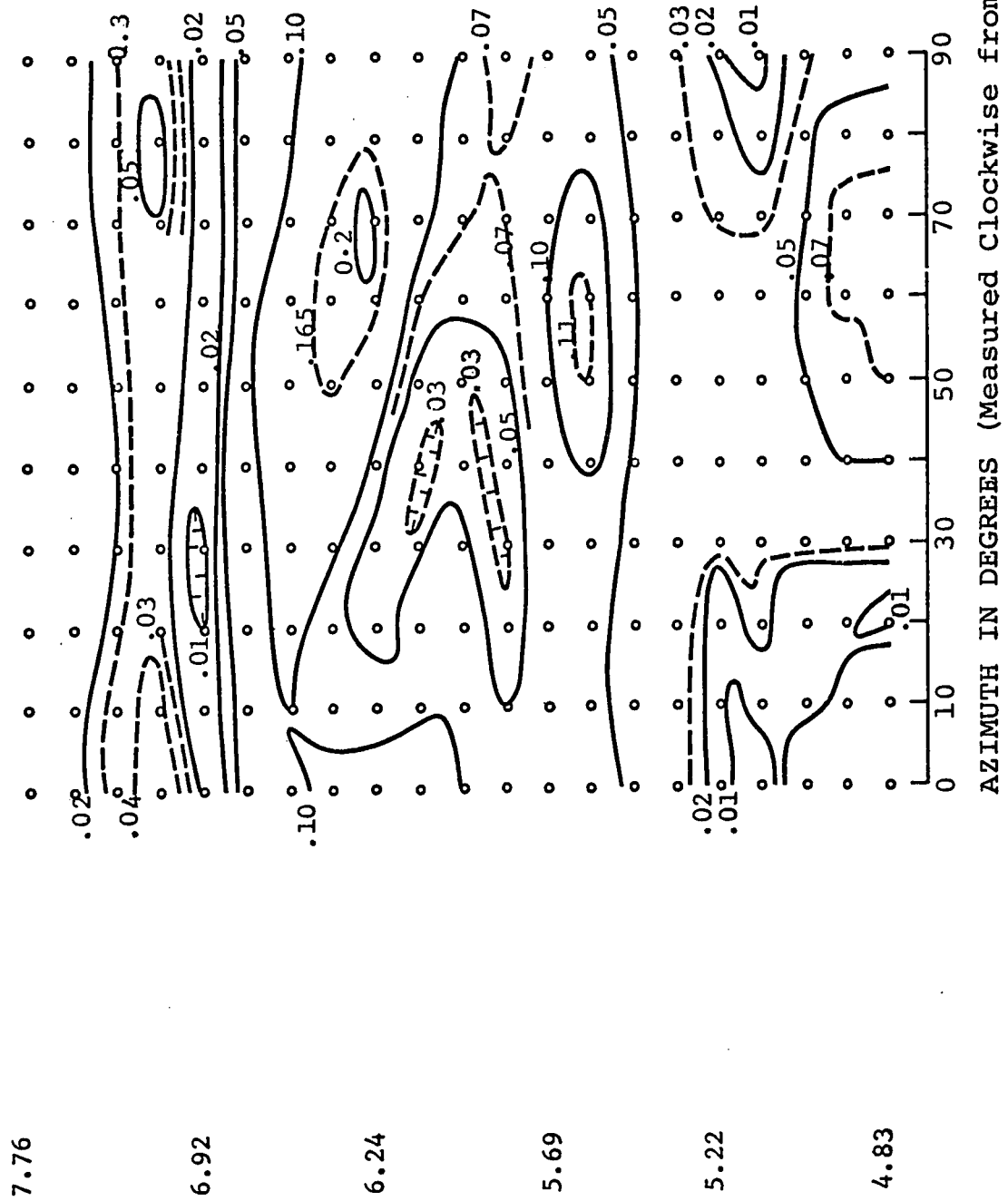


Fig. VI.5.c

COHERENCY BETWEEN THE HORIZONTAL COMPONENTS AT OTTAWA

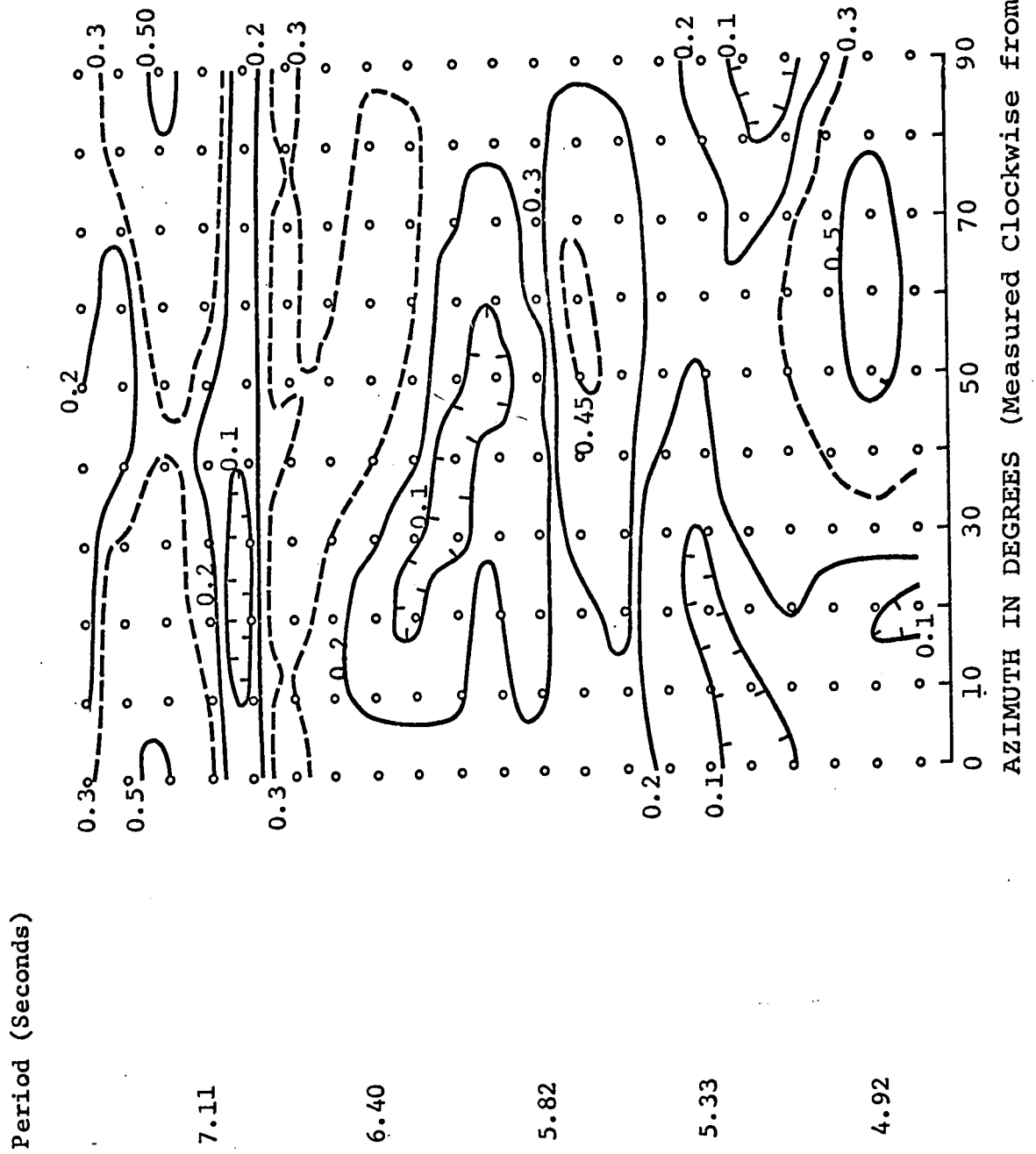


Fig. VI.5.d

these maps can also be observed in the direction of  $50^\circ$  a high at 5.69 seconds with a phase value of  $-153^\circ$ . On the contour map for crosspower between the horizontal components there is a high at 6.56 seconds (phase  $176^\circ$ ) and in the coherency map there is a high at 6.74 seconds (phase  $-147^\circ$ ), at directions of  $25^\circ$  and  $40^\circ$ . There are two more highs on these maps at 5.22 seconds (directions centred at  $25^\circ$ ) and 4.65 seconds (without a well defined direction), their phases being  $-22^\circ$  and  $170^\circ$  respectively.

At Penticton there is a peak on the autopower spectrum of the vertical component at 6.10 seconds. There is a marked high at this period on the contour map for the crosspower between the vertical and radial components (between  $120^\circ$  and  $160^\circ$ ) centred at  $140^\circ$  with a corresponding high on the coherency map at  $150^\circ$ . This direction actually falls in the northeast quadrant at  $50^\circ$  east of north. Since there is a  $180^\circ$  uncertainty in direction using this method this corresponds to a source in the Pacific  $40^\circ$  south of west. This choice of directions is also indicated by the low corresponding to this high at  $50^\circ$  west of north, which puts a low in the Pacific implying the absence of a source in that direction which is not true. The phase for this event is  $50^\circ$ . A second high at 6.24 seconds due west can be seen on both crosspower and coherency maps. Phase for this event is  $36.5^\circ$ . This high is actually merging into the first one, and thus the direction of approach is a cone

the sides of which make an angle of approximately  $50^{\circ}$ . A high at 4.64 seconds in the direction of  $45^{\circ}$  south of west can also be observed on the crosspower map. Even though there is a high of magnitude of 0.6 on the coherency map at this period, there is no well-defined direction for it. Phase for this event is  $-10^{\circ}$ . There is a high at 6.24 seconds on the contour map for the crosspower between the two horizontal components whose direction is  $20^{\circ}$  south of west. There is a corresponding high on the contour map of coherency between these two components. The phase for this is  $-177^{\circ}$ . A second high at 4.57 seconds can be seen on both crosspower and coherency maps for the horizontal components, with a phase value of  $175^{\circ}$ .

On the record chosen for Edmonton there are two peaks at 8.00 seconds and 4.27 seconds on the autopower spectrum of vertical component. Two highs (Directions of which are  $25^{\circ}$  north of west and  $10^{\circ}$  north of west) can be observed on the contour map for the crosspower between the vertical and radial components. Results on the coherency map are very ambiguous and no clear cut highs can be seen on this map. Both these events have the same coherency of 0.6 with directions of  $30^{\circ}$  north of west, and west. Phases for these two events are  $-6^{\circ}$  and  $-11^{\circ}$ . A high at 5.33 seconds can be seen on the contour map for the crosspower between the two horizontals at a direction of  $40^{\circ}$  north of west. Two highs on the coherency map for these two components

can be seen at 6.40 seconds and 4.00 seconds at the directions of  $45^{\circ}$  and  $55^{\circ}$  north of west. The phases for these two are  $-168^{\circ}$  and  $-175^{\circ}$ .

On the record chosen for Resolute there are two peaks on the autopower spectrum of the vertical component at 6.92 seconds and 5.45 seconds. There are two highs at 6.92 and 5.57 seconds with directions of  $30^{\circ}$  south of west and  $5^{\circ}$  south of west on the coherency contour map for vertical and radial components. The corresponding crosspower map shows highs at 6.92 seconds and 5.45 seconds, at directions of  $15^{\circ}$  north of west and  $30^{\circ}$  north of west. There is thus no agreement between the directions obtained from crosspower peaks and from coherency peaks. The phases for these two events are  $-88^{\circ}$  and  $-102^{\circ}$ , indicating Rayleigh motion. Three highs at 6.91, 5.57 and 4.92 seconds can be seen on the contour map of crosspower between the two horizontals at directions of  $55^{\circ}$  north of west,  $40^{\circ}$  north of west and  $55^{\circ}$  north of west. Three corresponding highs at 6.92, 5.69 and 5.02 seconds appear on the contour map of coherency between the two horizontals at directions of  $55^{\circ}$  north of west,  $40^{\circ}$  north of west and  $55^{\circ}$  north of west respectively. Their phases are  $172^{\circ}$ ,  $173^{\circ}$  and  $173^{\circ}$  respectively. Though Rayleigh and Love waves are indicated, their direction of approach is ambiguous at Resolute, but a cone of direction of  $55^{\circ}$  north of west to  $35^{\circ}$  south of west seems to indicate a source in the Pacific ocean. This large angular uncertainty



in direction is also verified by the broadness of the high in vertical-radial crosspower.

The autopower of the vertical component peaks at 6.40 seconds at Ottawa. The high on the contour map of the crosspower between the vertical and radial components occurs at  $60^\circ$  north of west. A high on the coherency map for these two components appears at 6.56 seconds with a direction of  $45^\circ$  north of west. The phase for this event is  $-179^\circ$ . There are four highs on the contour map of crosspower between two horizontal components at periods of 7.11, 6.24, 5.57 and 4.92 seconds. Their directions are  $80^\circ$  north of west,  $70^\circ$  north of west,  $55^\circ$  north of west and  $65^\circ$  north of west. Three of these are supported by highs on the coherency map for the two horizontals occurring at 7.31, 5.69 and 4.92 seconds. Their directions are north,  $60^\circ$  north of west and also  $60^\circ$  north of west, respectively. In addition there is a plateau of 0.3 coherency between 6.74 - 6.24 seconds with no well-defined direction. The phases for all these events are close to  $-180^\circ$  or  $0^\circ$ .

VI.4 The contour diagrams in general show highs in the North West or South West quadrants indicating a source in the Pacific Ocean. Lows are well marked (except in one or two cases) and  $90^\circ$  away from the highs in the case of vertical-radial system and  $45^\circ$  in the case of radial-transverse system as expected. In certain cases lows are more clearly defined than the highs, which tend to be broad.

A comparison of the four maps at a given location shows a general agreement between the directions of approach. It is only at Resolute that the directions obtained from the crosspower highs and the coherency highs for the vertical-radial system differ by as much as  $40^{\circ}$ , otherwise they are within  $\pm 10^{\circ}$  range. Not only do the directions obtained from two quantities in one set agree to  $\pm 10^{\circ}$  but they are also close to those obtained from the other set, viz. the radial-transverse system. It can be said therefore that the directions of approach of Rayleigh and Love waves differ at most by  $10^{\circ}$ . The discrepancy at Resolute is not readily explainable. As will be shown below the directions obtained here can be favourably compared with those of the storm locations.

Besides the directions, magnitudes of highs and lows offer very interesting features. It was pointed out earlier that the ratio between high and low provides a measure of the signal to noise ratio in the microseisms. Two such ratios exist in the two sets of computations; one corresponds to the crosspower and the other to coherency. The crosspower ratios are as low as 1.33 (for the 7.31 second event at Ottawa) and as high as 22 (for the 5.45 second event at Resolute); the average figure however seems to be around 8. Thus the amplitude signal to noise ratio is about 3. The range between the signal and noise level therefore varies from as low as 3db to well over 12db. This comes as no surprise in view of the sinusoidal appearance of the micro-

seisms on the records.

In most cases the noise level for coherency is about 0.1, although in one case it is as large as 0.5. But the very fact that the coherency in the direction of the arriving waves rarely exceeds 0.6 for the vertical-radial system coupled with the occurrence of spurious phase values, shows that other types of waves are recorded, especially on the vertical component. (Note that the coherency values for radial-transverse system are usually greater than 0.8). This conclusion is reinforced by the vertical to radial ratios calculated from these diagrams which rarely agree with theoretical ratios.

There are three cases where a Rayleigh type of motion could be identified. Two of them are at Resolute where the phase values indicate a retrograde motion; the third at Victoria where the phase value indicates a prograde motion. At Resolute, for this sample record, there is an excellent agreement between the observed and theoretical values of the vertical to radial ratios supporting the identification of a Rayleigh wave. At the other stations (including Victoria) the vertical component is usually larger than expected, and the phase is seldom appropriate for Rayleigh motion. If one were to interpret all these features (large values for vertical amplitude, wrong phase values, and yet high signal to noise ratio) as due to the presence of long period body waves (especially leaking P-

TABLE VI.1a

Period	Components	Power		Coherency		Station
(Secs)	V-Vertical R-Radial T-Transverse	High	Low	High	Low	
6.10	V					PENTICTON
6.24	V-R	320°	230°	300°	200°	
6.24	R-T	340°	30°	340°	30°	
4.65	V-R	315°	225°	-	-	
4.57	R-T	330°	10°	325°	10°	
6.40	V					OTTAWA
6.40	V-R	60°	150°	45°	135°	
7.31	R-T	75°	28°	85°	40°	
5.57	R-T	58°	10°	58°	10°	
4.92	R-T	65°	20°	60°	17°	
6.92	V					RESOLUTE
6.92	V-R	10°	100°	330°	-	
5.45	V	-	-	-	-	
5.45	V-R	30°	120°	355°	-	
6.92	R-T	330°	15°	325°	10°	
5.57	R-T	335°	20°	340°	290°	
5.12	R-T	325°	10°	325°	15°	
8.0	V					EDMONTON
8.0	V-R	25°	115°	30°	120°	
4.27	V	-	-	-	-	
4.27	V-R	10°	100°	0°	75°	
5.33	T-R	40°	90°	45°	90°	
6.56	V					VICTORIA
	V-R	40-80°	140-170°	50-70°	150°	
	R-T	20-30°	75°	40°	85°	
5.69	V-R	50°	140°	45°	140°	
4.74	V-R	60-80°	140-165°	60-90°	160°	
5.33	T-R	5-45°	80°			

TABLE VI.1b

Period	Components	Magnitude						Station
(Secs)	V-Vertical R-Radial T-Transverse	High	Low	Coherency High	Coherency Low	H/L	H/L	
6.10	V	60						PENNICTON
6.24	V-R	21.0	2.0	.55	0.1	10.5	very high	
6.24	R-T	13.0	1.0	0.40	0.1	13.0	"	
4.65	V-R	7.5	1.0	0.6	0.1	7.5	6	
4.57	R-T	7.0	1.0	0.9	0.1	7.0	9	
6.40	V	2						OTTAWA
6.40	V-R	0.7	0.15	0.9	0.16	4.6	5.6	
7.31	R-T	0.05	0.03	0.5	0.3	1.33	1.33	
5.57	R-T	0.11	0.05	0.45	0.2	2.2	2.25	
4.92	R-T	0.07	0.01	.55	0.1	7	5.5	
6.92	V	0.02						RESOLUTE
6.92	V-R	0.027	0.004	.66	0.5	6.7	1.32	
5.45	V	0.015						
5.45	V-R	0.022	0.001	0.71	0.4	22	1.7	
6.92	R-T	0.05	0.01	0.8	0.3	5	2.33	
5.57	R-T	0.049	0.005	0.85	0.2	10	4.25	
5.12	R-T	0.047	0.01	0.80	0.4	4.7	2.0	
8.0	V	15.0						EDMONTON
8.0	V-R	9.5	1.0	0.6	0.1	9.5	6.0	
4.27	V	11.0						
4.27	V-R	9.0	1.0	0.6	0.1	9.0	6.0	
5.33	T-R	6.5	0.5	0.9	0.1	13.0	9.0	
6.56	V	20.0						VICTORIA
	V-R	4.0	1.5	0.4	0.1	2.7	4	
	R-T	5.0	1.0	0.4	0.1	5.0	4	
5.69	V-R	4.5	0.5	0.5	0.1	9.0	very high	
4.74	V-R	1.0	0.1	0.5	0.1	10	"	
5.33	T-R	1.5	0.1	0.4	0.1	15	-	

TABLE VI.1c

Period	Components	V/R	V/R	Station
(Secs)	V-Vertical R-Radial T-Transverse	Observed	Theoretical	
6.24	V-R	2.9	.98	PENTICTON
6.40	V-R	2.9	0.72	OTTAWA
6.92	V-R	0.73	0.69	
5.45	V-R	0.75	0.69	RESOLUTE
8.0	V-R	1.6	1.1	
4.27	V-R	1.2	1.1	EDMONTON
6.56	V-R	5.0	0.9	
5.69	V-R	2.2		VICTORIA
4.74	V-R	2.5		

modes), one has to accept that the record at Resolute is unusual, and thus that pure Rayleigh waves in microseisms are the exception rather than the rule.

In table VI.-1 are summarized the several quantities computed from these diagrams and discussed above in sections VI.3 and VI.4.

VI.5 In summary then the following features can be recognized from these contour diagrams:

1. As a rule the contours tend to be broad in all cases. There are cases when the contours do centre around a small closed area but these are only exceptions.
2. Contour lines are broader for the radial-vertical system than for the radial-transverse system.
3. The broadness of the contours is indicative of uncertainty in direction of approach. The farther the station is removed from the coast, the broader are the contours.
4. There is no marked improvement in the values of coherency even after rotation.
5. Cross sections of the contours on the cross power grids do show very well marked peaks, a deduction made from the closely bunched nature of the contours.
6. The lows, the highs and the plateaux are very well shown on these diagrams.
7. Highs and lows are separated by  $90^\circ$  on radial-vertical contour maps and are repeated every full rotation ( $180^\circ$ ). The highs and lows on the contour maps for two horizontal components are separated by  $45^\circ$  and they are repeated every half rotation ( $90^\circ$ ).

8. A comparison was made between the directions obtained from rotated coherency and rotated cross power with the directions obtained from the bearings of storm locations. These comparisons are shown in Table VI.2. The uncertainty in the direction increases as one moves away from the coast. The best fit is for Victoria, the next best for Penticton, in that order Edmonton, Resolute and the worst for Ottawa. The discrepancy ranges from as low as  $-3^{\circ}$  to as high as  $54^{\circ}$ , but considering the limitations on the data, one has to admit that there is a good agreement between the directions obtained from cross power spectra and coherency.
9. From 3 and 8 above, it can be deduced that the seismic waves excited in the ocean bottom by the overlying water (due to second order pressure fluctuations) are channeled in the oceanic crust, which acts as a wave guide, until the energy reaches the coast at different points and is then propagated in the continental crust along several different paths. This effect of the coastline becomes more pronounced at sites very remote from the coast indicating that the coastline acts as a major source of waves. Thus the simple Longuet-Higgins theory needs to be modified to take into account interactions of the primary Rayleigh waves with the coastline and the subsequent generation of other wave types.
10. From the phase values, from the signal and noise levels as depicted by coherency values and from the power recorded in the vertical component, it is evident that body waves (P-waves in particular) of around 6-7 seconds are present in the microseisms.
11. Evidences for the presence of surface waves are cited where ever possible but they do not seem to form a dominant component of the microseisms.



TABLE VI.2  
COMPARISON OF DIRECTIONS

Station	Storm	Directions from								Discrepancy
		V-R	R-T	V-R	Coherency	Spectra	R-T	V-R	Spectra	
Victoria	43° NoFW	60° NoFW	25° NoFW	60° NoFW	40° NoFW	60° NoFW	+17°	+18°	+17°	-3°
Penticton	26° SoFW	50° SoFW	20° SoFW	60° SoFW	20° SoFW	60° SoFW	+24°	-6°	+34°	-6°
Edmonton	16° NoFW	25° NoFW	40° NoFW	30° NoFW	45° NoFW	30° NoFW	+9°	+24°	+14°	+29°
Resolute	40° SoFW	40° NoFW	35° SoFW	30° SoFW	35° SoFW	30° SoFW	+50°	-5°	-10°	-5°
Ottawa	37° NoFW	60° NoFW	75° NoFW	45° NoFW	85° NoFW	45° NoFW	+23°	+8°	+38°	+48°

12. The estimation of proportion of body waves in microseisms as compared to the surface waves is not feasible with the information available at present. An array of seismic stations separated by distances comparable to the wave-length of the surface waves would yield phase velocities of different waves which could then be used as criteria for this estimation.

## CHAPTER VII

### GENERAL DISCUSSION

VII.1 An attempt thus has been made to study microseisms recorded at five seismological observatories in Canada on dates when an atmospheric low pressure area was present on the Pacific Ocean. Spectral estimates were mainly utilized in identifying the wave types present in microseisms, in determining their direction of approach and in understanding the mechanism of the propagation over long distances. The data were Butterworth band pass filtered to draw Jensen's diagrams and particle motion trajectories.

No assumptions were made about the nature of the microseisms and the problem was approached with an entirely open mind. The results are revealing and at times discouraging; discouraging because of the limitations on the data, and not because of any method employed in understanding them. The data do not seem to be suited for constructing the Jensen's diagrams because of the very complex nature of the microseisms studied here. That this method has failed can be construed as an evidence of microseisms not containing solely surface waves. The presence of body waves (especially P-modes) in the period range of 6-7 secs and of 4-5 secs was suggested on the basis of several computations. The evidences for the presence of

body waves in microseisms can be cited in their order of occurrence in this work as follows:

1. Sequence of peaks in the velocity sensitivity spectra indicating a resonance phenomenon associated with the body waves (Phinney, 1964).
2. Phase values between the vertical and radial components which are usually  $0^\circ$  or  $180^\circ$ .
3. Amplitude ratios of vertical to radial components which are very high compared to the theoretical values suggesting that in addition to Rayleigh waves, long period P modes are recorded on the vertical component.
4. Jensen's diagrams which show a tremendous amount of scattering for the velocity vectors pointing that no simple Rayleigh and Love waves are being recorded on these instruments.

On the other hand several unmistakable surface wave examples were mentioned. It was also suggested that in addition to fundamental modes, higher modes of both Rayleigh and Love waves were present in microseisms superimposed in a complex fashion. In general surface waves have two dominant periods one between 6.0-7.0 sec and the other around 4.5 sec. A few examples of 2.5 second surface waves could be identified.

VII.2 Cross-power and coherency, as functions of two variables, viz. period and azimuth, were computed and plotted on a grid, using the resolved horizontal traces. This grid was then used to construct contour diagrams. The purpose of this was to determine the direction of approach of microseismic waves. The results were gratifying in so far as it was found that direction of approach

could be determined to an accuracy of  $\pm 10^\circ$ . Comparison of the directions obtained from cross power and coherency between the vertical and horizontal components provides a quadruple check on this measurement. Not always did these four directions agree, but seldom did they have a discrepancy of more than  $10^\circ$ . These directions were then compared with those obtained from the storm locations. Considering the limitations on the data, the agreement seems to be good.

VII.3 It is suggested here that the seismic waves excited in the ocean bottom by the second order pressure fluctuations in the overlying water (Longuit-Higgins, op. cit.) are propagated in multiple directions in the oceanic crust, which acts as a wave guide. The energy is then transferred from the oceanic crust to the continental crust and in so doing undergoes an interaction with the coastline which possibly acts as a number of secondary sources from which the waves travel in the continent, so that a recording site would look at different waves approaching the site in different directions. The farther is the site from the coast, the wider are the angles and hence the more uncertain is the direction of approach. It was found that the vertical component of the microseismic waves attenuates very nearly as  $\frac{1}{r}$  and the horizontal approximately as  $\frac{1}{r}$  also, where  $r$  is the distance from the source.

## BIBLIOGRAPHY

- Alpaslan, T., (1968), Spectral behavior of short period body waves and the synthesis of crustal structure in Canada, An M.Sc. thesis submitted to University of Alberta.
- Andrianova, Z. S., V.I. Keilis-Borok, A.L. Levshin, and M.G. Neigauz (1967), Seismic Love Waves, A special Research Report, Consultants Bureau, New York.
- Banerji, S.K., (1929) Microseisms associated with storms in the Indian Seas, Nature, Vol. 123, pp. 163-164.
- Banerji, S.K., (1930), Microseisms Associated with disturbed weather in the Indian Seas, Phil. Trans. Roy. Soc., London, Vol. 229, pp. 287-328.
- Banerji, S.K., (1935), Theory of Microseisms, Proc. Ind. Acad. Sci., Vol. 1, pp. 727-753.
- Basham, P.W., and K. Whitham, (1966) Microseismic noise on Canadian Seismograph records in 1962 and Station Capabilities, Pub. Dom. Obs., Vol. 32, No. 4.
- Blackman, R.B., and J.W. Tukey (1958), The measurement of Power Spectra, Dover Publications Inc., New York.
- Brune, J., and J. Dorman (1963), Seismic Waves and Earth Structure in the Canadian Shield, Bull. Seism. Soc. Am., Vol. 53, pp. 167-210.
- Butterworth, S., (1930), On the Theory of Filter Amplifiers, Wireless Engr, 1, pp. 536-541.
- Cumming, G.L., and E.R. Kanasevich (1966), Crustal Structure in Western Canada, Final Report. Contract AF19(628)-2835, AFCRL, Bedford, Mass.
- Darbyshire, J., (1950), Identification of microseismic activity with Sea Waves, Proc. Roy. Soc. London, A, Vol. 202, pp. 439-448.
- Darbyshire, J., (1954), Structure of Microseismic Waves: Estimation of Direction of Approach by Comparison of Vertical and Horizontal Components, Proc. R. Soc. London, A, Vol. 1152.

- Deacon, G.E.R., (1947), Relation between sea waves and microseisms, *Nature*, Vol. 162, pp. 419-421.
- Defant, A., (1961), *Physical Oceanography*, Vol. II, p. 54. A Pergamon Press Book, The Macmillan Company, New York.
- Dinger, J.E., (1952), Discussion on Ramirez's Paper, NAS-NRC. Publication, No. 306, pp. 12-16.
- Douze, E.J., (1964), Rayleigh waves in short period seismic noise, *Bull. Seism. Soc. Am.*, Vol. 54, pp. 1197-1212.
- Douze, E.J., (1967), Short Period Seismic Noise, *Bull. Seism. Soc. Am.*, Vol. 57, pp. 55-81.
- Ellis, R.M. and P.W. Basham (1968), Crustal characteristics from short period P-waves, *Bull. Seism. Soc. Am.*, Vol. 58, pp. 1681-1700.
- Ewing, W.M., W. S. Jardetzky, and F. Press (1957), *Elastic Waves in Layered Media*, New York, McGraw Hill Book Co. Inc.
- Gilmore, M.H., (1946), Microseisms and Ocean Storms, *Bull. Seism. Soc. Am.*, Vol. 36, pp. 89-119.
- Golden, R.M., and J. F. Kaiser (1964), Design of a wide band sampled data filter, *The Bell Telephone Technical Journal*, pp. 1533-1547.
- Gupta, I.N. (1965), Standing-wave Phenomena in short period Seismic Noise, *Geophysics*, Vol. 30, pp. 1179-1186.
- Gutenberg, B. (1958), *Advances in Geophysics*: New York, Academic Press. (Other references to Gutenberg's work can be found in this work.)
- Harkrider, D.G. and D.L. Anderson, (1962), Computation of Surface Wave Dispersion for Multilayered Anisotropic Media, *Bull. Seism. Soc. Am.*, Vol. 52, pp. 321-332.
- Haskell, N.A., (1953), The Dispersion of Surface Waves on Multilayered Media, *Bull. Seism. Soc. Am.*, Vol. 43, pp. 17-34.
- Jensen, H., (1958), A procedure for the determination of direction of Approach of Microseismic Waves, *Geodetisk Institut*, No. 36, Copenhagen.

- Jensen, H., (1959), Daily determinations of the Microseismic Direction in Copenhagen during the IGY (1958), Geodaetisk Institut, No. 38, Copenhagen.
- Jensen, H., (1961), Statistical Studies on the IGY microseisms from Copenhagen and Nord, Geodaetisk Institut, No. 39, Copenhagen.
- Jensen, H., (1965), Direction of Approach of Microseisms in Scoresbysund, Ivigtut, and Godhavn, Geodaetisk Institut, No. 40, Copenhagen.
- Lee, A.W., (1935), On the Direction of Approach of Microseismic Waves, Proc. Roy. Soc., A. 149, 183.
- Lee, Y.W., (1964), Statistical Theory of Communication, John Wiley & Sons, Inc., New York.
- Longuet-Higgins, M.S., (1950), A Theory of the origin of microseisms, Phil. Trans. Roy. Soc. A, Vol. 243, pp. 1-35.
- Longuet-Higgins, M.S., (1952), Can Sea Waves Cause Microseisms?, Symposium on Microseisms, NAS-NRC Publication No. 306 published in December, 1953.
- Macelwane, J.B., (S.J.) (1952), Sketch of the History of Microseismology, Symposium on Microseisms, NAS-NRC publication, No. 306, pp. 3-6.
- Omori, F., (1901), Publications on the Earthquake Investigation Committee in Foreign Languages, Tokyo, No. 5, pp. 1-82.
- Phinney, R.A., (1961), Leaking modes in the crustal waveguide, Part I, The oceanic PL wave, Journ. Geophys. Res. Vol. 66, pp. 1445-1469.
- Phinney, R.A., (1964), Structure of the Earth's Crust from Spectral Behavior of Long-Period Body Waves, Journ. Geophys. Res., Vol. 69, pp. 2997-3017.
- Press, F., D. Harkrider and C.A. Seafeldt, (1961), A fast, convenient program for computation of Surface-Wave Dispersion curves in Multilayered Media, Bull. Seism. Soc. Am., Vol. 51, pp. 495-502.
- Ramirez, J.E., (1940), An experimental investigation of the nature and origin of microseisms at St. Louis, Mo., Bull. Seism. Soc. Am., Vol. 30, pp. 35-84, 139-178.



- Roden, R.B., (1965), Horizontal and Vertical Arrays for Tele-seismic Signal enhancement, *Geophysics*, Vol. 30, pp. 597-608.
- Sander, G.W., and A. Overton, (1965), Deep Seismic Refraction Investigation in the Canadian Arctic Archipelago, *Geophysics*, Vol. 30, pp. 87-96.
- Seriff, A.J., C. J. Velzeboer and R.J. Haase, (1965), Possible P wave observations in short period seismic noise, *Geophysics*, Vol. 30, pp. 1187-1190.
- Thomson, W.T., (1950), Transmission of Elastic Waves Through a Stratified Medium, *Journ. App. Physics*, 21, p. 89.
- Weinberg, L., (1962), *Network Analysis and Synthesis*, McGraw Hill Book Co. Inc., Toronto, pp. 485-498.
- Weiner, N., (1964), *Extrapolation, Interpolation and Smoothing of Stationary Time Series*, The M.I.T. Press, Cambridge, Massachusetts.
- White, W.R.H., M.N. Bone and W.G. Milne, (1968), *Seismic Refraction Surveys in British Columbia, 1941-66: A Preliminary Interpretation*, Geophysical Monograph 12, AGU, NAS-NRC Publication 1687, pp. 81-93.
- White, W.R.H., and J.C. Savage, (1965), A seismic refraction and gravity study of the earth's crust in British Columbia, *Bull. Seism. Soc. Am.*, Vol. 55, pp. 463-486.
- Wickens, A.J., and F. Kollar, (1967), A Wide Range Seismogram Digitizer, *Bull. Seism. Soc. Am.*, Vol. 57, pp. 91-98.